

# A GIS-Based Approach for Determining Potential Runoff Coefficient and Runoff Depth for the Indian River Lagoon, Florida, USA

*Philip W. Bellamy and Hyun Jung Cho*

## Abstract

The Indian River Lagoon system (IRL), spanning ~40% of Florida's east coast, is one of the nation's biggest and most biodiverse estuaries. In 2011, a super algal bloom event occurred in the IRL with total nitrogen and phosphorus levels that exceeded historical levels. Scientists suspect that nonpoint source pollution through surface runoff may have had a significant impact on the recent recurring algal blooms. Digital Elevation Model, land cover/land use, and soil data were used to calculate a runoff coefficient for the IRL drainage basin. Rainfall data were used to calculate runoff depth for the study area between the years of 2006–2016. When the monthly runoff depth data for 2011 were compared to a previous study on the 2011 super algal bloom in the lagoon, areas with high runoff visually matched the areas with higher chlorophyll *a* concentrations. Land development was a significant variable for determining runoff depth ( $p < 0.0001$ ), and although used to derive runoff depths, the influence of precipitation was marginally significant ( $p = 0.06$ ). Significant spatial autocorrelation indicated local trends between land development and runoff depth ( $p < 0.0001$ ). Outputs will aid with decisions on stormwater management to more sustainable land development planning.

**Keywords:** surface runoff, runoff coefficient, stormwater, Indian River Lagoon, Halifax River, coastal watershed

## 1. Introduction

Algae blooms within coastal estuarine systems have been a threat to vital key ecosystem components causing the degradation of ecological integrity. With non-point source pollution being a primary concern, using geographic information system (GIS) approaches to assess the impacts is effective for stormwater management. Therefore, with the use of land use/land cover (LC/LU), soil, and elevation data, the Potential Runoff Coefficient (PRC) and runoff depth were calculated for the IRL and Halifax River watershed. The analysis consisted of manipulating the geospatial data to derive the potential runoff coefficients and runoff depths.

Considering the contributing factors of surface runoff, the overall goal of the study is to estimate the quantities of runoff within the Indian River Lagoon (IRL) watershed based on a method that encompasses those parameters. The findings can also address whether such method and similar approaches can indicate locations of algae blooms, and aid in stormwater/watershed management. The objectives of this study are listed respectively; **Objective 1:** to calculate the potential runoff coefficients within the IRL watershed. The values will be based on the satellite image classification and validation for land cover/land use, elevation data, and soil data of the study area. **Objective 2:** to calculate the runoff depth of the IRL watershed over an eleven-year duration (2006–2011) using the derived value of the runoff coefficients and rainfall data provided by National Oceanic and Atmospheric Administration National Weather Service (NOAA NWS) River Forecast Centers (RFCs) collected from the Hydrologic Rainfall Analysis Project (HRAP). The outcome will represent the actual quantity of rainfall that was converted to runoff for the year. **Objective 3:** to visually assess if there is a geographic correlation of surface runoff and algae concentrations during months of the 2011 super algal bloom. The finished products can aid in gaining coastal resilience to help adapt to storms, flooding events, and parameters can be used to determine suitability for stormwater parks and infrastructure. The data acquired from the public GIS databases include ground-truthed information and remotely sensed data which were carefully interpreted and validated by professionals.

### 1.1 The Indian River Lagoon system

The Indian River Lagoon (IRL), spanning ~40% of Florida's east coast, is one of the nation's biggest and most biodiverse estuaries. The IRL consists of barrier islands separating its water from Atlantic Ocean [1]. The exchange of the IRL water with the ocean occurs naturally at Ponce De Leon Inlet in New Smyrna Beach, and Jupiter Inlet near West Palm Beach. The other man-made inlets include Sebastian Inlet, Fort Pierce Inlet, Port Canaveral, and St. Lucie inlet. The estuary stretches 251 km along the east coast of Florida with numerous tributaries [2]. The IRL system is made up of three sub lagoons that include the Mosquito Lagoon, which is in the northern section, the Banana River, and the IRL (**Figure 1**). The natural sources of freshwater for the IRL include Crane Creek (Melbourne, FL), Eau Gallie River, St. Lucie River, St. Sebastian River, and Turkey Creek. A secondary natural source of freshwater in the IRL is the Tomoka River which is located west of the lagoon running north connecting to the Halifax River then eventually the Mosquito Lagoon. Although the Tomoka River is not directly connected to the IRL or in its watershed, the Halifax River (**Figure 1**) is partially connected to the northern lagoon at Ponce Inlet and therefore its watershed is included in this study. The IRL and Halifax River watershed contains ~40 cities. The developed urban land comprises impervious surfaces and residential communities that primarily contain turf grass.

In the summer of 2011, a super algal bloom event occurred in the IRL which reached a high biovolume of dinoflagellate *Pyrodinium bahamense var. bahamense* ( $33.9 \times 10^6 \mu\text{m}^3 \text{mL}^{-1}$ ) with mean chlorophyll *a* concentrations (6.2–16.4  $\mu\text{g/L}$ ) that positively correlated with total nitrogen and total phosphorus levels that exceeded historical levels in various locations [3]. Following the massive algae bloom, there have been recurrent blooms consisting of green macroalgae such as *Chaetomorpha* sp. since 2013 [4, 5]. As a result of the 2011 super algal bloom, the coverage of seagrass within the IRL drastically declined from the loss of photosynthetic light by the surface algae [6]. Although fluctuations in seagrass bed percent cover in the lagoon have been understood as a part of a natural cycle of decline and recovery as seagrass abundance,



**Figure 1.** A map of Indian River Lagoon and Halifax River, Florida. The Indian River Lagoon is composed of three waterbodies: the Mosquito Lagoon, Indian River, and the Banana Lagoon. The inset map provides a reference for the location of the lagoon in Florida.

scientists suspect that nonpoint source pollution via surface runoff may have had a significant impact on the recent recurring algal blooms in the lagoon [7, 8].

## 1.2 Surface runoff and runoff models

Surface runoff is water from rain or snowmelt that travels over the land before entering nearby waterbodies. Stormwater flowing across surrounding land transports various pollutants, and ultimately contributes to non-point source pollution. Surface runoff negatively affects many aquatic ecosystems as the runoff transports pollutants and other substances into waterbodies, which can alter turbidity, phosphorus and nitrogen concentrations, and organic matter content in receiving waterbodies [9]. The effects of surface runoff can also be intensified by climate change in specific regions that may have highly developed land and altered hydrology from the addition of artificial stormwater structures that modify the flow of water [10]. Human activities have been shown to have a stronger impact on runoff than climate change, but both stressors significantly impacts runoff quantities [10].

Hypothetical land cover change scenarios in a simulated hydrological study within the Lavrinha watershed in Minas Gerais State, Brazil showed that deforestation in the Atlantic Forest biome would lead to increases in soil moisture (5%), runoff (22%), and decreases in runoff interception (71%) from the loss of roots and extensive rhizomes [11]. Impervious surfaces in urban watersheds can influence the biogeochemical processes, organism's abundance, stress, and vulnerability from heated surface runoff during hot summers [12]. Incorporation of the contributing factors such as vegetative cover that may enhance or influence the effects is effective in hydrological modeling for determining the amount of runoff.

The characteristics of the land surrounding waterbodies affect the amount of surface runoff. During the process of rainfall becoming runoff, various characteristics of the land's surface, such as land use, soil type, and topography, will heavily impact the quantity of runoff [13]. Vegetative cover of the surrounding land can potentially act as a buffer for aquatic systems receiving runoff [14]. During rainfall events, impervious surfaces such as roads, parking lots, and other pavements increase runoff due to extremely limited infiltration into the ground. Areas with 75–100% imperviousness can yield runoff that represents up to 55% of any rainfall [15].

The potential runoff coefficient (PRC) represents the portion of rain that becomes surface runoff during a rain event, and it is determined by the land use, soil texture, and slope [16]. The potential runoff coefficient was derived from methods of developing a unit hydrograph (UH) for specific depths of rainfall. The hydrograph provided the assumption that discharge at any time is proportional to the volume runoff, and the temporal factors for a given duration are constant [17]. Runoff coefficients have been widely utilized in the hydrological modeling along with other computational factors for research in flood frequency, flood prediction, and storm management [18–20]. Hydrologic simulation model software's have been developed using spatial data and GIS [5]. Another method that includes runoff coefficients to hydrological modeling is the runoff curve number (CN) method created by the United States Department of Agriculture Natural Resources Conservation Service. Unlike the potential runoff coefficient, the CN can be calculated for each watershed and encompass the potential maximum retention of the soil over a given period of time.

PRC can be determined for land surfaces with different characteristics along with the quantity of runoff known as the “runoff depth.” Given the quantity of runoff being influenced by the determining conditions, spatial variation in PRC can be estimated for a specific time duration within a given estuarine drainage area. In order to demonstrate this, runoff coefficients and runoff depths were calculated using geographic information systems (GIS) for the drainage basin of the Indian River Lagoon (IRL), Florida, which recently had recurring severe algal blooms. Nonpoint source pollution from surface runoff may have had been a cause for the recurring algal blooms in the lagoon [7, 8]. Use of the spatially contiguous PRC across an area of interest provides additional resources and information for stormwater research within a coastal watershed. Runoff coefficients of a watershed along with other information can be utilized for analytical processes to gain further insight of stormwater dynamics on local and regional scales.

Since 2011, IRL experienced severe algal bloom events; and non-point source pollution through surface runoff is suspected to be one of the causes for the algal blooms. The goal of this study is to calculate the spatially contiguous PRC and runoff depth for the drainage basin of IRL and the connected estuary, the Halifax River, Florida for an eleven-year period (2006–2016) in order to determine which areas and factors contribute to the runoff. The 2011 monthly runoff depth of the draining areas was compared with the 2011 monthly algal bloom maps of a previous

study in order to see any visible correspondence between the locations of algal bloom initiation and the locations with high runoff depth values.

## **2. Data for model components**

The procedure to derive the PRCs and runoff depths for the IRL consisted of processing satellite imagery to derive the land cover and land use (LC/LU), collecting the soil textures throughout study area, and calculating slope using terrain elevation data within the watershed.

### **2.1 Land cover/land use**

Land cover and land use (LC/LU) is one of the factors for calculating PRC. The LC/LU was derived by classifying the European Space Agency (ESA) Sentinel 2 Level 1C 10 m satellite imagery from November of 2016. Four images were downloaded from the ESA Sentinel Scientific Data Hub website to encompass the elongated watershed of the IRL (<https://scihub.copernicus.eu/dhus/#/home>). The images were preprocessed with the ESA Sentinel Application Platform (SNAP) remote sensing software along with the Sentinel 2 toolbox. Before classifying LC/LU of the study area, an atmospheric correction was applied to the images using the Sen2cor 2.3.2 plugin within ESA SNAP to eliminate the effects of water vapor, aerosols, and cirrus clouds when utilizing spectral reflectance data. The preprocessing output of the Sentinel 2 data produces Sentinel Level-2A data which includes values that represent the radiation at the bottom of the atmosphere (BOA). Once the BOA output was produced, the four images were mosaicked to produce a continuous raster image of the IRL. By applying a supervised maximum likelihood classification in ENVI 5.4, the images were classified into five categories; forest, grass, bare soil, crop, and impervious.

### **2.2 Slope**

A digital elevation model (DEM) from the United States Geological Survey National Elevation Dataset (USGS NED) was used to generate terrain slope at a spatial resolution of 10 m (<http://viewer.nationalmap.gov/basic/?howTo=true>) within ESRI ArcMap 10.5 (380 New York Street, Redlands, CA 92373-8100). The elevation values were collected with Interferometric Synthetic Aperture Radar, and referenced to the North American Vertical Datum of 1988 (NAVD 88). A preliminary analysis of the DEM was performed to fill in the low areas or “sinks” that are considered to be errors so that modeled runoff would flow smoothly across the land’s surface. The filled output map was used to create the slope for the areas surrounding IRL. The percent slope was classified into three classes due to the low elevation throughout Florida.

### **2.3 Soil**

The soil data used in the analysis were obtained from the Web Soil Survey (WSS) (<http://websoilsurvey.sc.egov.usda.gov/App/WebSoilSurvey.aspx>). The WSS is operated by the United States Department of Agriculture Natural Resources Conservation Service (NRCS) and contains geospatial data and information produced by the National Cooperative Soil Survey. The NRCS soil data are produced from soil samples collected from NRCS State Soil Scientist for counties throughout the United States and are available in tabular and geospatial data. The spatial data

are provided in the Geographic Coordinate System and World Geodetic System of 1984 datum (GCS\_WGS\_84). The data for soil classification were acquired for six Florida coastal counties: Volusia, Brevard, Indian River, St. Lucie, Martin, and Palm Beach. Tabular information for the soil texture was extracted from the Web Soil Survey Microsoft Access Database file and imported into the ArcMap 10.5 software. The data contained a variety of different soil names for classification: muck, Myakka fine sand, and Turnbull muck, that are all used for determining the slope constant along with LC/LU.

## **2.4 Precipitation for runoff depth**

The runoff depth represents the amount of rainfall that is converted into runoff [16]. Therefore, rainfall data for the Halifax River and IRL watershed were collected to calculate the runoff depth using the runoff coefficients. The data were acquired from the National Oceanic and Atmospheric Administration (NOAA) National Weather Service (NWS) River Forecast Center (RFC) website. The data were downloaded in the ArcGIS shapefile format as point data with a projection of the Hydrologic Rainfall Analysis Projection (HRAP) grid coordinate system that has a North Pole Stereographic projection, and a grid resolution of 4762.5 m (<https://water.weather.gov/precip/download.php>). The rainfall data are acquired in a multi-sensor process that uses radar and rain gauge to estimate the precipitation. After extracting the point data, the shapefiles were converted into raster data. Due to estimation of multi-sensor collected data, the data are first stored in a binary file format called XMRG. This file is then read into the HRAP grid coordinate system through the NWSRFS Operational Forecast System using the NEXRAD Mean Areal Precipitation Preprocessor (MAPX) to associate grid points from XMRG data to represent the hourly average precipitation for each area [21].

## **3. Data analysis**

### **3.1 LC/LU accuracy assessment**

Before assessing the PRCs for the study area, the LC/LU image was tested for its accuracy. The accuracy assessment test consisted of collecting 600 referenced points using a stratified random method that randomly assigns points in each class. A 2016 Digital Globe basemap in ArcMap 10.5 of a higher spatial resolution (0.62 m) was utilized to visually interpret the land cover for each reference point. The output table consisted of a confusion matrix that displays the error of omission, the error of commission per class, and overall accuracy ranging from 0 to 1. Another test for accuracy of the LC/LU classification image included calculating the Cohen's kappa (K) coefficient [22].

### **3.2 PRC**

Potential runoff coefficient (PRC) values were derived to represent ratio of the rainfall that would convert to surface runoff per pixel. The PRC for the IRL area was determined by combining the soil texture, LC/LU, and the slope data. The PRC is calculated from a linear relationship between the runoff coefficients and slope, which is shown in Eq. (1) [23].

$$C = C_0 + (1 - C_0) \frac{S}{s + s_0} \quad (1)$$

$C$  is the PRC,  $S$  (%) is the slope of the land surface,  $C_0$  is the PRC for the near zero slope in reference to the first row of every land use class in PRC values for different land use, slope, and soil texture published in [23] which is sourced from published material [24–28].  $s_0$  represents the slope constant for different land use and soil textures that were empirically derived over a collection of studies. Following reclassification, classes for both parameters were assigned arbitrary weighted values and the soil and LC/LU values for the data were multiplied in the ArcMap 10.5 “Raster Calculator” tool. The arbitrary values were assigned to the classes to conveniently identify each combination of LC/LU and soil texture per pixel from the products. The products of the combinations helped derive the  $C_0$  and  $s_0$  per pixel in the image. The products for the variables were also used to calculate the PRC (Eq. (1)) using the Raster Calculator Tool.

### 3.3 Runoff depth

The total precipitation values were collected for eleven years (2006–2016), and imported into ArcMap 10.5 to be interpolated. The precipitation values (in.) for each of the years were interpolated using the Kriging method with a spherical semivariogram model. The method assumes that the values are more related when in close proximity, and the spatial autocorrelation decreases with distance. After the precipitation was interpolated for each year, the data were multiplied (cell-by-cell) by the PRC raster of the corresponding year using the raster calculator tool provided in ArcMap 10.5 toolboxes. The output of the images provided the runoff depth (centimeters) for each year, and the average runoff depth for the eleven-year period (2006–2016) was calculated per pixel (10 m). The outputs of this image can delineate potential sources of runoff for inland waterbodies that may be connected to the lagoon through a network of drainage systems.

Concentrations of chlorophyll  $a$  in the IRL during the 2011 super algal bloom were compared to runoff depth of surrounding areas. Kameronosky et al. [29] estimated and mapped the Chi  $a$  concentrations using the Medium Resolution Imaging Spectrometer (MERIS) platform aboard the European Space Agency (ESA) Environmental Satellite (ENVISAT) and calculated Normalized Difference Chlorophyll Index (NDCI) [29, 30].

### 3.4 Linear regression between LDI and runoff depth

In order to meet proper data conditions for linear regression analysis in ArcMap 10.5, the raster images were sampled into vector data as a point feature class. Land development intensity (LDI) data was collected from the Florida Department of Environmental Protection (FDEP) Geospatial Open Data Site (<http://geodata.dep.state.fl.us/>). The LDI serves as a human disturbance gradient that incorporates land use and energy used per unit area [31]. It is used in watershed modeling to delineate human-dominated areas, and to scale the human induced impacts on physiological, biological, and chemical processes. A total of 600 points were randomly placed within the Halifax River and IRL watershed via “Create Random Points” tool. Points that were placed over large waterbodies were deleted, leaving 528 sample points left for the analysis. Values from the LDI and runoff depth were extracted to the points.

To adequately assess the relationship between urbanized areas of intense impervious coverage and surface runoff, an ordinary least squares (OLS) regression analysis and geographically weighted regression (GWR) was performed in ArcGIS 10.5. These regression analyses use bandwidth methods to find the

optimal sampling distances between data points, adding a geospatial component to regression analysis. The OLS regression is designed as a “Global Model” with an assumption that the explanatory and dependent variables have global trends over a particular study area. In simplified context, it is assumed that the data are continuous throughout the area therefore being “stationary” data.

For the OLS analysis, the Jarque-Bera statistic tests for model bias that can arise from nonstationary data, misspecification of independent variables, and skewed residuals [32]. Due to the positively skewed data for LDI and runoff depth values, a logarithmic transformation was applied to data to ensure a normal distribution of the datasets while making the variance independent of the mean. The Koenker’s Studentized Breusch-Pagan (Koenker BP) statistic tests for nonstationary with a null hypothesis that the dependent and independent variables have a consistent relationship in geographic space, thus being stationary [33]. A rejected null hypothesis of this test indicates that there are local trends between the variables within the study area.

Presence of significant spatial autocorrelation using the Global Moran’s Index (Moran’s I) is based on the assumption of stationary data. In this case there will be clustering of standard residuals from heteroscedasticity, thus indicating a local model such as GWR is more appropriate. Therefore, the standard residuals produced from both regression analyses were tested for significant clustering using the Moran’s I test. On the other hand, a GWR is a “nonstationary” model that accounts for the local trends in relationships between the variables. In OLS analysis, LDI data from the FDEP and 11-year mean precipitation were used as the independent variable, and the 11-year mean runoff depth as dependent variable. The GWR only included the LDI as independent, and runoff depth as dependent variable due to collinear relationships with rainfall within clustered locations within the study area.

## **4. Results**

### **4.1 LC/LU classification**

There are six LC/LU classes delineated from the supervised classification. The land that mostly consists of agriculture occurs in the southern section of the watershed. The overall accuracy of the LC/LU classification image was 0.82, and the lowest accuracies were in the impervious (User accuracy of 0.65) and bare soil (0.53) classes. This may have been due to the spectral similarity between bare sand along the coast and impervious surfaces such as roof tops. The reference points that appeared to exist in unhealthy brown vegetation were misclassified as bare soil. The kappa coefficient for the LC/LU image was 0.77, with an overall average of 0.82.

### **4.2 Slope**

The slope for the study area was assigned a quantile classification to exclude the effects from outliers in the digital elevation map. The elevation in the state of Florida is relatively flat with an average slope of ~0.47 m per pixel. The areas of high percent slope are manmade structure such as buildings, walls, or homes in developed areas. Some manmade structures with unusually high slopes were identified as the outliers. The other cities have slopes ranging from 0.50 to 1.79 average percent.

### **4.3 Soil**

The soil texture classification for central east Florida consists of mostly fine with Myakka Fine Sand as a native soil, covering more than 1.5 million acres of land, and

labeled as the Florida Official State Soil [34]. The soil data were reclassified into the 12 different textures within the USDA Soil Texture Triangle to accurately implement the values: sand, loamy sand, sandy loam, silt loam, sandy clay loam, silty clay loam, sandy clay, silty clay, and clay. The total study area was composed of 67.7% sand, 4.5% loamy sand, and 8.7% silty clay.

#### 4.4 PRC

The PRC values range from 3 to 100% (**Figure 2**). The PRCs are higher in runoff values in developed areas that are in close proximity to the coastal waterbodies of the IRL and Halifax River. The spatial resolution (10 m) of the image shows a detailed delineation of the manmade infrastructure within urban coastal communities such as roads, buildings, homes, and airports.

#### 4.5 Precipitation

The precipitation data in the IRL watershed from 2006 to 2016 were divided into four quarters with each quarter representing the average of three-month intervals: January–March, April–June, July–September, and October–December. Although the quarterly intervals do not accurately align with seasons, the data are segmented to show the temporal shifts of the rainfall pattern in this area. The IRL watershed precipitation is usually the lowest within the first quarter averaging ~5.48 cm. As the seasonal rainfall increases in spring and summer moving from 10.03 cm in second quarter to 15.55 cm in the third quarter. The rainfall decreases towards the end of the year with an average of 5.58 cm.

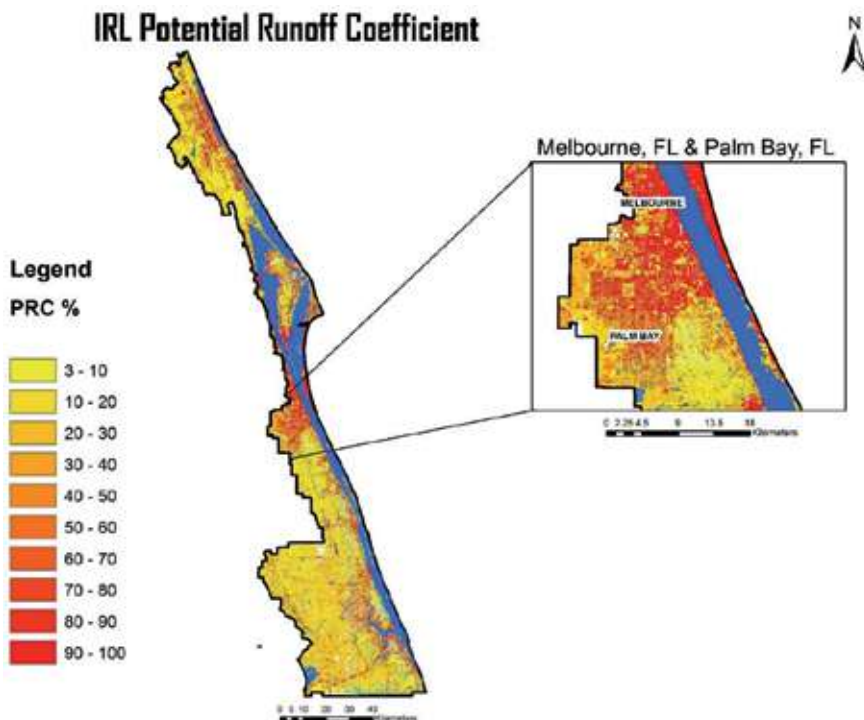


**Figure 2.** Map displaying the potential runoff coefficients (PRC; %) for the Indian River Lagoon and Halifax River watersheds, FL.

#### 4.6 Runoff depth

The runoff depth values for the IRL ranges from 2.51 to 141.48 cm. The monthly runoff depth was calculated for 2011, the year of the super algal bloom in the IRL, to serve as potential explanation for the contribution of high surface runoff to locations of the algal blooms (**Figures 3 and 4**). The average runoff per sub-basin (**Figures 3 and 4**) was compared to the chlorophyll *a* concentrations quantified from European Space Agency's Medium Resolution Imaging Spectrometer (MERIS) for 2011 [29] (**Figures 5 and 6**). The maps were all assigned the same symbology to aid easier depictions of changes in quantities, and for comparison between months.

#### 4.7 Ordinary least squares regression

For the OLS model, LDI is statistically significant ( $p < 0.0001$ ) for and robust probability. Precipitation determines the runoff depth, however, appears to be also significant at the 5%, but not as significant according to the robust p value ( $p = 0.05$ , robust  $p = 0.06$ ). The variance inflation factor (VIF) tests for the redundancy amongst the explanatory variables that are added to the model. If two or more explanatory variables tell the same story because they are linearly related, the error variances are inflated, and the resulting multicollinearity produces a higher VIF. Studies suggest that accepting VIFs fewer than 7.5 or 10 is the rule of thumb for determining if there is multicollinearity within a dataset [35].

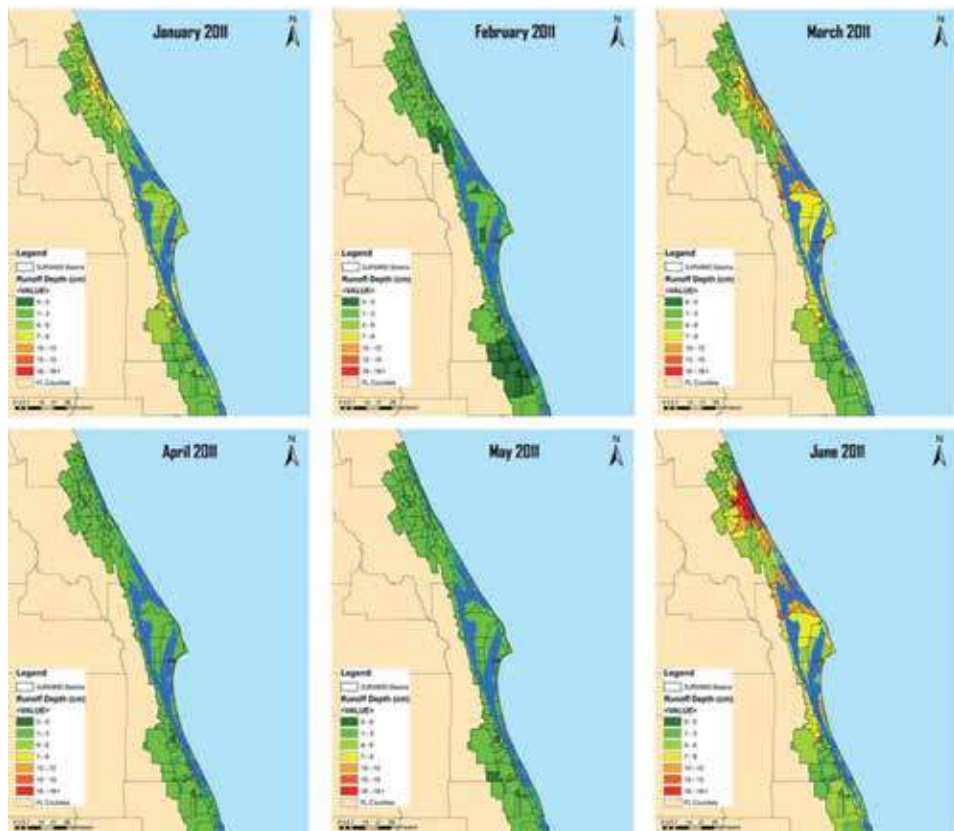


**Figure 3.** The monthly mean runoff depth per sub-basin in the Indian River Lagoon from January 2011 to June 2011. The values increase from dark green, to warmer colors.

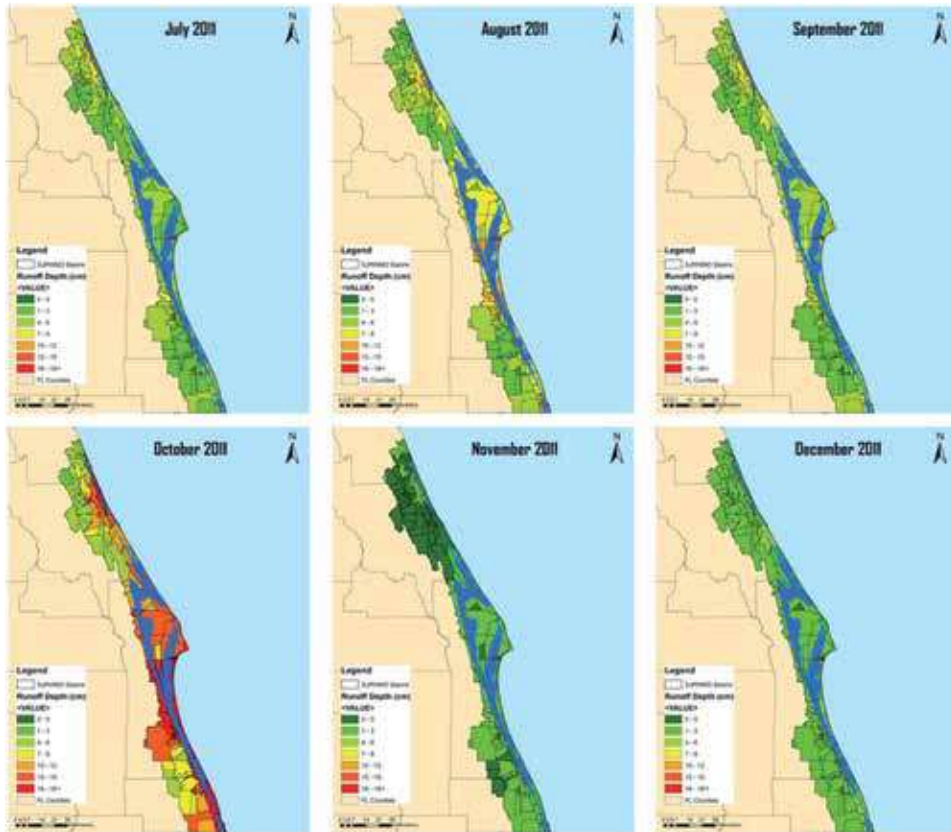


**Figure 4.** The monthly mean runoff depth per sub-basins in the Indian River Lagoon from July 2011 to December 2011. The values increase from dark green, to warmer colors.

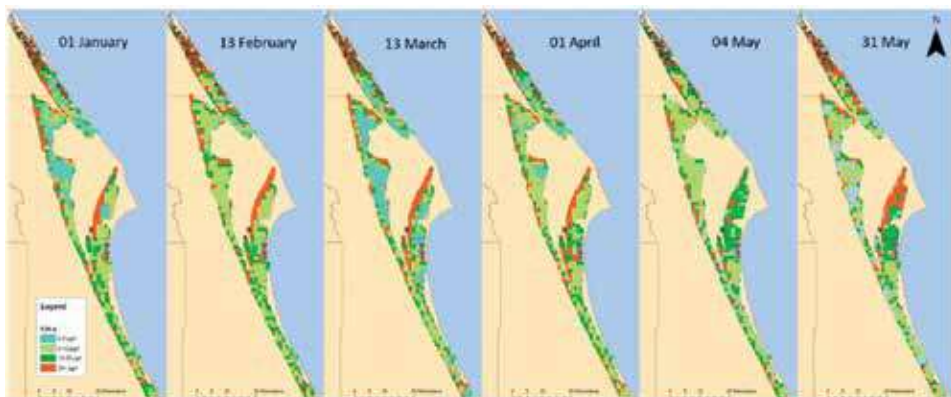


**Figure 5.** Indian River Lagoon chlorophyll a concentrations for spring 2011. The concentrations are estimated using medium resolution imaging spectrometer normalized difference chlorophyll index (image source: [29]).

Within the OLS diagnostic results, statistical values provide information describing the performance of the model along with indicators for choosing an alternative model to adequately address the overall question (**Table 1**). The Akaike's information criterion (AIC) measures the overall model performance, which can be used in comparison to other regression analyses [36]. The multiple  $R^2$  explains how

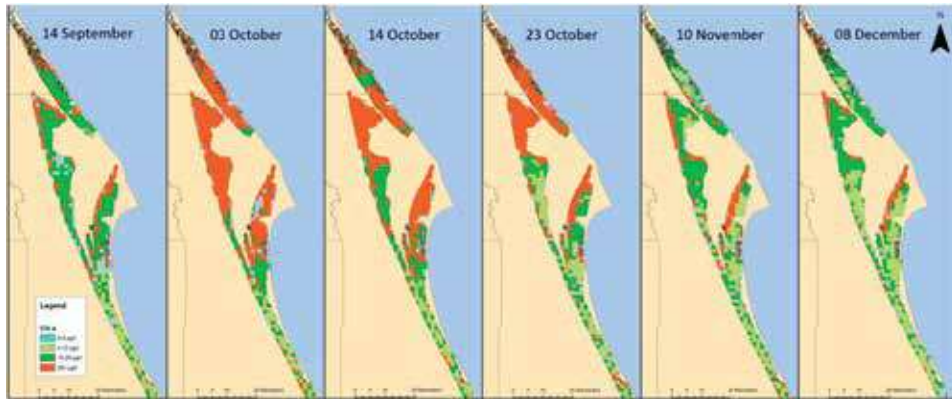


**Figure 6.** Indian River Lagoon chlorophyll a concentrations for 2011 (September–December 2011). The concentrations are estimated using medium resolution imaging spectrometer normalized difference chlorophyll index (image source: [29]).

Variable	Coefficient	Standard error	t-statistic	Probability	Robust SE	Robust probability	VIF
Intercept	1.032	0.531	1.943	0.053	0.571	0.071	
Precipitation	0.009	0.005	1.967	0.050	0.005	0.060	1.001
LDI	0.692	0.071	9.780	<0.0001	0.085	<0.0001	1.001

**Table 1.** A table of the ordinary least squares model variables.

much the independent variables explain the variation in the dependent variable. In relation to the multiple  $R^2$  the Adjusted  $R^2$  accounts for the model complexity. The multiple  $R^2$  the Adjusted  $R^2$  for this tests shows a small  $R^2$  between the variables ( $R^2 = 0.15$ ). The OLS regression also tests for the model significance with the Joint F-statistic and Joint Wald statistic to support the significance of  $R^2$  values (**Table 2**).

The Koenker’s BP statistic tests for nonstationary and heteroscedasticity. The null hypothesis is that the dependent and independent variables have a consistent relationship in geographic space, thus being stationary [33]. The Koenker’s BP statistic shows significant existence of nonstationary trends between runoff depth and LDI ( $p = 0.004$ ). Therefore, the model significance was interpreted based on the Joint Wald statistic ( $p < 0.0001$ ) which also indicates that the relationship was statistically significant. However, the overall measure of how well the explanatory variables explained the variation in the runoff depth from the OLS analysis was relatively small ( $R^2 = 0.15$ ). The Jarque-Bera statistic tests for model bias that can arise from nonstationary data, misspecification of independent variables, and skewed residuals [30]. In this case, the Jarque-Bera statistic shows no significant model bias ( $p = 0.064$ ). A Global Moran’s Index was performed on the residuals of the output file to test for the assumption of no spatial autocorrelation or clustering in the data. The Global Moran’s Index showed statistically significant clustering rejecting the null hypothesis that the data are randomly distributed spatially within a global assumption (Moran’s I = 0.07,  $p < 0.0001$ ). Therefore, the OLS results should not be used to adequately interpret relationship between the explanatory variables and runoff depth.

#### 4.8 Geographically weighted regression

Due to the detection of nonstationary and/or heteroscedasticity in the datasets, a GWR was used to adequately assess the relationship. The Global Moran’s Index and

Anselin Local Moran's Index was performed to test for clustering and local patterns of spatial association [37]. The Global Moran's I indicated that the standard residuals produced from the GWR were significantly dispersed indicating the absence of spatial autocorrelation (Moran's I =  $-0.025$ ,  $p = 0.111$ ). The algorithm calculated an index for every feature, and 96% of the local  $p$ -values were not significant ( $p > 0.05$ ). The validation for choosing the GWR also can be justified by the smaller AICc produced (AICc = 1522.83) compared to the OLS (1573). The  $R^2$  for the GWR increased ( $R^2 = 0.35$ ) with a lower adjusted  $R^2$  of 0.26. As previously stated, the GWR accounts for nonstationary data that contain local trends for the relationship between the variables. Local trends within the dataset relationships were inevitable due to the complexity of different LC/LU within urban communities. The locally weighted regression coefficients can be seen on the coefficient raster produced by the GWR analysis (**Figure 8**). The coefficients show that LDI influences runoff in locations with more impervious surfaces and higher runoff depths, and forested land cover that consists of low LDI values and low runoff. The coefficients increase from blue to yellow to red, indicating higher relationships between the two variables.

**Table 3** shows statistical values generated from the model according to the optimal sampling distance for nearest neighbors (bandwidth). The sampling kernel type for the GWR was fixed, and therefore provides the bandwidth in meters. The Residual Squares is the sum of squared residuals that represent the distance between the observed and estimated values. Therefore, the data are more related when this value is smaller. With a strong influence from bandwidth, the Effective Number is a measure of the complexity of the model that is used to calculate other variables within the GWR model, and it is useful when compared to other models. The sigma is the estimated standard deviation for the residual sum of squares, which shows

<b>Number of observations:</b>	<b>564</b>	<b>AICc</b>	<b>1573.001</b>
Multiple R-squared	0.151	Adjusted R-squared	0.147
Joint Wald statistic	67.250	Prob(>chi-squared), (2) df:	<0.0001
Koenker (BP) statistic	10.963	Prob(>chi-squared), (2) df:	0.004
Jarque-Bera statistic	5.500	Prob(>chi-squared), (2) df:	0.064

**Table 2.**  
*Statistical diagnostic results from the ordinary least squares regression.*

<b>Variable name</b>	<b>Values</b>
Bandwidth	11228.83 m
Residual squares	406.15
Effective number	66.62
Sigma	0.90
AICc	1522.83
R-squared	0.35
Adjusted R-squared	0.26
Dependent field	0.00
Explanatory field	1.00

**Table 3.**  
*Results from the geographic weighted regression analysis.*

that the standard deviation of the observed values for runoff depth were relatively close to the predicted values calculated for the regression model ( $\sigma = 0.90$ ).

## 5. Discussion

### 5.1 Spatially continuous PRC of the IRL and Halifax River watersheds

The goal of this research is to calculate spatially continuous potential runoff coefficient (PRC) and runoff depth. In order to demonstrate how spatial and temporal variation in PRC can be estimated within a given estuarine drainage area, this study calculated PRC as a proportion of rainfall becoming surface runoff and calculated the runoff depth that is the amount of rainfall converted to runoff.

The average PRCs increase from forest, grass, agriculture, bare soil, and to impervious. Ideally, forested areas would have the highest interception of precipitation because of high percent cover of vegetation. Forested areas also have an increase in absorption from the abundance of extensive rhizome systems in the substrate. Areas of grass may have high percent cover of vegetation, but the interception of storm water may not as efficient due to the small biomass of plants. The classification image shows that forest (27.4%) and grass (24.7%) are the most dominant land covers within the IRL watershed. Forests mostly cover the northern section of the IRL watershed and the Halifax River watershed westward of coastal cities. The higher PRC values are located along the Halifax River and IRL in more developed urban communities such as Daytona Beach, Melbourne, and Palm Bay, Florida. Throughout the state of Florida, St. Augustine grass (*Stenotaphrum secundatum* [Walt.] Kuntze) is a popular turf grass used for urban lawns. This rhizome structure of this grass is dense, but relatively short in length which increases yields in runoff and shoreline erosion. Regardless of specific lawn grass, runoff coefficients are higher than forest cover. The recommended runoff coefficient value table for Georgia Stormwater Management also shows different values for grass covered lands based on the soil texture and slope [38]. However, there is only one value for forested areas despite the slope and texture. Although different from forests PRCs used in this study, a change in land cover can impact runoff yields particularly in areas of dense vegetation.

Impervious surfaces make up 15.3% of the study area much of which is located along the coastlines. Based on the National Atlas of the United States Spatial Data collected from the Florida Geographic Data Library (FGDL), there is a total of 40 cities within the IRL watershed. For this study, the ten coastal communities with the highest cover of impervious surface were included: Palm Bay, Port St. Lucie, Melbourne, West Melbourne, Daytona Beach, Port Orange, Ormond Beach, New Smyrna Beach, Titusville, and Fort Pierce. The cities of the most impervious surfaces are Palm Bay with ~50,554 acres of impervious surfaces, and Port St. Lucie with ~73,959 acres of impervious cover.

### 5.2 Temporal variation in runoff depth

The runoff depth varies with changes in LC/LU and intensity of precipitation. The estimated average runoff depth for the IRL ranges from 2.5–141.5 cm for the 11-year interval. The runoff depth throughout the study area fluctuates among the years (**Figure 7**), due to the changes in precipitation. With PRC values, the areas with potential nonpoint source pollution can be used as target locations for management or mitigation. Runoff depth values above the 11-year mean varied across the area and amongst the years. Runoff deviation from the mean indicated

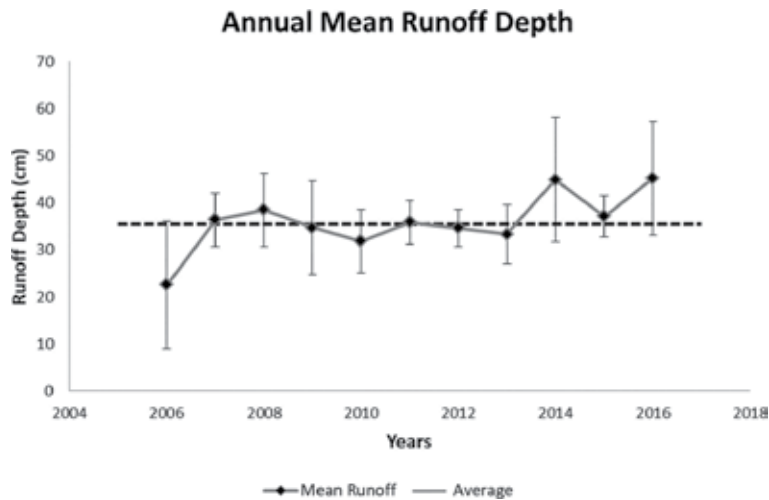


**Figure 7.** The mean of the total runoff depth for each year with standard error bars for standard deviation. The dotted line represents the average 11-year runoff depth ( $\mu = 35.89$  cm) (created in Microsoft Excel 2010).

that heavy runoff depth values above the 11-year mean are years of 2008, 2014, 2015, and 2016. Causes for runoff differences can be contributed to fluctuations in climatic and annual weather patterns for rainfalls. Climatic and temporal trends have been related to changes in the IRL water quality such as El Niño years linked to declines in salinity levels in 1997, and the extended period of La Niña drought events that persisted in autumn of 2006 and summer 2007 [3]. The precipitation data for the IRL were low quantities in 2006 and 2007, and a gradual increase to 2016. The runoff depth appeared to be above the 11-year mean (35.89 cm) throughout the watershed for the years of 2014 and 2016. These are the years of strong El Niño events during which recurrent algal blooms occurred in IRL. La Niña events in Florida have shown nitrate levels to higher in ground water than in streams, which results that nutrients in aquifers accumulates from fertilizer, septic tank effluent, and animal wastes [39, 40]. The average runoff depth for 2006 was the lowest of the years, with 2016 being the highest.

Nutrient loads vary with different land use. For example, golf courses are suspected to be a major contribution to nutrient loading in waterways aside from agricultural lands. Recorded nitrate and phosphorus concentrations significantly increased at the outflow locations from the inflow concentrations for the Morris Williams Municipal Golf Course in Austin, TX [41]. Above average runoff depths in such locations can be monitored as an indicator for early warnings of algal blooms.

### 5.3 Linear regression between runoff depth, precipitation, and land development

Developed land within the IRL watershed contains impervious surfaces consisting of roads, parking lots, and also vegetated lots that are highly altered by human development. Precipitation undoubtedly contributes to runoff quantities, but LC/LU, and development can influence runoff yields. The regression analyses were used to test the relationship between runoff and development, as well as between runoff and precipitation. The OLS regression (Tables 1 and 2), the test to analyze if precipitation is an important factor for determining areas and timing with high runoff contribution, could not be adequately assessed due to spatial autocorrelation (Moran's  $I = 0.07$ ,  $p < 0.0001$ ). However, the results appear to be marginally significant at the 95% confidence interval ( $p = 0.05$ ; robust  $p = 0.06$ ). The LDI

showed to be a significant ( $p < 0.0001$ ) variable at explaining a significant amount of variation in runoff depth. Presence of significant spatial autocorrelation using the Global Moran's I is based on the assumption of stationary data. In this case there will be clustering of standard residuals from heteroscedasticity, thus indicating a local model such as GWR is more appropriate. The Global Moran's Index indicated no spatial autocorrelation with a negative index and rejecting the null hypothesis at with 95% confidence (Global Moran's I =  $-0.025$ ,  $p = 0.111$ ).

Although the runoff depth was determined by precipitation, LC/LU can have a higher impact on the quantities of runoff. Empty grass lots within urban communities can have compacted soil from earlier construction activity which may decrease infiltration rates up to 70% in the central Florida region [42]. The runoff coefficients for the agricultural land surfaces include the effects of compacted soil from heavy machinery. Based on the coefficient raster generated from the GWR analysis, LDI values for forested and impervious areas may account for most of the linear relationship between development and runoff (**Figure 8**). The local trends between rainfall and runoff on smaller time intervals may have a strong linear relationship. However, the mean rainfall values may have reduced the weights in local rainfall-runoff relationships. This outcome also can be noticed within the 11-year mean runoff OLS regression from the existence of local relationships between runoff and the independent variables.

Precipitation estimates along the 251-kilometer IRL estuary and ~ 35-kilometer Halifax River varies within locations, with changing LC/LU as a factor. Areas with lower rainfall can have a higher runoff yield than areas with higher precipitation over forested areas that were assigned lower runoff coefficients. As a result, areas consisting of more human disturbance have a linear relationship with more runoff. Urban communities are often primary targets for some studies to analyze rainfall-runoff by enhancing methods to estimate the DCIA in developed catchments [43]. Based on the global trends of urbanization within coastal areas, stronger rainfall-runoff relationships have positive correlations with the increase of impervious cover percentages for urban zones within separate countries [44]. The purpose of choosing LDI was to indicate the contributions of surface runoff from vegetated lands affected by urban development. To further explain this relationship, future research should assess stormwater runoff using the impervious percentage images created by the USGS. The percentage of imperviousness can also be compared to increases in runoff depth.

#### **5.4 Runoff depth during the 2011 super algal bloom**

The IRL ecosystem recently suffered from a recurrence of algae blooms since 2011 which are heavily influenced by anthropogenic stressors within its watershed, such as surrounding developed land with possible higher surface runoff [8]. Based on a visual comparison; the runoff depth was higher prior to the algal bloom events between 2011 and 2016 particularly near the areas of recorded high Chlorophyll *a* concentrations (**Figures 3–6**). It is important to note that the monthly runoff reflects precipitation estimates collected at the end of the month. Therefore, the runoff depth map for March should be visually compared to the chlorophyll *a* concentrations in April 2011.

Although there is no available MERIS NDCI calculations collected throughout the summer, there was an increase of runoff to 10–18 cm in May and June for the Banana River (**Figures 5 and 6**). The increase may explain the 48.62  $\mu\text{g/L}$  spike in chlorophyll *a* May 2011 from April 2011. Based on the estimated concentrations by MERIS NDCI and water quality samples from SJRWMD, the algal bloom became higher on the 14 September 2011 with the highest concentrations in October [29].

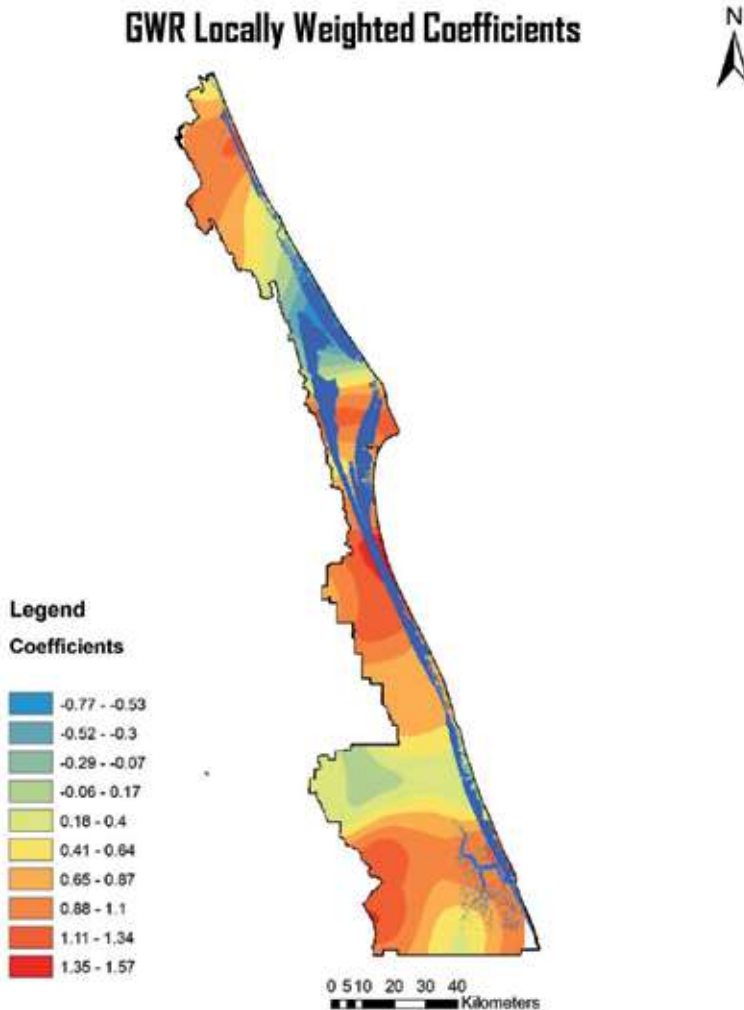


**Figure 8.**  
*The map above shows the geographically weighted regression locally weighted coefficients throughout the study area.*

The runoff depth for October 2011 showed the high runoff with values above 15 cm in the southern IRL and Northern IRL. Subsequently, concentrations of chlorophyll *a* gradually decreased throughout October, and further dropped in November and December. Results also indicate that there were also smaller contributions of runoff during those months with decreasing trends. Visual comparisons between the chlorophyll *a* and runoff depth indicate that there may be a correlation positive association between the two variables for 2011. However, further analysis including statistical measures should be performed to assess the relationship.

### 5.5 Implication for coastal water management

Delineation of PRCs and runoff depths can provide a geographic depiction for assessing lands of interest to implement sustainable developmental designs and structures. In this study, runoff coefficients were calculated for each pixel regardless of surrounding pixel values. Therefore, computational methods used in this study to determine runoff depth were not assessed using methods to incorporate Directly Connected Impervious Areas (DCIA). DCIAs are areas that are considered

to be hydraulically connected to the conveyance system according to the Southwest Florida Water Management District Resource Regulation Technical Guide [45]. Other study estimated runoff volumes in various sub-basins of rivers and tributaries within the IRL watershed using DCIA and non-DCIA methods [46]. Runoff from such studies use a measure called the Soil Conservation Survey Runoff Curve Number. The overall runoff was calculated from the sum of the DCIA and non-DCIA runoff, while runoff coefficients were derived by dividing the generated runoff by the total rainfall for the stations which was listed as “C values”. While this approach can be used to determine Total Maximum Daily Loads (TMDLs) for nutrients, PRCs from this study can be used to emphasize exact locations within the watershed that are suitable for LC/LU management practices.

Direct surface runoff into waterbodies can be significantly affected by impervious surfaces in close proximity. In other scenarios, runoff from developed lands may travel through vegetation before entering into a waterbody. The harmful effects of surface runoff from and on urban communities call for a need of more stringent regulations, and more efficient coastal urban planning and management. This approach of stormwater management provides a long term adaptation plan to be proactive to the future impacts from climate change. Delineation of potential runoff coefficients and runoff depths can provide a geographic depiction for assessing lands of interest to implement sustainable developmental designs and structures. Mean runoff depth and runoff coefficient values can be used to determine areas of high runoff to apply green infrastructure within a watershed. “Green Infrastructure” is the practice of utilizing natural vegetated areas for runoff treatment by mimicking natural stormwater flow paths, and is composed of many low impact development (LID) designs [47]. Developed land within the IRL watershed contains impervious surfaces consisting of roads, parking lots, and also vegetated lots that are highly altered by human development.

Precipitation undoubtedly contributes to runoff quantities, but LC/LU, and development can influence runoff yields. The regression analyses were used to test the relationship between runoff and development, as well as between runoff and precipitation. The OLS regression, the test to analyze if precipitation is an important factor for determining areas and timing with high runoff contribution, could not be adequately assessed due to spatial autocorrelation (Moran’s  $I = 0.07$ ,  $p < 0.0001$ ). However, the results appear to be marginally significant at the 95% confidence interval ( $p = 0.05$ ; robust  $p = 0.06$ ). The LDI showed to be a significant ( $p < 0.0001$ ) variable at explaining a significant amount of variation in runoff depth. Presence of significant spatial autocorrelation using the Global Moran’s  $I$  is based on the assumption of stationary data. In this case there will be clustering of standard residuals from heteroscedasticity, thus indicating a local model such as GWR is more appropriate. The Global Moran’s Index indicated no spatial autocorrelation with a negative index and rejecting the null hypothesis at with 95% confidence (Global Moran’s  $I = -0.025$ ,  $p = 0.111$ ).

Although the runoff depth was determined by precipitation, LC/LU can have a higher impact on the quantities of runoff. Empty grass lots within urban communities can have compacted soil from earlier construction activity which may decrease infiltration rates up to 70% in the central Florida region [42]. The runoff coefficients for the agricultural land surfaces include the effects of compacted soil from heavy machinery. Based on the coefficient raster generated from the GWR analysis, LDI values for forested and impervious areas may account for most of the linear relationship between development and runoff. The local trends between rainfall and runoff on smaller time intervals may have a strong linear relationship. However, the mean rainfall values may have reduced the weights in local

rainfall-runoff relationships. This outcome also can be noticed within the 11-year mean runoff OLS regression from the existence of local relationships between runoff and the independent variables.

Mitigation of stormwater runoff often includes developing more sustainable development strategies within urban communities. An aggregation of developmental designs for combating runoff in an urban community showed reductions in runoff, and also projected expansions in bare soil, impervious cover, and soil alteration will lead to higher runoff volumes [48]. As with vegetated and undeveloped surfaces within riverine systems, the hydrological changes in volume and base flows are reduced with this hybrid design. In reference to GIS approaches to correlating surface runoff to LCLU, urban areas and bare land also corresponded to the degradation of stormwater quality [49].

## **6. Conclusion**

The PRCs for the IRL were applied to land surfaces based on soil, land cover, and slope. These coefficients were used as ratios to determine the runoff depth per pixel within the IRL using precipitation data. After calculating the runoff depth for an 11-year period (2006–2016), it was found that the recent years (2014, 2016) were above the average 11-year runoff matched years of strong El Niño. The runoff deviation from the 11-year mean was also calculated per pixel for each year and highlighted higher runoff quantities closer to the shore of the IRL within the watershed. It is well known that impervious surfaces decrease infiltration, thus increasing runoff yields. Even with vegetated landscape, highly developed land can have poor infiltration from compact soil. The linear regression analysis showed that land development has a significant relationship with runoff depth, and there are local trends between the variables. During the 2011 super algal bloom, the months of March and April 2011 showed increases in runoff, which matched the areas with higher chlorophyll *a* mapped with MERIS in the Mosquito Lagoon in the Northern IRL [29]. In October 2011, extremely high concentrations were detected from MERIS and sampled from St. Johns River Water Management District; this research also calculated high runoff depth concentrations, delineated in the IRL watershed for October 2011. Based on these analyses, the output of this research can possibly delineate areas within the coastal communities that experience higher runoff, and help locate more suitable areas for stormwater parks, green infrastructure, and sustainable stormwater structures. Future research can include using the indices such as LDI to further correct the runoff coefficients for a particular watershed. PRCs can be applied to other watersheds of coastal ecosystems for as a visual reference, or used as a parameter for more advanced hydrologic modeling.

## **Acknowledgements**

This publication was made possible by the National Oceanic and Atmospheric Administration, Office of Education Educational Partnership Program award (NA16SEC4810009). Its contents are solely the responsibility of the award recipient and do not necessarily represent the official views of the U.S. Department of Commerce, National Oceanic and Atmospheric Administration.

Any opinions, findings, conclusions, or recommendations expressed in this publication are those of the author(s) and do not necessarily reflect the view of the U.S. Department of Commerce, National Oceanic and Atmospheric Administration.

## **Conflict of interest**

There is no conflict of interest.

## **Author details**

Philip W. Bellamy and Hyun Jung Cho\*  
Bethune-Cookman University, Daytona Beach, Florida, USA

\*Address all correspondence to: [choh@cookman.edu](mailto:choh@cookman.edu)

## **IntechOpen**

---

© 2019 The Author(s). Licensee IntechOpen. This chapter is distributed under the terms of the Creative Commons Attribution License (<http://creativecommons.org/licenses/by/3.0>), which permits unrestricted use, distribution, and reproduction in any medium, provided the original work is properly cited. 

## References

- [1] Smithsonian Marine Station. An Overview of the Indian River Lagoon Species Inventory Project [Internet]. 2014. Available from: <https://www.curriki.org/oer/Smithsonian-Marine-Station-at-Fort-Pierce-The-Indian-River-Lagoon-Species-Inventory-150548> [Accessed: 25 February 2019]
- [2] De Freese DE. Connecting people to the sea: The Indian River Lagoon. In: Schue K, editor. *Naturally Central Florida: Fitting the Pieces Together*. Orlando, FL: "myregion.org" and University of Central Florida. [Accessed: 15 December 2005]
- [3] Philips EJ, Badylak S, Christman MC, Lasi MA. Climatic trends and temporal patterns of phytoplankton composition, abundance, and succession in the Indian River Lagoon, Florida, USA. *Estuaries and Coasts*. 2010;**33**:498-512. DOI: 10.1007/s12237-009-9166-8
- [4] Whitehouse LN, Lapointe BE. Comparative ecophysiology of bloom-forming macroalgae in the Indian River Lagoon, Florida: *Ulva lactuca*, *Hypnea musciformis*, and *Gracilaria tikvahiae*. *Journal of Experimental Marine Biology and Ecology*. 2015;**47**:208-216. DOI: 10.1016/j.jembe.2015.06.012
- [5] Philips EJ, Badylak S, Lasi MA, Chamberlain R, Green WC, Hall LM, et al. From red tides to green and brown tides: Bloom dynamics in a restricted subtropical lagoon under shifting climatic conditions. *Estuaries and Coasts*. 2014;**38**:886-904. DOI: 10.1007/s12237-014-9874-6
- [6] Gobler CJ, Koch F, Kang Y, Berry DL, Tang YZ, Lasi M, et al. Expansion of harmful brown tides caused by the pelagophyte *Aureoumbra lagunensis* De Yoe et Stockwell, to the US east coast. *Harmful Algae*. 2013;**27**:29-41. DOI: 10.1016/j.hal.2013.04.004
- [7] Lapointe BE, Herren LW, Debortoli DD, Vogel MA. Evidence of sewage-driven eutrophication and harmful algal blooms in Florida's Indian River Lagoon. *Harmful Algae*. 2015;**43**:82-102. DOI: 10.1016/j.hal.2015.01.004
- [8] Breininger DR, Breininger RD, Hall CR. Effects of surrounding land use and water depth on seagrass dynamics relative to a catastrophic algal bloom. *Conservation Biology*. 2017;**31**:67-75. DOI: 10.1111/cobi.12791
- [9] da Silva RM, Santos CAG, de Lima Silva VC, Pereira e Silva L. Erosivity, surface runoff, and soil erosion estimation using GIS-coupled runoff-erosion model in the Mamuaba catchment, Brazil. *Environmental Monitoring and Assessment*. 2013;**185**:8977-8990. DOI: 10.1007/s10661-013-3228-x
- [10] Hao X, Chen Y, Xu C, Li W. Impacts of climate change and human activities on the surface runoff in the Tarim River basin over the last fifty years. *Water Resources Management*. 2008;**22**:1159-1171. DOI: 10.1007/s11269-007-9218-4
- [11] Alvarenga L, de Mello C, Colombo A, Cuartas L, Bowling L. Assessment of land cover change on the hydrology of a Brazilian headwater watershed using the distributed hydrology-soil-vegetation model. *Catena*. 2016;**14**:7-17. DOI: 10.1016/j.catena.2016.04.001
- [12] Hester ET, Bauman KS. Stream and retention pond thermal response to heated summer runoff from urban impervious surfaces stream and retention pond thermal response to heated summer runoff from urban impervious surfaces. *Journal of the American Water Resources Association*. 2013;**49**:328-342. DOI: 10.1111/jawr.12019

- [13] Wilson C. Land use/land cover water quality nexus: Quantifying anthropogenic influences on surface water quality. *Environmental Monitoring and Assessment: An International Journal Devoted to Progress in the Use of Monitoring Data in Assessing Environmental Risks to Man and the Environment*. 2015;**187**:1-23. DOI: 10.1007/s10661-015-4666-4
- [14] Donovan GH, Butry DT, Mao MY. Statistical analysis of vegetation and stormwater runoff in an urban watershed during summer and winter storms in Portland, Oregon, U.S. *Arboriculture & Urban Forestry*. 2016;**42**:318-328
- [15] Paul MJ, Meyer JL. The ecology of urban streams. *Annual Review of Ecology and Systematics*. 2001;**32**:333-365. DOI: 10.1146/annurev.ecolsys.32.081501.114040
- [16] Mahmoud SH, Mohammad FS, Alazba AA. A GIS-based approach for determination of PRC for Al-baha region, Saudi Arabia. *Arabian Journal of Geosciences*. 2014;**7**:2041-2057. DOI: 10.1007/s12517-014-1303-4
- [17] Sherman L. Stream flow from rainfall by the unit graph method. *Engineering News Record*. 1932;**108**:501-505
- [18] Viji R, Prasanna PR, Ilangoan R. GIS based SCS-CN method for estimating runoff In Kundahpalam watershed, Nilgries district, Tamilnadu. *Earth Sciences Research Journal*. 2015;**19**:59-64. DOI: 10.15446/esrj.v19n1.44714
- [19] Crăciun AI, Haidu I, Magyari-Sáska Z, Imbroane AI. Estimation of runoff coefficient according to soil moisture using GIS techniques. *Geographia Technica*. 2009;**8**:1-10
- [20] Costea G. Deforestation process consequences upon surface runoff coefficients. catchment level case study from the Apuseni Mountains, Romania. *Geographia Technica*. 2013;**17**:28-33
- [21] Reed S, Maidment D. Coordinate transformations for using NEXRAD data in GIS-based hydrologic modeling. *Journal of Hydrological Engineering*. 1999;**4**:174-182. DOI: 10.1061
- [22] Cohen J. A coefficient of agreement for nominal scales. *Educational and Psychological Measurement*. 1960;**20**:37-46. DOI: 10.1177/001316446002000104
- [23] Liu YB, De Smedt F. WetSpa extension, a GIS-based hydrologic model for flood prediction and watershed management [thesis]. Vrije Universiteit Brussel; 2004
- [24] Corbitt RA. Stormwater Management. *Standard Handbook of Environmental Engineering*. 2nd ed. 1990. pp. 1-7. ISBN: 9780070131606
- [25] Chow VT, Maidment DR, Mays LW. *Applied Hydrology*. 1st ed. New York City, NY: McGraw-Hill; 1988. ISBN: 0 07-010810-2
- [26] Fetter CW Jr. *Applied Hydrogeology*. Columbus, Ohio: Charles E. Merrill and Co; 1980. p. 484. ISBN: 013-088239-9
- [27] Kirkby MJ, Beven KJ. A physically based, variable contributing area model of basin hydrology (Unmodèle à base physique de zone d'appel variable de l'hydrologie du bassin versant). *Hydrological Sciences Journal*. 1979;**24**:43-69. DOI: 10.1080/02626667909491834
- [28] Mallants D, Feyen J. Kwantitatieve en Kwalitatieve Aspecten Van Oppervlakte en Grondwaterstroming. Vol. 21. 1990. p. 76
- [29] Kameronosky A, Cho HJ, Morris L. Monitoring of the 2011 super algal bloom in Indian River Lagoon, FL, USA, using MERIS. *Remote Sensing*.

2015;7:1441-1460. DOI: 10.3390/rs70201441

[30] Mishra S, Mishra DR. Normalized difference chlorophyll index: A novel model for remote estimation of chlorophyll a concentration in turbid productive waters. *Remote Sensing of Environment*. 2011;**117**:394-406. DOI: 10.1016/j.rse.2011.10.016

[31] Brown MT, Vivas MB. Landscape development intensity index. *Environmental Monitoring and Assessment*. 2005;**101**:289-309. DOI: 10.1007/s10661-005-0296-6

[32] Jarque CM, Bera AK. A test for normality of observations and regression residuals. *International Statistical Review*. 1987;**55**:163-172. DOI: 10.2307/1403192

[33] Fotheringham SA, Brunson C, Charlton M. *Geographically Weighted Regression: The Analysis of Spatially Varying Relationships*. Hoboken, NJ: John Wiley & Sons; 2002. ISBN-10: 0471496162

[34] Florida's State Soil-Myakka Fine Sand. 1993. Available from: <https://soils.ifas.ufl.edu/media/soilsifasufledu/sws-main-site/pdf/about/Myakka-Fl-State-Soil.pdf> [Accessed: 25 February 2019]

[35] O'Brien RM. A caution regarding rules of thumb for variance inflation factors. *Quality & Quantity*. 2007;**41**:673-690. DOI: 10.1007/s11135-006-9018-6

[36] Burnham KP, Anderson DR. *Model Selection and Multimodel Inference: A Practical Information-Theoretic Approach*. 2nd ed. New York: Springer; 2010. pp. 2-444. ISBN: 0-387-95364-7

[37] Anselin L. Local indicators of spatial association-LISA. *Geographical Analysis*. 1995;**27**:93-115. DOI: 10.1111/j.1538-4632.1995.tb00338.x

[38] Georgia Stormwater Management. *Georgia Storm water Management Manual Volume 2* [Internet]. 2001. Available from: <http://www.lex-co.com/Departments/PublicWorks/GSMMVol2.pdf> [Accessed: 20 April 2019]

[39] Cao H. El Niño-La Niña events, precipitation, flood-drought events, and their environmental impacts in the Suwannee River watershed, Florida. *Environmental Geosciences*. 2000;**7**:90-98. DOI: 10.1046/j.1526-0984.2000.72002.x

[40] Pittman JR, Hatzell HH, Oaksford ET. Spring contributions to water quantity and nitrate loads in the Suwannee river during base flow in July 1995. U.S. Geological Survey Water-Resources Investigations Report. 1995. 12. pp. 97-4152

[41] King KW, Balogh JC, Hughes KL, Harmel RD. Nutrient load generated by storm event runoff from a golf course watershed. *Journal of Environmental Quality*. 2007;**36**:1021-1030. DOI: 10.2134/jeq2006.0387

[42] Gregory JH, Dukes MD, Jones PH, Miller GL. Effect of urban soil compaction on infiltration rate. *Journal of Soil and Water Conservation*. 2006;**61**:117-124

[43] South Florida Water Management District. *Surface Water Improvement and Management (SWIM) Plan for the Indian River Lagoon*. Palatka, FL: 1995

[44] Hwang J, Rhee DS, Seo Y. Implication of directly connected imperious areas to the mitigation of peak flows in urban catchments. *Water*. 2017;**9**:696-710. DOI: 10.3390/w9090696

[45] Dietz ME. Low impact development practices: A review of current research and recommendations for future directions. *Water Pollution and Soil*. 2017;**186**:351-363. DOI: 10.1007/s11270-007-9484-z

[46] Ebrahimian A, Wilson BN, Gulliver JS. Improved methods to estimate the effective impervious area in urban catchments using rainfall-runoff data. *Journal of Hydrology*. 2016;**536**:109-118. DOI: 10.1016/j.jhydrol.2016.02.023

[47] Goldshleger N, Shoshany M, Karnibad L, Arbel S, Getker M. Generalising relationships between runoff-rainfall coefficients and impervious areas: An integration of data from case studies in Israel with data sets from Australia and the USA. *Urban Water Journal*. 2009;**6**:201-208. DOI: 10.1080/15730620802246355

[48] Paule-Mercado M, Lee B, Memon S, Umer S, Salim I, Lee C. Influence of land development on stormwater runoff from a mixed land use and land cover catchment. *Science of the Total Environment*. 2017;**59**:2142-2155. DOI: 10.1016/j.scitotenv.2017.05.081

[49] Paule MA, Memon SA, Lee B, Umer SR, Lee C. Stormwater runoff quality in correlation to land use and land cover development in Yongin, South Korea. *Water Science and Technology*. 2014;**70**:218-225. DOI: 10.2166/wst.2014.207

# Autonomous Systems for the Environmental Characterization of Lagoons

*Monica Rivas Casado, Marco Palma and Paul Leinster*

## Abstract

This chapter reviews the state of the art in robotics and autonomous systems (RAS) for monitoring the environmental characteristics of lagoons, as well as potential future uses of such technologies that could contribute to enhancing current monitoring programmes. Particular emphasis will be given to unmanned aerial vehicles (UAVs), autonomous under water vehicles (AUVs), remotely operated underwater vehicles (ROVs) and (semi-)autonomous boats. Recent technological advances in UAVs, AUVs and ROVs have demonstrated that high-resolution data (e.g. 0.4 cm imagery resolution) can be gathered when bespoke sensors are incorporated within these platforms. This in turn enables the accurate quantification of key metrics within lagoon environments, such as coral morphometries. For example, coral height and width can now be estimated remotely with errors below 12.6 and 14.7 cm, respectively. The chapter will explore how the use of such technologies in combination could improve the understanding of lagoon environments through increased knowledge of the spatial and temporal variations of parameters of interest. Within this context, both advantages and limitations of the proposed approaches will be highlighted and described from operational, logistical, and regulatory considerations. The chapter will be based on recent peer-reviewed research outputs obtained by the authors.

**Keywords:** emerging technologies, robotics, autonomous systems, environmental monitoring, UAVs, autonomous underwater vehicles, ROVs, semi-autonomous boats

## 1. Introduction

Lagoons are shallow bodies of water separated from larger bodies of water by barrier reefs, coral reefs, sandbars or other natural barriers such as shingle or rocks (**Figure 1**). Monitoring of lagoons is a regulatory requirement in Europe under the Water Framework Directive [1]. These requirements need to be interpreted alongside those of other directives such as the Nitrates Directive, Habitats Directive and the Marine Strategy Framework Directive and the EU strategy on adaptation to climate change [2, 3]. Implementation of these regulatory requirements has increased the focus on characterizing lagoon environments and in developing periodic and routine monitoring programmes (e.g. [4]), with government across the European Union having to reconsider their approach to lagoon monitoring.

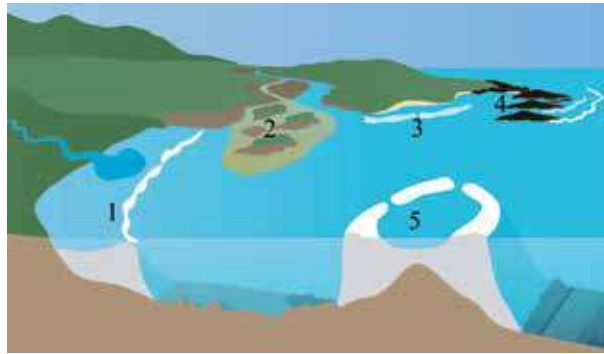


**Figure 1.** Schematic diagram depicting different types of lagoon environments. (1) sandbar coastal lagoon; (2) river delta and tidal lagoon; (3) coastal coral reef lagoon; (4) archipelago's lagoon; (5) atoll coral reef lagoon. Modified from IAN image library, Tracey Saxby ([ian.umces.edu/imagelibrary/](http://ian.umces.edu/imagelibrary/)).

For example, Scotland's common standards for saline lagoon habitat monitoring were abandoned in 2008 as they were not considered to be fit for purpose and were not in accordance with these new regulatory requirements [3]. The development of periodic and routine monitoring programmes has required consideration of how to increase the spatial and temporal understanding of lagoon environments and has resulted in increased spatio-temporal coverage, resolution, larger data sets and more sophisticated data analysis approaches [3, 5].

The range of parameters that potentially could be monitored is wide and varied [4, 6]. **Table 1** summarizes the key parameters that are typically monitored to characterize lagoon environments [1]. These include biological, physico-chemical and hydromorphological parameters. Traditional monitoring methods rely on visual observation or direct manual measurements of these key parameters [1]. In general, such methods are highly time-consuming and costly. They can also require destructive sampling and are therefore limited in the spatial extent within which they can be implemented.

Remote sensing techniques based on satellite imagery have been used to overcome some of these limitations (e.g. [7–9]). Satellite imagery enables the monitoring of large extents. However, the resolution provided by satellite imagery is, in many cases, not sufficient to characterize a lagoon environment to the required level of detail. Information derived from satellite imagery cannot be used for physical measurements of water quality and does not enable characterization of the sub-surface properties of lagoons in the deepest areas.

Recent technological advances within the area of robotics, autonomous systems and machine learning have been identified as potential solutions to overcome the limitations mentioned above. Both robots and autonomous systems have been identified by the UK government as one of the eight great technologies [10] where the UK will be global leaders. Robots and autonomous systems that are able to monitor the environment independently of human control could revolutionize lagoon monitoring in the next decades. Such technologies have already been used in a diverse range of environments, with some authors reporting some applications in lagoons [11]. Both robots and autonomous systems require bespoke algorithms that enable them to carry out their tasks, from path planning during autonomous navigation to the analysis of the data collected. Machine learning methods enable the development and implementation of such algorithms. Machine learning techniques have already been successfully used in multiple environments to detect fish species automatically from imagery collected with underwater cameras [12] and to predict trophic status indicators in coastal lagoons [13].

Parameter	Description	
Biological	Phytoplankton	Changes in phytoplankton composition indicate changes in the dynamics of the lagoon. Changes in nutrients, salinity or environmental stressors have an impact on the primary production. Key metrics look at the presence of harmful algal species, species configuration of assemblages, phytoplankton variation over time, growth and biomass [14, 15]
	Other aquatic flora	This includes floating (emergent) and submerged plants. The key parameters used to describe other aquatic flora include community structure, taxonomic composition, abundance, coverage, diversity and species richness
	Habitat	Habitat characterization focuses on the quality and diversity of the habitat present within the lagoon and surrounding areas. Key metrics include species composition, species coverage gain/loss, habitat alteration, complexity, patchiness and stabilization [14]
	Macro-invertebrates	Abundance and diversity of macro-invertebrates are ecological indicators of water-level fluctuations and human pressures. Taxonomic composition, abundance, species richness, community structure and diversity indexes are key parameters
	Fish	Fish community composition (diversity and structure), abundance and seasonality are the key parameters used to characterize fish communities in lagoons. Changes in these parameters are indicators of environmental change and anthropogenic impact
Physico-chemical	Salinity	Salinity patterns provide information about the vertical and horizontal stratification of water in the lagoon, tidal patterns and the rate of saline and fresh water ingress-egress
	Temperature	Temperature measurements provide information about the temporal and spatial variation patterns in the lagoon and the occurrence of thermoclines. It also provides information about the influence of insolation and evaporation processes
	pH	An indicator of acidification and algal activity
	Oxygen	Oxygenation levels in lagoons are an indication of primary production and general organic matter consumption
Hydromorphological	Tidal range	The tidal range is the difference in water level between high tide and low tide. The tidal range is an indicator of the likely patterns of saline and fresh water ingress-egress
	Hydrology	Hydrological characterization focuses on quantifying existing hydrological processes within lagoons. These include evaporation, insolation, internal circulation (saline and freshwater ingress-egress, groundwater), groundwater input and mixing processes, amongst others
	Morphology	Quantity, structure and substrate of the bed, depth variation and continuity and structure of the intertidal zone are key morphological parameters. More detailed characterizations look at the properties of the barrier, backbarrier stratigraphy, absence/presence of tidal inlet [16] and detailed bathymetry

**Table 1.**  
 Key parameters used for lagoon characterization based on the water framework directive [1].

The aim of this chapter is to review applications of recent technological advances within the context of lagoon environmental monitoring and define the implications for future remote sensing-based monitoring of these environments and the associated management strategies. In particular, this chapter reviews reported uses of robotics and autonomous systems for the characterization of lagoon ecosystems. It also highlights future applications of such technology and interprets the findings within the context of lagoon management and protection. The first section highlights how unmanned aerial vehicles, autonomous underwater vehicles and autonomous on-water platforms have been used to enhance existing lagoon environment monitoring practices. The second section describes the implications of the use of such technology for survey design, their potential to provide continuous information in time and space and the need for tailored data processing methods. The last section identifies some of the advantages and limitations of these remote sensing monitoring methods within the context of environmental management and current practice.

## **2. Robots and autonomous systems**

### **2.1 Background**

In the last decade, the uptake of robotics and autonomous systems (RAS) for environmental monitoring has increased significantly. The low cost and availability of some of the technologies in the market have facilitated the integration of RAS solutions within the environmental sector. Perhaps the most significant uptake of RAS relates to unmanned aerial vehicles (UAVs) and autonomous underwater vehicles (AUVs). UAVs are small aircraft controlled remotely (i.e. with no human pilot on board). When equipped with specific sensors, they enable on-demand and generally high-resolution data collection. This overcomes some of the limitations of more traditional remote sensing methods such as satellites. Their capabilities also enable the collection of information under low cloud cover, thus increasing the operational window for environmental monitoring.

A wide range of sensors are currently available in the market for integration on existing off-the-shelf platforms (**Figure 2**). These sensors include multispectral, thermal, hyper-spectral and high-resolution red, green and blue (RGB) cameras and water quality probes. RGB cameras are the most accessible and therefore currently the most used sensor for environmental monitoring. However, recent advances in sensor miniaturization (e.g. [17]) facilitate the integration of combined sensors on a single platform, enabling RGB imagery to be coupled with other sources of information.

### **2.2 Unmanned aerial vehicles**

Within the context of lagoon characterization, UAVs have been used to assess the preferred locations and distribution at a fine scale of blacktip reef sharks and pink whiprays within a coral lagoon and reef systems off French Polynesia (Morea) [11]. This study focused on the assessment of the differences in species presence along reef habitats such as fringing, channels and sandflats. Density estimates of both species were estimated from the video footage recorded with a GoPro Hero 3+ Silver Edition camera fitted to a DJI Phantom II UAV quadcopter. The study highlighted the usefulness of UAVs to detect statistically significant differences in species densities across lagoon habitats [11].

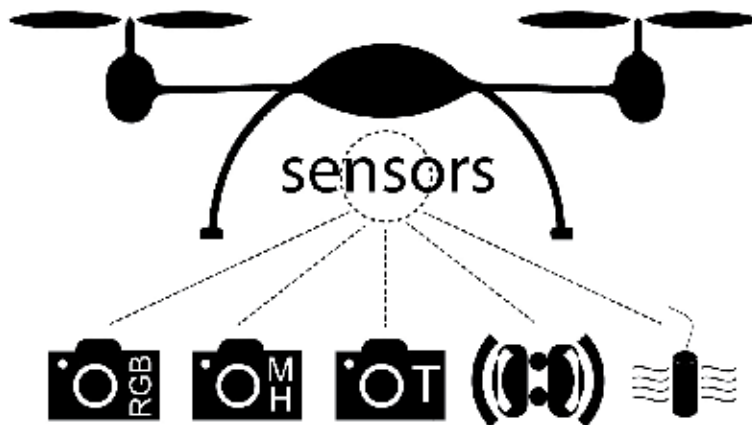


**Figure 2.** Schematic diagram showing an array of sensors that can be integrated to drone platforms [i.e. red, green and blue (RGB) camera, multispectral camera, thermal camera, hyper-spectral camera, laser scanner, conductivity-temperature-depth probe].

UAVs have also been used to make water surface elevation (i.e. orthometric water height above mean sea level) and bathymetry observations in lagoons of the Yucatan Peninsula (Mexico) [18]. In Ref. [18], the authors used a DJI hexacopter Spreading Wings S900 UAV equipped with an RGB high-resolution camera (Sony DSC-RX100) and lower-resolution fish-eye lens Eken H9 camera to characterize water surface elevation. The UAV was enabled to control a tethered sonar sensor (Deeper Smart Sonar PRO + Deeper, UAB, Vilnius, Lithuania) able to map the bathymetry of the lagoons. The information thus gathered enabled the estimation of water depth. The authors reported the technology to be accurate and fit for purpose, with errors less than 7 cm for water surface elevation estimation and less than 3.8% of the actual water depth. The study also highlighted the flexibility and low cost of the technology and its capacity to monitor remote areas that are difficult to access by human operators.

Lally et al. [19] reviewed the latest advances in UAV technology (platforms, payload and probe integration) for water sample capture and physico-chemical analysis. The potential of UAVs to gather water samples in lagoons is still unexplored. To date and to the authors' knowledge, only a few examples exist of this application of the technology [19] but none within lagoon environments. Multiple limitations still curtail the uptake of the technology and include water samples are too small to be representative, restrictive drone technology, low rate of sample collection and low reliability [19]. For the technology to be transferable and cost-effective for lagoon characterization, a range of enhancements are required such as increased payload capability, increased battery endurance, beyond visual line of sight operation and real-time physico-chemical measurement [19].

### 2.3 Autonomous underwater vehicles, ROVs and on-water platforms

It is evident that the use of the technology for water sample collection would be of benefit to managers and conservationists alike, especially within a regulatory context where water quality assessment of such ecosystems is required on a regular basis. In England, for example, there are 52 coastal saline lagoons defined in Special Protection Areas or Special Areas of Conservation, with an additional 28 lagoonal water bodies identified under the Water Framework Directive [6]. All these lagoons and lagoonal water bodies require monitoring, assessment and reporting of the

ecological quality. The use of autonomous or semi-autonomous UAVs to gather water samples could de-risk the overall activity, provide samples from inaccessible locations (increased representativeness) and increase the cost-effectiveness of the monitoring programme.

A faster route to achieve autonomous water sampling capability is the use of autonomous or semi-autonomous on-water platforms (**Figure 3**). Small boats with autonomous capability will overcome some of the limitations highlighted for UAV technology. In addition to water quality parameters, the capability of on-water platforms could be expanded to include factors such as water depth, bathymetry mapping, underwater habitat and emergent/submerged vegetation assessment. This would facilitate the temporal and spatial collocation of sampling for multiple variables. Recent studies have looked at their use within the context of freshwater ecosystem monitoring [20]. For example, Vandrol et al. [20] presented a structure-from-motion-based approach for the characterization of habitat and morphology in rivers for small boats capable of navigating autonomously along rivers. The methodology presented could also be transferred to lagoon environment characterization. Fornai [21] presented the small-size autonomous surface vessel (ASV) able to perform water column monitoring with a bespoke sampling probe (**Figure 3**). The autonomous solar-powered vessel “BUSCAMOS-RobObs” equipped with side scan sonar, sub-bottom sonar, laser systems, ultrasound sonar, depth metres, a multi-parametric probe and a GPS for collecting georeferenced oceanic data has been tested at the coastal lagoon system of Mar Menor (Spain) [22] (**Figure 3**). Low-budget and portable autonomous vessels have also been proved to be efficient with the collection of bathymetry and other variables in remote and dangerous coastal areas [23] (**Figure 3**).

Characterization of the euphotic and epipelagic zones can be achieved with both autonomous underwater vehicles (AUV) and remotely operated underwater vehicles (ROVs) (**Figure 4**). AUVs are robots able to travel underwater at different depths without the need of input from an operator. Remotely operated underwater vehicles (ROVs) are a variant of this type of robot. ROVs are directed by an operator via a remote control or an umbilical. Both AUVs and ROVs have been used for lagoon environment monitoring. For example, AUVs have been used in the Mar Menor (Murcia, Spain) coastal lagoon in different studies. The Mar Menor lagoon is separated from the Mediterranean Sea by a 20 km long dune cord that acts as a barrier to seawater ingress and ensures the protection of

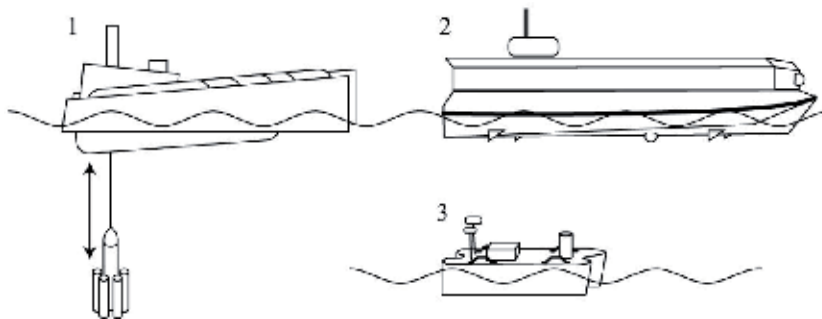


**Figure 3.** Schematic diagram showing multiple autonomous surface vessels (ASV) used in coastal areas and lagoon systems. (1) ASV equipped with a winch system for autonomous water column sampling [21]; (2) the solar-powered ASV equipped with a large range of sensors is able of self-mooring [22]; (3) the affordable and portable size ASV used in coastal surveys in Greenland [23].

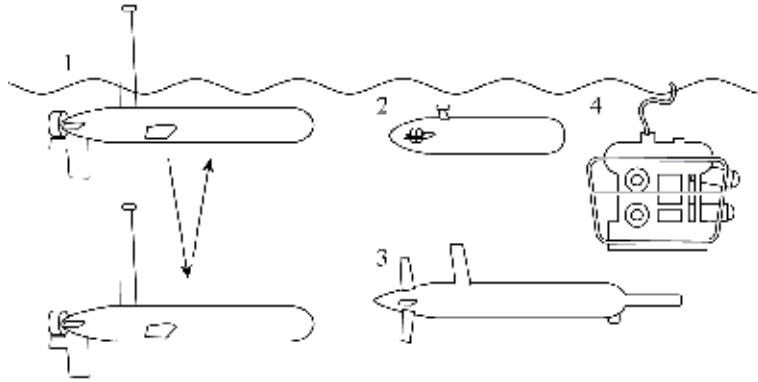


**Figure 4.** Schematic diagram showing multiple autonomous underwater vehicles (AUV) and a remotely operated vehicle (ROV). (1) Guanay II [27]; (2) SPARUS [28]; (3) Seacon [26]; (4) general remotely operated vehicle (ROV).

the characteristics of both environments. In [24], the AEGIR [25], Seacon [26], Guanay II [27] and SPARUS AUV [28] were deployed in the Mar Menor lagoon to better understand the ingress-egress of marine and freshwater into the environment. The multiple AUVs were equipped with probes to capture real-time measures of salinity. Similarly, in the Indian River Lagoon (Florida, USA) [29], AUVs have been used to collect spatially dense water quality data to study the spatial variability of conditions related to algal blooms. The Indian River Lagoon extends across three estuaries for over 160 miles. Phytoplankton blooms are frequent within the lagoon and are well known to have an ecological impact on the three estuaries. The AUV was used to measure water quality parameters that provide indicators of algal activity, temperature, conductivity, pH, dissolved oxygen, turbidity, total chlorophyll and phycocyanin fluorescence. In [30], the authors developed an AUV system able to track a leopard shark tagged with an acoustic Lotek MM Series transmitter along the SeaPlane Lagoon (Los Angeles, USA). The AUV was fitted with a stereo-hydrophone and receiver system able to detect acoustic signals. Further applications of AUVs exist in marine environments [31], many of which could be transferred to lagoon environments. Predicted improvements of the technology, such as enhanced hovering capability, long endurance and rapid response capabilities [31], will facilitate further monitoring applications in lagoon environments.

## 2.4 Concluding remarks

The use of RAS for lagoon environmental monitoring has proved to be successful for multiple variables. The cost-effectiveness of such methods is yet unknown and needs to be understood in relation to comprehensive and more integrative monitoring programmes. The capabilities provided by RAS could further benefit lagoon environment monitoring via the integration of different platforms—e.g. UAVs, AUVs, ROVs and bespoke sensors. The technology readiness level of such approaches is still constrained by a number of factors, such as the miniaturization of sensors, but initial conceptual models have already been tested [32, 33]. Successful design of integrated solutions will require a significant degree of collaboration between experts from different disciplines, including engineers, biologists, ecologists, environmental scientists, marine scientists, data analysts and software developers. Future developments and investment should focus on further

advancing the technology towards achieving an integrated system that enables the collection of collocated spatio-temporal information of all the parameters required for lagoon characterization (**Table 1**).

### 3. Implications for survey design

Standardization of monitoring protocols across lagoons, although a EU regulatory requirement [34], is challenging because of the complex and varied range of conditions encountered across such environments. Identification of the best location where specific samples of water quality, habitat or phytoplankton are to be taken is usually difficult to determine due to the spatio-temporal variability present within and between lagoon environments and a priori lack of knowledge of the conditions within the lagoon. Recent studies have looked at developing statistically robust sampling protocols to address this gap in knowledge. The use of robotics and autonomous systems introduces continuous monitoring capability. This makes survey design easier by prioritizing continuous data collection over point sampling. From a statistical perspective, such approaches to data collection enables the estimation of unbiased measures of dispersion and central tendency, with less intensive requirements on determining where point sample should be taken. This is of special relevance when trying to disentangle the effects that multiple factors (e.g. management practice) have on the quality of the lagoon.

Palma et al. [35] studied the effect of sampling design on coral reef characterization when collecting high-resolution (0.4 cm) RGB imagery with semi-autonomous water vehicles (**Figures 5 and 6**). The authors were interested in determining seascape metrics that would provide information about the configuration of coral reefs in Ponta do Ouro Partial Marine Reserve (Mozambique) and the morphology of the site (**Table 1**). A range of sampling scales (quadrats of size 0.5 m × 0.5 m, 2 m × 2 m, 5 m × 5 m, 7 m × 7 m) and densities (from 1 to 100 quadrats) were compared. Results showed that sampling scales equal to or coarser than 5 m × 5 m and sampling densities equal to or larger than 30 were most effective along the 1655 m<sup>2</sup> case study area. The study highlighted that special attention needs to be given to the design of coral reef monitoring programmes, with decisions being based on



**Figure 5.** The driver propulsion system (DPV), a remotely operated vehicle (ROV), equipped with a waterproof (wp) tablet and cameras. The tablet is used to coordinate data collection and steer vehicle direction.

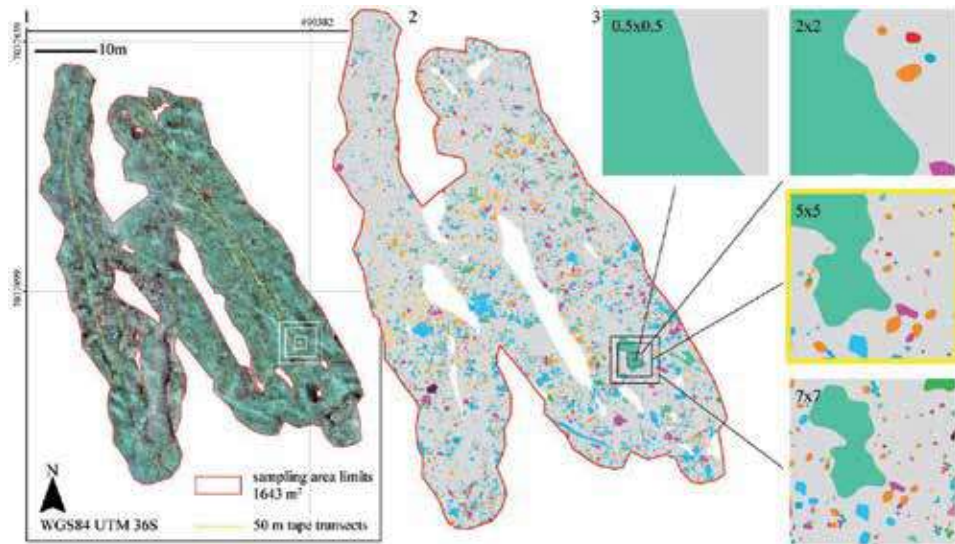


**Figure 6.** Coral reef area sampled at Ponta do Ouro partial Marine Reserve in Palma et al. [35]. The image shows the different sampling strategies compared in the study ( $0.5\text{ m} \times 0.5\text{ m}$ ,  $2\text{ m} \times 2\text{ m}$ ,  $5\text{ m} \times 5\text{ m}$  and  $7\text{ m} \times 7\text{ m}$ ). Each sampling strategy depicts a different spatial configuration of the number and coverage of species (colored polygons) present within the area.

the seascape metrics and statistics being determined. Although the Ponta do Ouro Partial Marine Reserve is not classed as lagoon, the results obtained are transferable to lagoon environments.

More recent studies, also transferable to lagoon environments, have looked at the combined use of structure-from-motion (SfM) approach and ROV to map coral reefs and reduce the need for destructive sampling. In particular, Palma et al. [36] developed a framework for wide-scale benthic monitoring which is transferable to lagoon environments. The authors estimated population structure, morphology and biomass automatically from imagery collected with a (i) a GoPro Hero4 Black Edition (Woodman Labs, Inc., San Mateo, CA, USA) recording maximal resolution still images ( $4000\text{ pixels} \times 3000\text{ pixels}$ ) and (ii) a Sony Alpha NEX7 Digital Camera (Sony Corporation, Minato, Tokyo, Japan) recording full high-definition ( $1920\text{ pixels} \times 1080\text{ pixels}$ ) videos mounted on a ROV—the driver propulsion system (DPV) (Figure 7). The point clouds generated with both cameras contained more than 6.5 million points. Both the point cloud and the high-resolution imagery collected enabled the estimation of coral morphometrics, such as height, width and planar surface of coral colonies. With the methodology proposed in [36], the error in coral height estimation was always  $<12.6\text{ cm}$ . For coral width estimation, the error was always  $<14.7\text{ cm}$ , whereas for the estimation of the planar surface, the error was  $533\text{ cm}^2$ . Palma et al. [36] were also able to develop the methodology further to estimate coral ash free dry weight (AFDW) from the imagery collected based on the planar surface estimated. AFDW is the biomass weight present within the coral after oxidation of the organic component occurs at high temperatures. Eq. (1) is specific for *Paramuricea clavata* [37]. The results provided information on the overall health of coralligenous habitats within the Marine Protected Area of Portofino (Punta del Faro, Italy). The technology enabled sampling of  $52\text{ m}^2$  within 6 minutes, with data analysis requiring under 10 hours of post-processing work:

$$AFDW = A \cdot 0.0047 \cdot 0.1515 \quad (1)$$

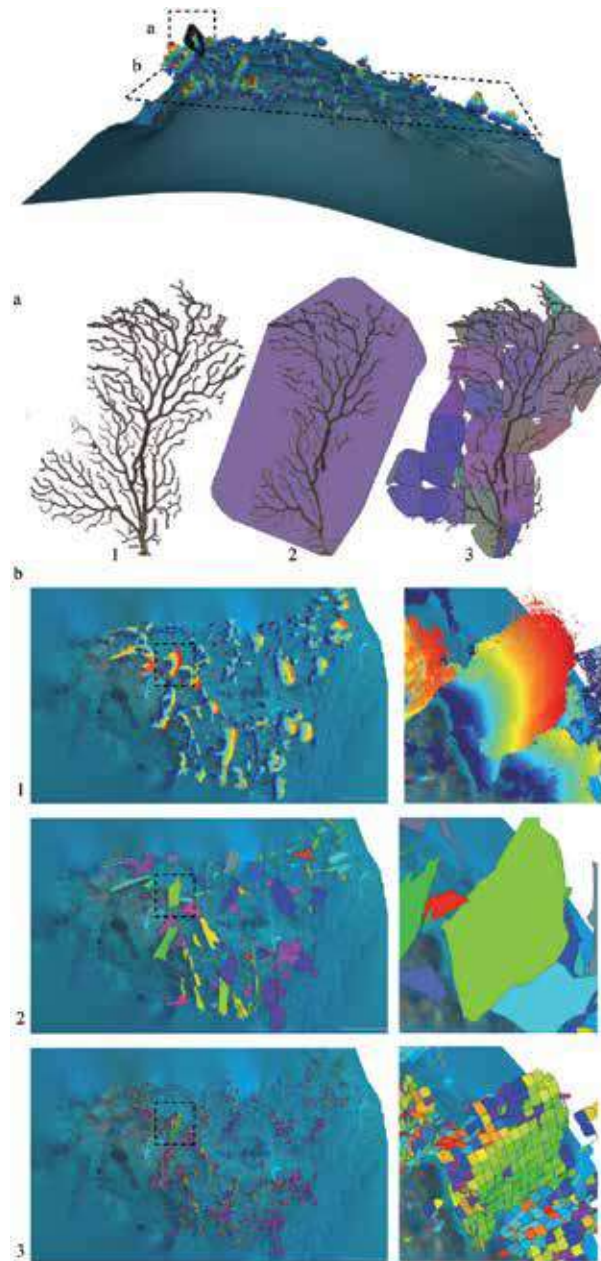


**Figure 7.** Image depicting the structure-from-motion methodology developed by Palma et al. [36] to sample corals without the need for destructive sampling. Overall view of the sampled area within the marine protected area of Portofino (Punta del Faro, Italy); (a) detailed view of a scanned coral branch and the automated estimation of its surface area; (b) sequence of images showing the implementation of the estimation of the surface area of corals on-site using SfM methods: (b1) point cloud generation, (b2) delineation of outmost boundary and (b3) estimation of the coral surface area via a small set of polygons.

Technological advances in RAS and data processing algorithms enable more comprehensive data sets to be produced that facilitate more informed management decisions. The increased quality and quantity of data collected provides a robust foundation for the use of more advanced statistical methods than the estimation of measures of central tendency and dispersion.

## 4. Management considerations

### 4.1 Key challenges

Remote sensing approaches including the use of satellites, UAVs, remote-controlled boats and underwater vehicles provide the potential for significant advances in the understanding of the environmental characteristics and functioning of lagoons. They can facilitate a better understanding of the temporal and spatial variation of environmental quality parameters, of habitat extent and condition, of risks, pressures and resultant responses and of the effectiveness of mitigation measures. They can contribute to coordinating and implementing nature-related policies [2], to the standardization of monitoring programmes ([34]) and to identifying environmental management priorities. They could also be used to better understand climate change impacts.

Recent studies [2] have highlighted the need to increase research and technology development (RTD) to enhance current lagoon management practices. For example, current understanding of the functioning and ecological quality of European lagoons is currently impaired by limited and incomplete data sets [2] such as lack of water quality measurements, gauging records, climate stations or water level stations. Further data weaknesses identified included insufficient water quality data in spatial and temporal dimensions for lagoon model calibration and validation. Based on a total of four case study areas, the work by Stålnacke et al. [2] concluded that effective lagoon management critically depends on high-quality data in geospatial format. Such data can be obtained with the remote sensing RAS solutions described in previous sections. However, there are several challenges to the deployment of remote sensing approaches and their widespread uptake by those responsible for the management and oversight of lagoons. Many of the techniques are still predominately the domain of the research community. There is as yet no purpose driven overarching monitoring and surveillance protocol for lagoons into which the use of remote sensing can be easily positioned. Thought has to be given to the use that will be made of the data that will be collected. For example, is it being collected because it is now possible to collect it or it will inform and improve the management of a lagoon.

Remote sensing approaches clearly have an important role to play in the baseline assessment of a lagoon enabling detailed characterizations of habitats, morphology and quality. They can then be used to determine how these parameters vary within and between years including the impact of climate change. In addition, they can enable a better assessment of the condition of a lagoon, the pressures, responses and effectiveness of interventions, than existing methodologies. Whether such detailed characterizations are needed for all lagoons will be for individual managers and organizations to determine.

There are few agreed protocols for the collection and interpretation of data using these techniques. This can limit their use in demonstrating compliance with legislative requirements. However, if remote sensing techniques do gain greater utilization in terms of routine monitoring including for legislative purposes, then this will significantly increase data transfer and storage capabilities and requirements. These monitoring approaches generate significant quantities of data that will have to be managed—the transfer and storage of this data could be a challenge. Agreed data collection and analysis protocols would facilitate the exchange of information and enable intercountry comparisons to be made.

These technologies produce information that has not routinely been available previously [31, 38], for example, spatial and temporal variations in a range of water

quality parameters obtained using on-water platforms with a variety of probes [39]. Such information will enable modeling outputs to be ground-truthed and better management decisions to be made. Although this information will enable a greater understanding of lagoons, it will require expenditure that previously was not required. Business cases will therefore need to be made to justify expenditure on initial characterization studies and then for routine surveillance. Such capital and revenue requirements could form a barrier to entry of these techniques into routine use. It may take a significant time before these techniques have widespread uptake by wildlife trusts, government agencies and regulatory bodies.

Some of the techniques will substantially reduce the cost of data collection and improve the health and safety of those collecting the information such as the use of small boat-mounted ACDP sensors to measure flow. However, for others it was not possible to collect the type of information that can now be gathered such as the spatial distribution of water quality parameters. To collect such information would therefore result in costs that were not previously incurred. Additional funding will therefore be necessary, and the case is made as to why such information is useful and justifies the level of expenditure proposed.

## **4.2 Technology acceptance**

Technological uptake and integration in standard monitoring programmes will depend upon the factors highlighted in previous sections as well as the cost-effectiveness of the technology and the acceptance of the results produced by government agencies.

There could be resistance to the use of such systems because of the associated cost or initial capital investment. In addition, some people will resist the introduction of new technologies. Innovation is not always welcomed. There can be a level of conservatism in people working in a science or technical area to new approaches. It is not the way that they were taught to do things, and efficiencies can lead to some people losing their jobs or having to do something else. For example, the use of UAVs may be constrained by concerns that the technology can be used to violate individuals' privacy, their link to war-fare and the risk of collision with aircraft [40, 41]. Technological advances occur very fast within the context of RAS. However, the rate-determining step in their uptake can be the associated business and governance processes.

Technology acceptance and adoption models could be used to determine the key factors that will drive the uptake of remote sensing RAS monitoring solutions [42]. These models consider internal antecedents of behaviour-like attitudes, values and intentions, norms, incentives and institutional constraints to provide an estimate of the likelihood of technology uptake. Further research is required to better understand how the uptake of RAS-based remote sensing technology for lagoon environment monitoring can be facilitated.

## **4.3 Concluding remarks**

Lagoons have been difficult environmental features to characterize and assess with the typically used monitoring approaches. They are extensive, and their characteristics vary spatially and temporally. Remote sensing approaches and RAS developments therefore provide new opportunities to better understand and assess lagoon environments. They also provide the means of better understanding what management approaches work in practice and assessing the effectiveness of interventions. They can also be used to inform the design of routine monitoring programmes.

However, there are real challenges in translating research and development and investigative approaches into repeatable and robust monitoring techniques that can be used on a routine and standardized basis for regulatory and compliance purposes. There will therefore need to be a concerted effort if the clear benefits that the developing remote sensing and RAS technologies provide are to be realized in the management of lagoon environments. The risk of not using such techniques and approaches is that the lagoon environments will continue to suffer environmental degradation.

## **Conflict of interest**

The authors declare no conflict of interest.

## **Author details**

Monica Rivas Casado<sup>1\*</sup>, Marco Palma<sup>2</sup> and Paul Leinster<sup>1</sup>

1 Cranfield University, Bedfordshire, UK

2 Università Politecnica delle Marche, Ancona, Italy

\*Address all correspondence to: [m.rivas-casado@cranfield.ac.uk](mailto:m.rivas-casado@cranfield.ac.uk)

## **IntechOpen**

---

© 2020 The Author(s). Licensee IntechOpen. This chapter is distributed under the terms of the Creative Commons Attribution License (<http://creativecommons.org/licenses/by/3.0>), which permits unrestricted use, distribution, and reproduction in any medium, provided the original work is properly cited. 

## References

- [1] European Commission. Directive 2000/60/EC of the European Parliament and of the Council of 23 October 2000 Establishing a Framework for Community Action in the Field of Water Policy. Vol. L327. Brussels; 2000. pp. 1-72
- [2] Stålnacke P, Lillebø AI, Gooch GD. Management of coastal lagoons-lessons learnt and recommendations. In: Lillebø AI, Stålnacke P, Gooch GD, editors. Coastal Lagoons in Europe: Integrated Water Resource Strategies. London: IWA Publishing; 2015. p. 222
- [3] Angus S. Monitoring and surveillance of a highly variable habitat: The challenge posed by Scottish saline lagoons. *Regional Studies in Marine Science*. 2016;8:20-26
- [4] Joint Nature Conservation Committee Common Standards Monitoring Guidance for Lagoons; 2004. Available from: <http://data.jncc.gov.uk/data/9b4bff32-b2b1-4059-aa00-bb57d747db23/CSM-Lagoons-2004.pdf>
- [5] Plana Q, Alferes J, Fuks K, Kraft T, Maruéjols T, Torfs E, et al. Towards a water quality database for raw and validated data with emphasis on structured metadata. *Water Quality Research Journal*. 2019;54:1-9
- [6] Bamber RN. Coastal Saline Lagoons and the Water Framework Directive - NECR039. Peterborough, UK: Natural England; 2010
- [7] Erena M, Domínguez JA, Aguado F, Soria J, García-Galiano S. Monitoring coastal lagoon water quality through remote sensing: The mar Menor as a case study. *Water*. 2019;11:1468
- [8] López García MJ, Caselles V. A multi-temporal study of chlorophyll-a concentration in the albufera lagoon of Valencia, Spain, using thematic mapper data. *International Journal of Remote Sensing*. 1990;11:301-311
- [9] Blondeau-Patissier D, Gower JFR, Dekker AG, Phinn SR, Brando VE. A review of ocean color remote sensing methods and statistical techniques for the detection, mapping and analysis of phytoplankton blooms in coastal and open oceans. *Progress in Oceanography*. 2014;123:123-144
- [10] Willets D. The Eight Great Technologies. London: Policy Exchange; 2013. Available from: <https://policyexchange.org.uk/wp-content/uploads/2016/09/eight-great-technologies.pdf>
- [11] Kiszka J, Mourier J, Gastrich K, Heithaus M. Using unmanned aerial vehicles (UAVs) to investigate shark and ray densities in a shallow coral lagoon. *Marine Ecology Progress Series*. 2016;560:237-242
- [12] Rathi D, Jain S, Indu DS. Underwater fish species classification using convolutional neural network and deep learning. Ninth International Conference on Advances in Pattern Recognition (ICAPR). 2017. Available from: [https://www.researchgate.net/publication/330026877\\_Underwater\\_Fish\\_Species\\_Classification\\_using\\_Convolutional\\_Neural\\_Network\\_and\\_Deep\\_Learning](https://www.researchgate.net/publication/330026877_Underwater_Fish_Species_Classification_using_Convolutional_Neural_Network_and_Deep_Learning)
- [13] Béjaoui B, Ottaviani E, Barelli E, Ziadi B, Dhib A, Lavoie M, et al. Machine learning predictions of trophic status indicators and plankton dynamic in coastal lagoons. *Ecological Indicators*. 2018;95:765-774
- [14] Kennish MJ, Paerl HW. Coastal Lagoons: Critical Habitats of Environmental Change. Boca Raton, Florida: CRC Press; 2010. Available from: <https://www.crcpress.com/Coastal-Lagoons-Critical-Habitats->

of-Environmental-Change/Kennish-Paerl/p/book/9781138111844#googlePreviewContainer

[15] Padedda BM, Pulina S, Magni P, Sechi N, Lugliè A. Phytoplankton dynamics in relation to environmental changes in a phytoplankton-dominated Mediterranean lagoon (Cabras lagoon, Italy). *Advances in Oceanography and Limnology*. 2012;**3**:147

[16] Duffy W, Belknap DF, Kelley JT. Morphology and stratigraphy of small barrier-lagoon systems in Maine. *Marine Geology*. 1989;**88**:243-262

[17] Lin Y, Hyyppä J, Jaakkola A. Mini-UAV-borne LIDAR for fine-scale mapping. *IEEE Geoscience and Remote Sensing Letters*. 2011;**8**:426-430

[18] Bandini F, Lopez-Tamayo A, Merediz-Alonso G, Olesen D, Jakobsen J, Wang S, et al. Unmanned aerial vehicle observations of water surface elevation and bathymetry in the cenotes and lagoons of the Yucatan peninsula, Mexico. *Hydrogeology Journal*. 2018;**26**:2213-2228

[19] Lally HT, O'Connor I, Jensen OP, Graham CT. Can drones be used to conduct water sampling in aquatic environments? A review. *Science of the Total Environment*. 2019;**670**:569-575

[20] Vandrol J, Rivas Casado M, Blackburn K, Waive T, Leinster P, Wright R, et al. In-Channel 3D models of riverine environments for Hydromorphological characterization. *Remote Sensing*. 2018;**10**:1005

[21] Fornai F, Ferri G, Manzi A, Ciuchi F, Bartaloni F, Laschi C. An autonomous water monitoring and sampling system for small-sized ASVs. *IEEE Journal of Oceanic Engineering*. 2016;**42**:1-8

[22] González-Reolid I, Molina-Molina J, Guerrero-González A, Ortiz F, Alonso D. An autonomous

solar-powered marine robotic Observatory for Permanent Monitoring of large areas of shallow water. *Sensors*. 2018;**18**:3497

[23] Carlson DF, Fürsterling A, Vesterled L, Skovby M, Pedersen SS, Melvad C, et al. An affordable and portable autonomous surface vehicle with obstacle avoidance for coastal ocean monitoring. *HardwareX*. 2019;**5**:e00059

[24] González J, Masmitjà I, Gomáriz S, Molino E, del Río J, Mánuel A, et al. AUV based multi-vehicle collaboration: Salinity studies in mar Menor coastal lagoon. *IFAC Proceedings*. 2012;**45**:287-292

[25] García-Córdova F, Guerrero-González A. Intelligent navigation for a solar powered unmanned underwater vehicle. *International Journal of Advanced Robotic Systems*. 2013;**10**:185

[26] Sousa J, Carvalho C. The SeaCon AUV system: Technology evaluation, training and development of concepts of operation for the Portuguese navy. In: *Proc. Maritime Systems and Technology Conference*. Stockholm: Suecia; 2009

[27] Gomáriz S, Masmitjà I, González J, Masmitjà G, Prat J. GUANAY-II: An autonomous underwater vehicle for vertical/horizontal sampling. *Journal of Marine Science and Technology*. 2015;**20**:81-93

[28] Mallios A, Ridao P, Carreras M, Hernandez E. Navigating and mapping with the SPARUS AUV in a natural and unstructured underwater environment. In: *OCEANS'11 MTS/IEEE KONA*. Waikoloa, HI, USA: IEEE; 2011. pp. 1-7. Available from: <https://ieeexplore.ieee.org/document/6107105>

[29] US Department of the Interior Autonomous Underwater Vehicle Water-Quality Surveys for Indian River Lagoon, near Titusville, Florida, August 2016–November 2017- Data.

- gov. Available from: <https://catalog.data.gov/dataset/autonomous-underwater-vehicle-water-quality-surveys-for-indian-river-lagoon-near-titusvill-2017> [Accessed: 07 July 2019]
- [30] Clark CM, Forney C, Manii E, Shinzaki D, Gage C, Farris M, et al. Tracking and following a tagged leopard shark with an autonomous underwater vehicle. *Journal of Field Robotics*. 2013;**30**:309-322
- [31] Wynn RB, Huvenne VAI, Le Bas TP, Murton BJ, Connelly DP, Bett BJ, et al. Autonomous underwater vehicles (AUVs): Their past, present and future contributions to the advancement of marine geoscience. *Marine Geology*. 2014;**352**:451-468
- [32] Combined USV and AUV System Maps Ocean Floor|Unmanned Systems Technology. Available from: <https://www.unmannedsystemstechnology.com/2018/01/combined-usv-auv-system-maps-ocean-floor/> [Accessed: 07 July 2019]
- [33] Zolich, A. Systems Integration and Communication in Autonomous Unmanned Vehicles in Marine Environments. Doctoral theses at Norges teknisk-naturvitenskapelige universitet. 2018. Available from: <https://ntnuopen.ntnu.no/ntnu-xmlui/handle/11250/2584513>
- [34] Poikane S, Zampoukas N, Borja A, Davies SP, van de Bund W, Birk S. Intercalibration of aquatic ecological assessment methods in the European Union: Lessons learned and way forward. *Environmental Science & Policy*. 2014;**44**:237-246
- [35] Palma M, Rivas Casado M, Pantaleo U, Cerrano C, Palma M, Rivas Casado M, et al. High resolution Orthomosaics of African coral reefs: A tool for wide-scale benthic monitoring. *Remote Sensing*. 2017;**9**:705
- [36] Palma M, Casado M, Pantaleo U, Pavoni G, Pica D, Cerrano C, et al. SfM-based method to assess gorgonian forests (*Paramuricea clavata* (Cnidaria, Octocorallia)). *Remote Sensing*. 2018;**10**:1154
- [37] Mistri M, Ceccherelli VU. Growth and secondary production of the Mediterranean gorgonian *Paramuricea clavata*. *Marine Ecology Progress Series*. 1994;**103**:291-296
- [38] Underwater Vehicles - an overview|ScienceDirect Topics. Available from: <https://www.sciencedirect.com/topics/agricultural-and-biological-sciences/underwater-vehicles> [Accessed: 20 October 2019]
- [39] An Autonomous Surface Vehicle for water quality monitoring|Request PDF. Available from: [https://www.researchgate.net/publication/46574629\\_An\\_Autonomous\\_Surface\\_Vehicle\\_for\\_water\\_quality\\_monitoring](https://www.researchgate.net/publication/46574629_An_Autonomous_Surface_Vehicle_for_water_quality_monitoring) [Accessed: 20 October 2019]
- [40] Lidynia C, Philipsen R, Ziefle M. Droning on about drones—Acceptance of and perceived barriers to drones in civil usage contexts. In: *Advances in Intelligent Systems and Computing*. Vol. 499. Switzerland: Springer Verlag; 2017. pp. 317-329. Available from: <https://link.springer.com/book/10.1007/978-3-319-41959-6#>
- [41] Clothier RA, Greer DA, Greer DG, Mehta AM. Risk perception and the public acceptance of drones. *Risk Analysis*. 2015;**35**:1167-1183
- [42] Taherdoost H. A review of technology acceptance and adoption models and theories. In: *Procedia Manufacturing*. Vol. 22. Tirgu, Mures, Romania: Elsevier BV; 2018. pp. 960-967. Available from: <https://www.sciencedirect.com/science/article/pii/S2351978918304335>

# Process-Based Statistical Models Predict Dynamic Estuarine Salinity

*Christina L. Durham, David B. Eggleston and Amy J. Nail*

## Abstract

Climate change is increasing variation in freshwater input and the intensity of this variation in estuarine systems throughout the world. Estuarine salinity responds to dynamic meteorological and hydrological processes with important consequences to physical features, such as vertical stratification, as well as living resources, such as the distribution, abundance and diversity of species. We developed and evaluated two space-time statistical models to predict bottom salinity in Pamlico Sound, NC: (i) *process* and (ii) *time* models. Both models used 20-years of observed salinity and contained a deterministic component designed to represent four key processes that affect salinity: (1) recent and long-term fresh water influx (FWI) from four rivers, (2) mixing with the ocean through inlets, (3) hurricane incidence, and (4) interactions among these variables. Freshwater discharge and distance from an inlet to the Atlantic Ocean explained the most variance in dynamic salinity. The final *process* model explained 89% of spatiotemporal variability in salinity in a withheld dataset, whereas the final *time* model explained 87% of the variability within the same withheld data set. This study provides a methodological template for modeling salinity and other normally-distributed abiotic variables in this lagoonal estuary.

**Keywords:** estuaries, space-time model, spatial covariance, freshwater inflow, process-based model, salinity

## 1. Introduction

Estuarine salinity responds to dynamic meteorological and hydrological processes [1] with important consequences to physical features, such as vertical stratification, as well as living resources, such as the distribution, abundance and diversity of species [2–5]. For example, relatively low mixing and subsequent salinity stratification can lead to hypoxia in areas where organically-rich sediments are not adequately re-oxygenated, causing emigration of mobile fauna and degradation of ecosystem functions [5–9]. Rapid salinity changes, such as those associated with large rainfall events or tropical cyclones, can cause death of postlarval stages that are sensitive to unusually low salinities [10], and mass seaward migration and subsequent hyper-aggregation of mobile, commercially important species that can result in (1) shifts of juveniles from primary nursery areas protected from trawling to secondary non-nursery areas vulnerable to fishing pressure [11], (2) overharvest of adults due to increases in fishery catchability [12],

or (3) bias fishery-independent surveys that leads to over-inflated population abundance estimates [12]. Thus, the need to accurately predict the spatiotemporal dynamics of salinity is unprecedented. The specific goals of this study were to: (1) evaluate several statistical models to hindcast and forecast salinity in the second largest estuary and largest lagoonal estuary in the United States—Pamlico Sound, North Carolina, USA, and (2) assess salinity observations, predictions, and standard errors under five hydrologic scenarios characteristic of historic and future climate changes.

Pamlico Sound (PS) is a relatively shallow estuary with a mean depth of 4 m and a maximum depth of 7 m. PS circulation is dominated by wind-driven currents and freshwater input [13, 14]. Seasonal cyclonic storms are also an important climatological component of the PS system. Since 1996, over three tropical storms or hurricanes have passed within 300 km of the North Carolina coast per year [10]. Given the important role that salinity plays in the abiotic and biotic system components of estuaries, and the likelihood that global climate change will increase the frequency of extreme weather events (e.g., floods, droughts, hurricanes—[9, 15, 16]), there is a critical need for models that can accurately forecast spatiotemporal variation in salinity (e.g., [17]). A recent review by Iglesias et al. [17] highlights the strengths of applying numerical modeling tools to characterize morpho-hydrodynamic processes in estuarine and coastal systems. *Numerical methods* can include a large variety of models and techniques, such as finite element, finite difference, finite volume, or Eulerian-Lagrangian models (e.g., [17–19]). Complex, three-dimensional numerical models used for simulation and forecasting of dynamic estuarine salinity can require significant effort and computation time that is beyond the capabilities of many local management agencies. Local management agencies sometimes require a quick turnaround time for long-term simulations or short-term forecasts of estuarine salinity conditions, which could be produced using location-specific statistical models. Therefore, the goals of this study were to (1) develop and evaluate two types of *statistical models* of bottom salinity in PS, and (2) apply the best models to produce sound-wide retrospective maps of bottom salinity based on observational data. Bottom (as opposed to surface) salinity was chosen as the variable of interest because it characterizes habitats of mobile demersal species that are important members of benthic food webs, and that are the targets of valuable commercial and recreational fisheries. Hereafter, the term ‘salinity’ will always refer to bottom salinity unless otherwise noted.

### 1.1 Statistical models to predict dynamic salinity

Producing retrospective salinity maps based on observational data does not require a statistical model based on hydrological mechanisms that affect salinity; it is possible to perform individual spatial interpolations for each time period of interest using an ordinary kriging model or a universal kriging model with a simple spatial trend. Predicting salinity under a hypothetical set of conditions, however, does require a model that can ‘learn’ about hydrological mechanisms based on retrospective data (e.g., [20, 21]). Thus, the more comprehensive goal of this study was to produce retrospective maps of salinity by developing a space-time statistical model in which the mean function represents the hydrological mechanisms that affect salinity, and a spatial covariance function makes up the difference between the observed salinity data and the mean function’s salinity prediction.

To create such a model, we constructed explanatory variables that accounted for the effect of riverine freshwater inflow (FWI), distance to inlet sources of oceanic saltwater, and hurricane incidence on salinities at different locations in PS. We used

a forward-selection process to choose which of these variables to keep in the model. Standard errors based on the covariance function allowed for assessment of strengths and weaknesses of the representation of the hydrology in the mean function. Since an additional goal of this study was to provide a template for researchers to build process-based models of normally-distributed estuarine variables, we considered only models that could be fit using procedures in the SAS<sup>®</sup> software package, yet can be adopted to R-statistical software.

Other process-based models of PS salinity in the literature—all of which are differential-equation-based deterministic models—provided important insights into how different variables influenced spatiotemporal salinity variation in PS ([22, 23], and others). However, these models ultimately lacked the spatial resolution and/or coverage of the entire area of interest of this study, and none quantified uncertainty at every space-time prediction location. For example, Xu et al. [24] predicted surface and bottom salinity, and temperature at 30-second intervals over a spatial grid with varying cell size (200–800 m<sup>2</sup>) in the Pamlico River Estuary (PRE), a PS tributary, using a customized extension of the Environmental Fluid Dynamics Code [25] to incorporate FWI from major tributary rivers, as well as tide and wind effects on circulation. Although this model incorporated environmental variation and produced salinity predictions suitable to assess long-term space-time trends, the PRE makes up only 18% of the area of PS. Predicting salinity across the entire PS using this model would require spatial domain expansion and re-parameterization, and such extensions are not planned (J. Lin, NC State University, pers. comm. on behalf of Xu et al. [24]).

Though we are unaware of researchers that have constructed space-time statistical models of salinity in PS, there are examples of applying statistical models for spatial prediction of salinity in other estuaries. For example, Rathbun [26] used independent multiple linear regression models with spatially-correlated errors to predict salinity and dissolved oxygen (DO) in Charleston Harbor, SC over a two-week time period in 1988 as a function of spatial coordinates and distance to the estuary mouth. Chehata et al. [27] performed three-dimensional spatial interpolation of salinity and DO measurements in Chesapeake Bay. Qiu and Wan [20] developed a salinity model based on time series analyses of salinity data for the Caloosahatchee River Estuary, Florida, USA. The structure of their model consisted of an autoregressive term representing the system persistence and an exogenous term accounting for physical drivers including freshwater inflow, rainfall, and tidal water surface elevation that cause salinity to vary. The model was calibrated and validated using up to 20 years of measured data collected they found that the time series model offers comparable or superior performance compared with its 3-D, numerical counterpart. This model has been used as a tool for water resources management projects relating to ecosystem restoration and water control in south Florida [20]. Similarly, Ross et al. [21] examined the response of salinity in the Delaware Estuary, USA to climatic variations using statistical models and long-term (1950-present) records of salinity from the U.S. Geological Survey and the Haskin Shellfish Research Laboratory. The statistical models included non-parametric terms and were robust against auto-correlated and heteroscedastic errors. After using the models to adjust for the influence of streamflow and seasonal effects on salinity, several locations in the estuary showed significant upward trends in salinity. Insignificant trends are found at locations that are normally upstream of the salt front. The models indicate a positive correlation between rising sea levels and increasing residual salinity, with salinity rising from 2.5 to 4.4 psu per meter of sea-level rise. The results suggest that continued sea-level rise in the future will cause salinity to increase regardless of any variation in fresh water influx [21]. Urquhart

et al. [28] present the results of multiple statistical models that predicted daily, gridded surface salinity at 1 km resolution across Chesapeake Bay, USA as a function of surface reflectance estimates of salinity from the NASA Moderate Resolution Imaging Spectroradiometer (MODIS), onboard the Aqua platform satellite. Eight statistical methods were tested, and sea surface salinity was accurately predicted via remote sensed products with an accuracy that was more than sufficient for many physical and ecological applications [28].

None of these previous studies, however, attempted to explicitly represent the hydrological processes by which fresh and saltwater mixing affects estuarine salinity. In this paper, we describe the development of candidate explanatory variables to represent mechanisms affecting PS salinity and how that development led to consideration of two fundamentally different mean functions. We then describe the forward selection process by which candidate variables were chosen to be retained in the models, and how candidate covariance functions were selected to pair with each mean function. Next, we examined maps of salinity observations, predictions, and standard errors under five hydrologic scenarios, analyzed these results, and provided overall implications of the findings.

## 2. Methods and results

### 2.1 Data and notation

We used bottom salinity values measured by the North Carolina Division of Marine Fisheries (NC DMF) Pamlico Sound Trawl Survey Program 195 (*the survey*) every June and September from 1987 to 2006. The survey is conducted only in June and September each year. Designed to assess species abundance at depths over 2 m, the survey uses a weighted stratified random sampling design. For each time period, coordinates of stations are randomly generated within each of seven water body strata, with more stations allocated to larger strata, for a total of 54 stations per time period. Hereafter, we denote with  $S$  the spatial domain that includes all points sampled within the seven strata mentioned over the entire 1987–2006 temporal domain. **Figure 1** shows the geographic location of each sampling station in  $S$ . Salinity was measured using a YSI-85 multi-function meter at the beginning of each trawl and recorded along with depth and spatial reference coordinates. All spatial coordinates used in this analysis were converted from decimal degrees to northings and eastings in nautical miles (nmi) from a reference point (the origin in **Figure 1**) located southwest of  $S$  at  $34.6^\circ\text{N}$ ,  $-77.1^\circ\text{W}$ . Salinity is always reported using the Practical Salinity Scale.

The temporal domain contains  $T = 40$  time periods, or month/year combinations, indexed by the subscript  $t$ , so that  $t = 1, \dots, T$ . A time period is approximately 2.5 weeks long, the time it takes to sample all stations. Since locations of the 54 stations sampled in each time period differed slightly, and since some data were missing in each time period, let  $n_t$  represent the number of sites in time period  $t$ . Site refers to a specific spatial location nested within a particular time period and is indexed using the subscript  $i$  where  $i = 1, \dots, n_t$ . The dataset included  $N = 2100$  total observations of salinity, where  $N = \sum_{t=1}^T n_t$ . Denoted with  $sal_{it}$  observed salinity at site  $i$  in time period  $t$ .

The fresh water influx (FWI) data represented watersheds of the Neuse, Pamlico, Roanoke, and Chowan rivers, which comprise 80% of the land draining into PS [29]. FWI observations were average daily river discharge rates collected by one

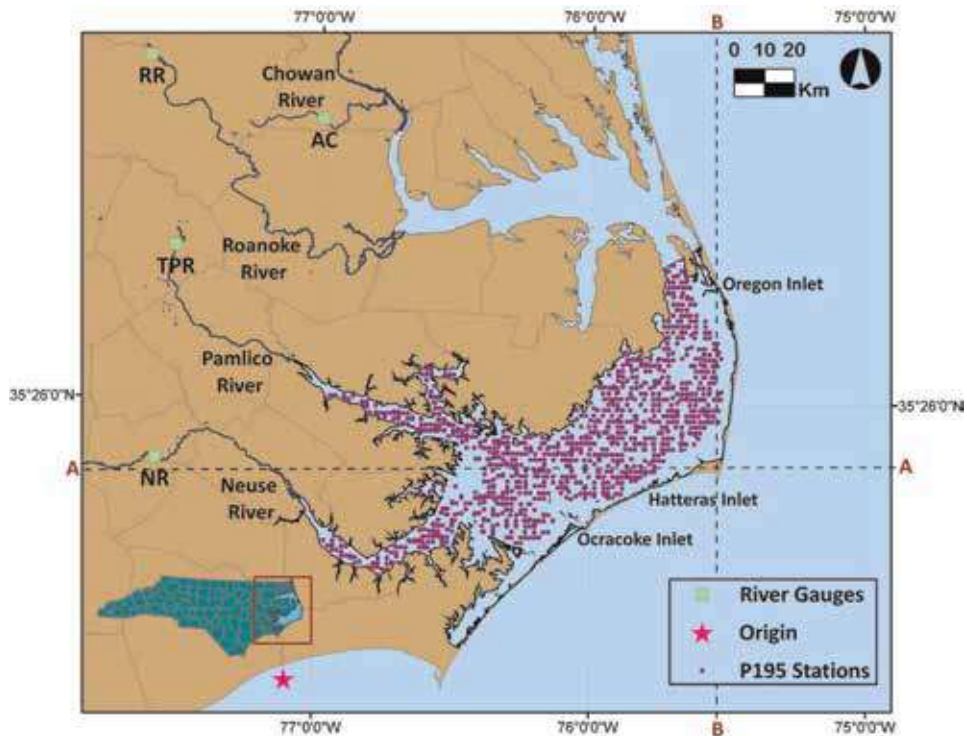


**Figure 1.** Pamlico Sound, NC and the Chowan, Roanoke, Pamlico, and Neuse Rivers. Green squares show the four river gauge stations used in this study. Purple dots indicate all P195 trawl survey sample stations for the 1987–2006 time domain. The pink star indicates the reference point from which northings and eastings were calculated. As referenced in Section 3.5, Parallel A is located at 35° 16' N latitude and meridian B is at 75° 42' W longitude.

US Geological Survey (USGS) gauge station per tributary (**Figure 1**): Neuse River (NR) station 02089500 in Kinston; Tar-Pamlico River (TPR) station 02083500 in Tarboro; Roanoke River (RR) station 02080500 in Roanoke Rapids; and Ahoskie Creek (AC) station 02053500 in Ahoskie, which gauges Chowan River inflow. Discharge rates in  $\text{ft}^3/\text{s}$  for every day during the time domain (7305 days) were downloaded from the USGS Water Resources website for the state of North Carolina (USGS 2009) and were converted to  $\text{m}^3/\text{s}$ . For each river, the gauge chosen was the furthest downstream gauge that recorded data over the entire temporal domain.

## 2.2 Candidate explanatory variables

The creation of explanatory variables reflects the modeling context—the objectives, the geographical features of the spatial domain, and the space-time coverage and resolution of the data—but the general thought process can be modified by other researchers in a different context. We index the term *it* as any variable that varies in both space and time, and with *t* any variable that varies over time but is constant over *S* within a time period.

## 2.3 Freshwater influx indices

Sixty-one days is the average freshwater residence time of the four major rivers flowing into PS [30–32], accounting for the temporal lag between the upriver

gauging of freshwater and the delivery of that water to  $S$ . Therefore, we defined the long-term metric  $2moFWI_{r_t}$  for river  $r$  and time period  $t$  where  $r = 1, \dots, 4$ , and  $t = 1, \dots, T = 40$  as the average daily discharge rate in the 61 days prior to  $m_t$ , the first day of the survey in time period  $t$ . Because Ramus et al. [33] calculated a seven-day residence time for the Neuse and Pamlico Rivers after Hurricanes Dennis and Floyd deposited 1 m of rainfall in eastern NC less than 2 weeks before the September 1999 survey, we defined the short-term metric  $1wkFWI_{r_t}$ , by averaging daily discharge rates in the 7 days prior to  $m_t$ .

Since freshwater from river  $r$  in time period  $t$  should have more of an effect on  $sal_{it}$  the closer site  $i$  is to the river, a unique measure of the influence of  $1wkFWI_{r_t}$  and  $2moFWI_{r_t}$  for each site was formed by dividing each by  $dist_{r_{it}}$ ,  $r = 1, \dots, 4$ , the distance separating the gauge on river  $r$  from site  $i$  within time period  $t$ :

$$1wkFWII_{r_{it}} = \frac{1wkFWI_{r_t}}{dist_{r_{it}}}, \text{ and } 2moFWII_{r_{it}} = \frac{2moFWI_{r_t}}{dist_{r_{it}}} \quad (1)$$

The coordinates of each gauge station were used to calculate distance because the gauge was the location of the  $1wkFWI_{r_t}$  and  $2moFWI_{r_t}$  observations. Like all distances in this study,  $dist_{r_{it}}$  represents distance “as the crow flies” as opposed to water-path distance. Though the superiority of using water-path distance when modeling water-quality variables in stream and estuarine systems seems intuitive, results from studies that compare these two distance metrics are inconclusive. For example, Gardner et al. [34] found more accurate predictions of stream temperatures when models incorporated water-path distance, but only when this distance was modified and weighted by stream order. Peterson and Urquhart [35] predicted various nutrient concentrations in 17 Maryland rivers and concluded that using water-path distance works well when modeling certain nutrients, but not others, and that the crow-flies distance appeared to be the most suitable distance measure overall. Comparing the accuracy of predictions of water quality parameters generated from two different multiple linear regression models containing the explanatory variable “distance to inlet mouth”, Little et al. [36] found that predictions from models using water-path distance were no more accurate than those from models using crow-flies distance. None of these studies demonstrated marked predictive improvement using water-path distance, therefore we used crow-flies distance from each of the four river gauges to each of 2100 sample stations and over 6000 prediction locations.

The plot in **Figure 2** of  $sal_{it}$  against Roanoke River  $2moFWII_{r_{it}}$  typifies the relationships between salinity and each of the eight  $1wkFWII_{r_{it}}$  and  $2moFWII_{r_{it}}$  variables. Larger values of the metric are associated with smaller values of salinity, but groups of observations have different slopes. Closer examination revealed that the different groups corresponded to different time periods. We attempted to account for the different slopes in two ways, first by considering the 28 pair-wise interactions among the  $1wkFWII_{r_{it}}$  and  $2moFWII_{r_{it}}$  and second by considering 39 time-period indicator variables defined as

$$timeper_{1t} = \begin{cases} 1 & \text{if } t = 1 \\ 0 & \text{otherwise} \end{cases}, \dots, timeper_{\tau t} = \begin{cases} 1 & \text{if } t = \tau \\ 0 & \text{otherwise} \end{cases}, \dots, timeper_{39t} \\ = \begin{cases} 1 & \text{if } t = 39 \\ 0 & \text{otherwise} \end{cases}$$

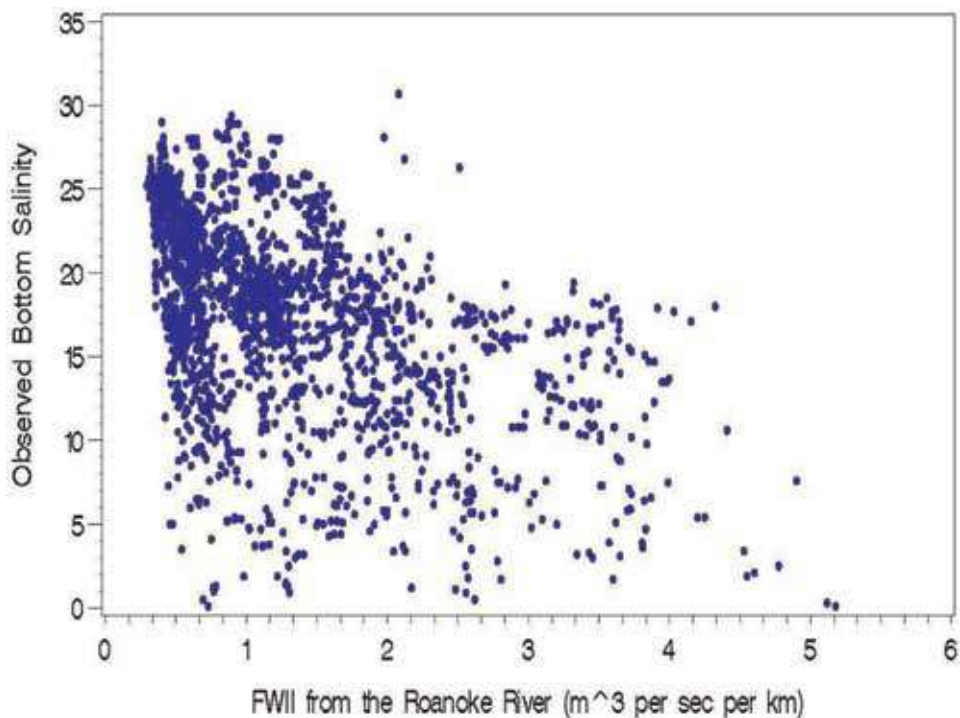


**Figure 2.** Observed bottom salinity (psu) vs. the Roanoke River two-month relative freshwater influx index ( $2moFWII_{rit}$ ) in  $m^3 s^{-1} km^{-1}$  from 1987 to 2006. Groups of values within the same time period exhibit relationships with different slopes.

(A fortieth indicator variable was not used because it would create a non-full-rank design matrix, and the effect for the fortieth time period can be derived using the intercept.) This latter consideration led to the creation of two distinct mean function models: the *process* and *time* models. The first has process variables only, and the second has process variables in addition to the time-period indicator variables to address the possibility that salinity is affected by some aspect of physical phenomena that is not accounted for by any other variable in the model.

## 2.4 Saltwater mixing and tidal signal

Although salinity on the inner-continental shelf of the U.S. Southeast Atlantic coast exhibits some spatial variability near PS [37], we follow Xie et al. [38] and assume constant open ocean salinity. This assumption allows for modeling the effect of ocean water mixing as a function of only the distance to inlet, as opposed to distance interacting with the salinity of the ocean water, from each spatial location in the sound to each of the major PS inlets: Oregon, Hatteras, and Ocracoke. Exploratory analyses reveal that models using a single variable (distance to the nearest inlet) rather than three variables (distances to each of the three inlets), explains the same amount of variability in salinity when other explanatory variables are also included. Therefore, we consider for inclusion in subsequent models the variable *closest\_inlet\_dist<sub>it</sub>*, defined to be the distance separating site *i*, sampled in time period *t*, from the center of the most proximate inlet.

## 2.5 Wind speed and direction

A prevailing wind field that is north/northeast from March to August and south/southwest from September to February is the primary driver of currents in PS [39]. Thus, wind speed and direction were incorporated into the modeling process using the categorical variable  $month_t$ , where

$$month_t = \begin{cases} 1 & \text{if } t \text{ is in Sept} \\ 0 & \text{if } t \text{ is in June} \end{cases}$$

is used to examine the effects of seasonal wind patterns on the spatial distribution of salinity.

## 2.6 Evaporation and direct precipitation

Holding other factors constant, sound-wide salinity in time periods that experience more evaporation of water from the surface of PS would likely be higher than those in time periods that experienced less evaporation, but no evaporation data were available for the space-time domain of interest. Salinity in time periods for which there was more direct precipitation into  $S$  should be lower than those in lower-precipitation time periods, however precipitation data were only available at two weather stations on the edges of PS from which information about individual spatial locations within PS would be difficult to infer. Giese et al. [40] found that direct precipitation constitutes only 8% of mean PS freshwater input, thus the signal from riverine FWI should dominate in explaining salinity variability. Therefore, we did not include evaporation or direct precipitation variables in our models.

## 2.7 Spatial coordinates

Estuarine salinity varies over space such that functions of spatial coordinates might explain variability in salinity not accounted for by the other variables. Scatterplots of salinity versus easting and northing suggested that salinity is quadratic in the former and cubic in the latter. The quadratic function of easting can be explained by examining a west-to-east path through PS along the 35° 16' N parallel (A in **Figure 1**): salinity should initially increase, reach a maximum at the saltwater plume near Ocracoke and Hatteras Inlets, and decrease again on the other side of the plume in the waters on the western shore of Hatteras Island near Buxton, NC. The cubic function of northing is best described by examining a north-to-south path along longitude of 75° 42' W (B in **Figure 1**), where salinity should increase traveling south from Albemarle Sound, reach a local maximum near Oregon Inlet, decrease continuing past the saltwater inlet plume, and increase again as the Hatteras Inlet saltwater plume is reached. Thus,  $easting_{it}$ ,  $easting_{it}^2$ ,  $northing_{it}$ ,  $northing_{it}^2$ , and the interactions  $northing_{it} * easting_{it}$ ,  $northing_{it}^2 * easting_{it}$ ,  $northing_{it} * easting_{it}^2$ , and  $northing_{it}^2 * easting_{it}^2$  are considered as explanatory variables. All coordinates are centered before they are squared or cubed by subtracting the mean over all observations.

## 2.8 Hurricanes

Hurricanes can rapidly introduce large volumes of freshwater to estuaries via riverine influx, push large volumes of saltwater in through inlets via storm surge,

and alter circulation patterns through abrupt changes in wind speed and direction [7, 10]. Hurricanes can also open new inlets to PS, which can alter current flow and increase saltwater intrusion [41]. The variable  $1wkFWII_{r_{it}}$  should capture variability in salinity due to hurricane-produced FWI. Three additional variables may account for non-FWI-related variability in salinity due to hurricane passage. These variables are unique to a given time period  $t$  but are constant over all sites  $i$  within  $t$ . The continuous variable  $inverse\_days\_survey_t$  is the reciprocal of the number of days between the most recent hurricane and  $m_t$ , except when there is no hurricane within the 61 days, and then it takes the value zero. The categorical variable  $category_t$  equals the category of the most recent hurricane rated on the Stafford-Simpson scale (1, ..., 5), but if no hurricane made landfall in the 61 days prior to  $m_t$ , it takes the value zero. Finally, the discrete variable  $num\_storms_t$  equals the number of hurricanes making landfall in NC in the 61 days prior to  $m_t$ .

## 2.9 Variable selection

Section 3 identifies 46 candidate explanatory variables for the process model mean function:  $1wkFWII_{r_{it}}$  and  $2moFWII_{r_{it}}$  (8), plus selected pair-wise interactions (explained below) (24); spatial coordinates, their powers, and specified interactions (9);  $closest\_inlet\_dist_{it}$ ;  $month_t$ ; and hurricane variables  $inverse\_days\_survey_t$ ,  $category_t$ , and  $num\_storms_t$ . For the time model, there were an additional 39 time period indicator variables. Some variables—in either model—may be redundant. There is overlap among the hurricane variables, and spatial coordinates may not be necessary if other variables explain more variability in salinity. The set of variables included in the final model(s) should balance goodness-of-fit with parsimony. We first describe the variable-selection process for the process model, then for the time model.

## 2.10 Process model

The results of eight separate ordinary least squares linear regression models of salinity make up the rows **Table 1**. The first five consist of an intercept and a single explanatory variable:  $closest\_inlet\_dist_{it}$ ,  $category_t$ ,  $inverse\_days\_survey_t$ ,  $num\_storms_t$ , and  $month_t$ . The sixth and seventh contain an intercept plus, respectively, the sets of four short and long-term freshwater influx indices  $\{1wkFWII_{r_{it}}, r = 1, \dots, 4\}$ , and  $\{2moFWII_{r_{it}}, r = 1, \dots, 4\}$ . We treated the short and long-term sets of indices as groups assuming that if an index evaluated for one river is meaningful, then it is also meaningful for other rivers. We discuss the eighth row in Section 4.2.

Adjusted  $R^2$  is a modification of  $R^2$  that penalizes the number of explanatory variables. While  $R^2$  increases as more variables are added to a model, adjusted  $R^2$  increases only if the added variable decreases the error sum of squares enough to offset the loss in error degrees of freedom.

The model with the long-term freshwater influx indices had the largest adjusted  $R^2$  at 0.38, followed by the model with the distance from the nearest inlet (0.34), and the model with the short-term FWI indices (0.27). None of the other four models explained more than 5% of the variability in salinity. We chose the model with the long-term freshwater influx indices as the base upon which to build the mean function.

To this base model we added the variable  $closest\_inlet\_dist_{it}$  since the model containing this variable had the second-best performance, thus beginning a forward-selection process. Each time we added a variable or set of variables to the model, we kept it in the model if the new adjusted  $R^2$  exceeded the old. Variables

Explanatory variable or set of explanatory variables	Adj R <sup>2</sup>
<i>closest_inlet_dist<sub>it</sub></i>	0.34
<i>category<sub>t</sub></i>	0.049
<i>inverse_days_survey<sub>t</sub></i>	0.035
<i>num_storms<sub>t</sub></i>	0.029
<i>month<sub>t</sub></i>	0.015
$1wkFWII_{r_{it}}, r = 1, \dots, 4$	0.27
$2moFWII_{r_{it}}, r = 1, \dots, 4$	0.38
$timeper_{\tau_t}, \tau = 1, \dots, 39$	0.41

**Table 1.**

Adjusted R<sup>2</sup> for the eight initial linear regression models. All regressions include an intercept plus the variables listed.

from the seven initial models were then added in order of decreasing adjusted R<sup>2</sup>. Following this procedure, the mean trend model grew to contain 10 variables —{ $2moFWII_{r_{it}}, r = 1, \dots, 4$ }, *closest\_inlet\_dist<sub>it</sub>*, { $1wkFWII_{r_{it}}, r = 1, \dots, 4$ }, and *inverse\_days\_survey<sub>t</sub>*—with adjusted R<sup>2</sup> 0.57.

Because the effect of FWI from one river on a given location in PS could change based on the FWI from another river during the same time period, we evaluated the addition of the 6 pair-wise interactions among the four  $1wkFWII_{r_{it}}$ , the 6 pair-wise interactions among the four  $2moFWII_{r_{it}}$ , and the twelve interactions between the  $1wkFWII_{r_{it}}$  and the  $2moFWII_{r_{it}}$ , excluding interactions of one river's  $1wkFWII_{r_{it}}$  with its own  $2moFWII_{r_{it}}$ . Despite a decrease in error degrees of freedom by 24, adjusted R<sup>2</sup> was 0.66, so the set was retained.

Spatial coordinate variables were evaluated last in groups according to their polynomial order, with squared and cubic terms added before interactions. We considered these variables last because we wanted to include them only if they explained additional variability in the response after more interpretable variables were included. We determined that including all variables except  $northing_{it}^2 * easting_{it}^2$  increased the adjusted R<sup>2</sup>. The final process model mean function thus had an adjusted R<sup>2</sup> of 0.73 and included the following: { $2moFWII_{r_{it}}, r = 1, \dots, 4$ }; *closest\_inlet\_dist<sub>it</sub>*; { $1wkFWII_{r_{it}}, r = 1, \dots, 4$ }; { $1wkFWII_{r_{it}} * 1wkFWII_{q_{it}}, r \neq q$ }; { $2moFWII_{r_{it}} * 2moFWII_{q_{it}}, r \neq q$ }; { $1wkFWII_{r_{it}} * 2moFWII_{q_{it}}, r \neq q$ }; *inverse\_days\_survey<sub>t</sub>*; *easting<sub>it</sub>*, *easting<sub>it</sub>*<sup>2</sup>, *northing<sub>it</sub>*, *northing<sub>it</sub>*<sup>2</sup>, and interactions  $northing_{it} * easting_{it}$ ,  $northing_{it}^2 * easting_{it}$ , and  $northing_{it} * easting_{it}^2$ .

## 2.11 Time model

To build the time model, we followed the same procedure described above, selecting for the base of the mean function a set of time period indicator variables because a linear regression of *sal<sub>it</sub>* on these variables had an adjusted R<sup>2</sup> of 0.41 (Table 1). (Note that such a model is equivalent to fitting an ANOVA model using the time periods as groups.) Again, we added other sets of explanatory variables in order of decreasing adjusted R<sup>2</sup>. Before evaluating interactions, the mean trend time model had an adjusted R<sup>2</sup> of 0.78 and contained 48 variables:

{ $timeper_{\tau_t}, \tau = 1, \dots, 39$ }, { $2moFWII_{r_{it}}, r = 1, \dots, 4$ }, *closest\_inlet\_dist<sub>it</sub>*, and { $1wkFWII_{r_{it}}, r = 1, \dots, 4$ }. When interactions among the { $timeper_{\tau_t}, \tau = 1, \dots, 39$ } and the { $2moFWII_{r_{it}}, r = 1, \dots, 4$ } were added, the

model was not full rank (not all columns in the design matrix were linearly independent). Because we created this second model to evaluate these interactions, we removed the  $\{1wkFWII_{rit}, r = 1, \dots, 4\}$ , the most recent variable addition, to include them. This new model, including the interactions, became the base since its adjusted  $R^2$  (0.89) was larger than that of the previous mean trend time model (0.78). After investigating spatial coordinate variables, the final mean trend time model (below) had an adjusted  $R^2$  of 0.91 and included 204 variables:  $\{timeper_{\tau t}, \tau = 1, \dots, 39\}$ ,  $\{2moFWII_{rit}, r = 1, \dots, 4\}$ ,  $closest\_inlet\_dist_{it}$ ,  $\{timeper_{\tau t} * 2moFWII_{rit}; \tau = 1, \dots, 39; r = 1, \dots, 4\}$ ,  $eastings_{it}$ ,  $eastings_{it}^2$ ,  $northing_{it}$ , and  $northing_{it}^2$ . To avoid confusion later, note that the adjusted  $R^2$  of 0.73 for the process model and 0.91 for the time model were based on fitting each model to the full dataset. In the next section, we report  $R^2$  (not adjusted  $R^2$ ) based on a cross-validation dataset.

## 2.12 Modeling spatially correlated error

The variable selection analyses above used ordinary least squares (OLS) regression to model salinity as a function of explanatory variables. That model can be written as

$$sal_{it} = \beta_0 + \beta_1 x_{1it} + \beta_2 x_{2it} + \dots + \beta_P x_{Pit} + \varepsilon_{it}, \quad t = 1, \dots, 40, \quad i = 1, \dots, n_t \quad (2)$$

where  $x_{pit}$  represents the value of the  $p^{th}$  explanatory variable at space-time location  $it$ , for  $p = 1, \dots, P$ , where  $P$  is the total number of explanatory variables.  $\beta_0, \beta_1, \dots, \beta_P$  represent the intercept and regression coefficients, and deviations from the mean trend  $\varepsilon_{it}$  are assumed to be independent and identically distributed  $\varepsilon_{it} \sim N(0, \sigma^2)$  with mean 0 and variance  $\sigma^2$ . The model can be equivalently written as  $sal_{it} = \mathbf{x}_{it}^T \boldsymbol{\beta} + \varepsilon_{it}$ , where  $\mathbf{x}_{it}$  is the  $(P + 1) \times 1$  vector containing the values of the explanatory variables at space-time location  $it$ , and  $\boldsymbol{\beta}$  represents the  $(P + 1) \times 1$  vector of regression coefficients. The same model written in matrix form is

$$\mathbf{Y} = \mathbf{X}\boldsymbol{\beta} + \boldsymbol{\varepsilon}, \quad \boldsymbol{\varepsilon} \sim N(\mathbf{0}, \sigma^2 \mathbf{I}), \quad (3)$$

where bold print indicates vectors so that  $\mathbf{Y}$ ,  $\boldsymbol{\varepsilon}$ , and  $\mathbf{0}$  are  $N \times 1$  vectors containing, respectively, all observations of salinity in the space-time domain, all deviations from the mean function, and all zeros.  $\mathbf{X}$  is the  $N \times (P + 1)$  design matrix whose rows represent space-time locations and whose columns contain the values of the explanatory variables (with a column of ones for the intercept), and  $\mathbf{I}$  is the  $N \times N$  identity matrix. Since a histogram of salinity observations is somewhat symmetric and bell-shaped, use of the normal distribution is justified.

Rarely, however, does the assumption of independent and identically distributed errors hold for observations of natural phenomena associated with locations in space and time. While it is intuitive that values of salinity located close together in space should be similar, it is also generally the case that the deviations from the mean function of observations located close together are similar. That similarity is referred to as spatial covariance, and the spatial covariance between deviations from the mean trend at two locations within the same time period can be modeled as a function of the distance separating them. Including in the overall model both a deterministic mean function and a spatial covariance function allowed predictions of salinity at locations where there were no observations.

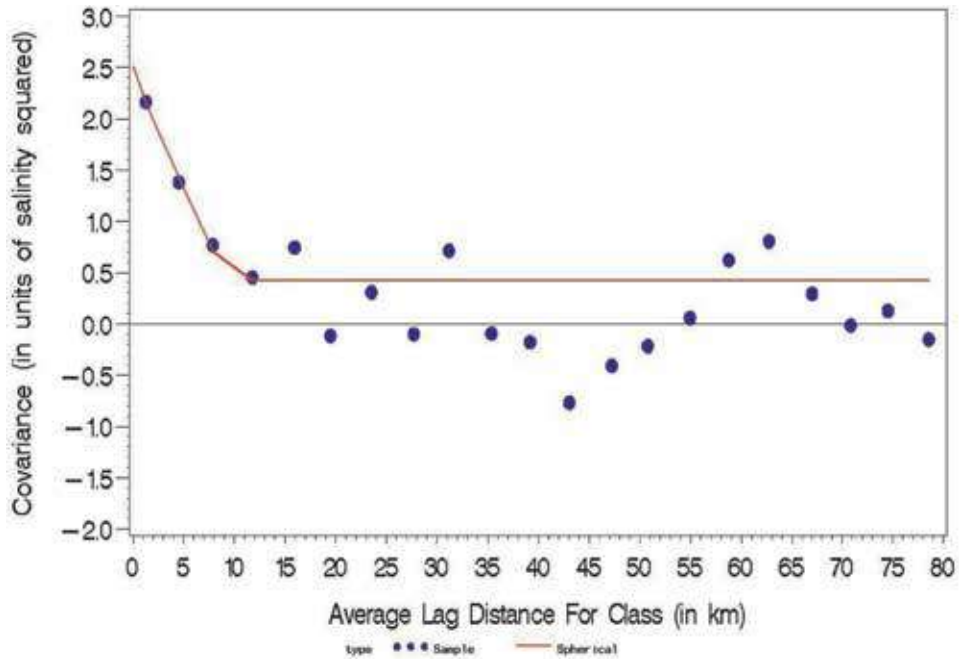


**Figure 3.** Sample covariogram for June 1994 calculated from process model residuals (blue dots). The solid red line illustrates a spherical covariance function fit to the covariogram. Covariance is in units of salinity squared.

Valid covariance functions ensure that the covariance matrix will be positive definite, which, in turn, ensures that variances will be non-negative. Each covariance function has a shape defined by a range parameter, a partial sill, and sometimes a nugget effect. Appendix Table A1 gives formulas for determining spatial covariance according to the exponential, Gaussian, and spherical covariance functions, each with and without a nugget effect. **Figure 3** shows an example of the spherical covariance function—the solid red line—fit to a sample covariogram—the blue dots—of deviations from the process model for June 1994. The range parameter— $\theta$  for the exponential and Gaussian covariance functions,  $\rho$  for spherical—is related to the distance that must separate two sites before their deviations are independent, where independence corresponds to a covariance of zero or virtually zero. In **Figure 3**, the range is approximately 10 km. In the absence of a nugget effect, the partial sill  $\sigma^2$  is the value of the covariance at distance zero—that is, it is the variance of deviations from the mean—and in **Figure 3** this value is approximately 2.5 squared units of salinity. In the presence of the nugget  $\sigma_n^2$ , there is a discontinuity in the covariance function at distance zero, so that the intercept is slightly greater than the limit of the smooth part of the function as distance approaches zero. In this case, the variance of the deviations is equal to the sum of the partial sill and nugget:  $\sigma^2 + \sigma_n^2$ . It may be the case that variance is higher when values of deviations are higher. Since covariance parameters represent physical quantities that may change over time, we used the capabilities of SAS<sup>®</sup> Proc Mixed to allow a different partial sill and range parameter for each time period.

Model (3), modified to include spatial correlation, becomes

$$Y = X\beta + \epsilon, \quad \epsilon \sim N(\mathbf{0}, \Sigma), \tag{4}$$

where  $\Sigma$  represents the  $N \times N$  block-diagonal covariance matrix

$$\Sigma = \begin{bmatrix} \Sigma_1 & \mathbf{0} & \mathbf{0} & \mathbf{0} \\ \mathbf{0} & \Sigma_2 & \mathbf{0} & \mathbf{0} \\ \mathbf{0} & \mathbf{0} & \ddots & \mathbf{0} \\ \mathbf{0} & \mathbf{0} & \mathbf{0} & \Sigma_T \end{bmatrix},$$

where zero matrices for off-diagonal elements indicate that deviations in one time period are not correlated with those in another. We make this assumption partially due to the long time span separating June and September, but also because no SAS<sup>®</sup> procedure has the capacity to model such space-time correlation while at the same time allowing every time period to have different spatial covariance parameters and allowing a mean function to be fit. Diagonal elements  $\Sigma_1, \Sigma_2, \dots, \Sigma_t, \dots, \Sigma_T$  are individual spatial covariance matrices for each time period with dimensions  $n_t \times n_t$ , and elements  $[\Sigma_t]_{ij} = Cov\{\varepsilon_{it}, \varepsilon_{jt}\}$  representing the spatial covariance between sites  $i$  and  $j$  in time period  $t$ .

Understanding how predictions of salinity and prediction standard errors are generated from this model will make the results and analysis in Sections 6 and 7 easier to understand. To predict salinity at space-time locations where it is not observed, the following results are needed. Superscripts differentiate between locations where salinity is observed and unobserved. Model (4), represents observations of salinity (by virtue of the dimensions of the vectors and matrices), but we model salinity observations and unobserved values of salinity at other space-time locations using a similar model, the joint distribution of unobserved and observed salinity, given by

$$\begin{pmatrix} \mathbf{Y}^o \\ \mathbf{Y}^u \end{pmatrix} \sim N \left\{ \begin{pmatrix} X^o \boldsymbol{\beta} \\ X^u \boldsymbol{\beta} \end{pmatrix}, \begin{pmatrix} \Sigma^o & \Sigma^{ou} \\ \Sigma^{uo} & \Sigma^u \end{pmatrix} \right\}. \quad (5)$$

Here,  $\mathbf{Y}^o$  represents the  $N \times 1$  vector of salinity observations, and, letting  $N^u$  represent the number of space-time locations at which we want to predict salinity,  $\mathbf{Y}^u$  represents the  $N^u \times 1$  vector of unknown values of salinity at these locations. All the symbols in (5) have the same meaning as in (4), except for the distinction between observed and unobserved locations. The  $N \times N^u$  matrix  $\Sigma^{ou}$  contains the cross-covariance between observed and unobserved locations. Thus,

$$\Sigma^{ou} = \begin{bmatrix} \Sigma_1^{ou} & \mathbf{0} & \mathbf{0} & \mathbf{0} \\ \mathbf{0} & \Sigma_2^{ou} & \mathbf{0} & \mathbf{0} \\ \mathbf{0} & \mathbf{0} & \ddots & \mathbf{0} \\ \mathbf{0} & \mathbf{0} & \mathbf{0} & \Sigma_T^{ou} \end{bmatrix},$$

and  $\Sigma^{uo} = (\Sigma^{ou})^T$ . The elements  $[\Sigma_t^{ou}]_{ij} = Cov\{\varepsilon_{it}^o, \varepsilon_{jt}^u\}$  also come from the spatial covariance function.

Let  $\boldsymbol{\psi}$  represent the vector that contains all spatial covariance parameters for every time period—either 80 or 81 parameters depending on whether a nugget effect is used. Standard normal distribution theory gives the distribution of unobserved salinity  $\mathbf{Y}^u$  conditioned on knowing the values of observations  $\mathbf{Y}^o$  and all of the parameter values:

$$\mathbf{Y}^u | \mathbf{Y}^o, \boldsymbol{\beta}, \boldsymbol{\psi} \sim N \left\{ X^u \boldsymbol{\beta} + \Sigma^{uo} (\Sigma^o)^{-1} (\mathbf{Y}^o - X^o \boldsymbol{\beta}), \Sigma^u - \Sigma^{uo} (\Sigma^o)^{-1} \Sigma^{ou} \right\}. \quad (6)$$

The pipe symbol ( $|$ ) means “given” or “conditioned on knowing the values of” the terms following the pipe symbol. The terms before the comma represent the mean of the multivariate normal distribution, which is used for the salinity prediction, and the terms after the comma represent the variance-covariance matrix, which is used for prediction standard errors. Salinity predictions are the sum of the mean trend,  $X^u\beta$ , and the spatial interpolation of observation deviations from the mean trend,  $\Sigma^{uo}(\Sigma^o)^{-1}(\mathbf{Y}^o - X^o\beta)$ . If the deviations  $(\mathbf{Y}^o - X^o\beta)$  are large for a given time period, then the partial sill  $\sigma_i^2$  will be large for that time period, so that diagonal elements of  $\Sigma^o$  and  $\Sigma^u$  will be large. For a given location, the prediction standard error is the diagonal element of the matrix  $\Sigma^u - \Sigma^{uo}(\Sigma^o)^{-1}\Sigma^{ou}$ . If the diagonal elements of  $\Sigma^o$  and  $\Sigma^u$  are large, then the diagonal elements of  $(\Sigma^o)^{-1}$  are small, and the prediction standard error is a large number minus a small number. That is, the prediction standard error will be high for time periods in which observation deviations from the mean function are large. When observation deviations from the mean trend are small, the reverse is true, and prediction standard errors tend to be low for that time period.

The salinity predictor

$$X^u\beta + \Sigma^{uo}(\Sigma^o)^{-1}(\mathbf{Y}^o - X^o\beta) \quad (7)$$

is an *exact predictor*: the prediction of salinity at a site where there is an observation will exactly equal the observation. For this reason, to determine which spatial covariance function to use, we randomly selected 10% of the observations to withhold as a cross-validation dataset, the *test dataset*; the remaining 90% we term the *base dataset*. For every combination of the two mean functions—process and time—and the six spatial covariance functions in Appendix Table A1, we fit model (4) to the base dataset, and predicted salinity values at the space–time locations of the test dataset using the results given in (5) and (6). When the model predicted salinity to be less than zero, we set the prediction equal to zero before calculating the following statistics. Predictions of negative values could be avoided using a truncated normal distribution, but SAS<sup>®</sup> Proc Mixed does not permit specification of this distribution. The root mean squared error (RMSE) of predictions—with the same units as salinity—are given in **Table 2**, along with the slope, intercept, and coefficient of determination ( $R^2$ ) from a regression of actual salinity values in the test dataset on predictions of them. If predictions were perfect, this regression would have slope equal to one, intercept equal to zero, and  $R^2$  equal to 1.

Salinity predictions are better when a spatial covariance function is combined with either mean function. For example, of the time models, the exponential covariance function with a nugget produced predictions with the lowest RMSE (2.1), slope closest to one (0.92), and intercept closest to zero (1.55). Comparing process models, the exponential and spherical, each with and without a nugget, performed equally well, and better than the time models. To select the best model from this group of four, we examined statistics based on how well the model fit the base dataset. The model with an exponential covariance function with a nugget had the lowest AIC (7580.0) and BIC (7711.7) and was thus chosen as the final model. It explained 89% of variability in the test dataset and generated predictions with RMSE 2.0.

Next, we fit this model using the full dataset, and produced retrospective maps of salinity predictions and standard errors at evenly spaced 1 nmi (1.85 km) increments for each time period. Forty-two salinity predictions—less than 0.1% of the total number of predictions—were negative and set to zero.

	Model type	-2 log likelihood	AIC	BIC	RMSE (psu)	Slope/ $\beta_1$	Intercept/ $\beta_0$	R <sup>2</sup>
Process	IID	9935.9	9937.9	9943.5	2.9	0.98	0.84	0.74
	Exponential	7430.7	7584.7	7714.7	2.0	0.95	1.03	0.89
	Exponential + $\sigma_n^2$ *	7424.0	7580.0	7711.7	2.0	0.96	0.96	0.89
	Gaussian	8198.0	8356.0	8489.5	2.3	0.94	1.37	0.84
	Gaussian + $\sigma_n^2$ *	7532.0	7686.0	7816.0	2.1	0.94	1.15	0.87
	Spherical	7570.0	7722.0	7850.4	2.0	0.95	1.07	0.88
	Spherical + $\sigma_n^2$ *	7571.6	7727.6	7859.3	2.0	0.96	0.93	0.89
Time	IID	7077.5	7079.5	7084.9	2.6	0.83*	3.47*	0.83
	Exponential	Infinite						
	Exponential + $\sigma_n^2$	6217.1	6367.1	6493.7	2.1	0.92*	1.55*	0.87
	Gaussian	6281.0	6433.0	6561.3	2.2	0.90*	1.98*	0.86
	Gaussian + $\sigma_n^2$ *	6214.0	6366.0	6494.4	2.2	0.91*	1.90*	0.86
	Spherical	6199.6	6315.6	6479.9	2.2	0.91*	1.86*	0.86
	Spherical + $\sigma_n^2$	6201.3	6357.3	6489.1	2.2	0.91*	1.86*	0.86

Process and time mean functions with no spatial covariance (IID) and with each of six covariance functions were used. The symbol " $\sigma_n^2$ " indicates that a nugget was included. Stars (\*) indicate rejection of the appropriate null hypothesis at the  $\alpha = 0.05$  level of significance:  $H_{01}$ :  $\sigma_n^2 = 0$ ;  $H_{02}$ :  $\beta_1 = 1$ ;  $H_{03}$ :  $\beta_0 = 0$ . The exponential plus nugget process model is highlighted as it was chosen as the best model of PS salinity for our modeling context.

**Table 2.** Summary statistics comparing salinity observations in the test dataset to predictions based on fitting models to the base dataset.

### 2.13 Examining freshwater influx scenarios

To examine variations in the spatial distribution of salinity under drought, average, and flood conditions, we classified freshwater influx from each river within each time period ( $1wkFWI_{r_t}$  and  $2moFWI_{r_t}$ ) as LOW if it fell below the 25th percentile of observed FWI across all time periods, MODERATE if it fell between the 25th and 75th percentiles, HIGH if it fell between the 75th and 95th percentiles, and FLOOD if it fell above the 95th percentile. Next, we classified one-week and two-month FWI for the entire time period as LOW (or HIGH) if at least two rivers exhibited low (or high) inflow, MODERATE if at least three rivers exhibited moderate inflow, and FLOOD if at least one river exhibited extremely high (>95th percentile) inflow. These classifications are mutually exclusive, though some of the 40 time periods did not fall into any of them. The first two columns of **Table 3** list the 16 combinations of classifications, and the third column shows the classification and salinity rank for each time period. Time periods were ranked 1–40 by mean predicted salinity (1 = highest mean salinity; 40 = lowest).

Moderate-to-moderate FWI. June 2005 (**Figure 4**) experienced moderate FWI in both the 2 months and 1 week prior to the survey in PS with predicted salinity ranked 37th—the lowest of the moderate-to-moderate time periods. Legend colors for model predictions in the left pane and observations in the upper right pane of **Figure 4** (as well as **Figure 5A** and **B**, **6A** and **B**) are based on percentiles of the distribution of observed salinity across all time periods: minimum to 5%; 5–10%; 10–25%; 25–50%; 50–75%; 75–90%; 90–95%; and 95% to maximum. From the left pane of **Figure 4**, predicted salinity in June 2005 increased moving east across PS,

<i>2mo_FWI<sub>t</sub></i>	<i>1wk_FWI<sub>t</sub></i>	Time periods and mean predicted salinity rank (mmyy, r)
Flood	Flood	(0603, 40), (0999*, 30)
	High	none
	Moderate	(0687, 28), (0689, 27)
	Low	None
High	Flood	(0903*, 39), (0690, 29)
	High	(0904*, 32)
	Moderate	(0698, 38), (0693, 36), (0697, 35)
	Low	None
Moderate	Flood	(0996*, 33)
	High	(0696, 26), (0900, 24)
	Moderate	(0605, 37), (0989, 31), (0601, 26), (0600, 22), (0604, 21), (0688, 16), (0990, 13), (0692, 10)
	Low	(0694, 17)
Low	Flood	(0987, 18)
	High	(0695, 6)
	Moderate	(0905, 20)
	Low	(0997, 15), (0699, 12), (0901, 8), (0902, 7), (0993, 5), (0602, 4), (0988, 3), (0994, 1)

*Only time periods that fit each scenario as defined in Section 6 are listed; the remaining 7 time periods were not classified. Boldfaced time periods are examined in Section 6. Stars (\*) indicate time periods in which hurricanes occurred within the 61 days prior to the survey.*

**Table 3.** Sixteen combinations of *2mo\_* and *1wk\_FWI<sub>t</sub>* classifications; time periods that exhibit each set of conditions; and mean predicted salinity rank (1 = highest).

reaching a maximum just south of Oregon Inlet. We note the same east-west salinity gradient when comparing this pane to the June 2005 map of observed salinities (top right pane), indicating that prediction maps typically mirror trends seen in observation maps. The area of highest predicted salinity corresponds to a lone purple observation of 26.5 just south of Oregon Inlet (**Figure 4**). Plumes of relatively higher salinity are evident in the vicinity of all three ocean inlets (**Figure 4**).

The lower right pane of **Figure 4** (as well as **Figure 5A and B, 6A and B**) displays prediction standard errors (SE) with the same units as salinity. The same eight percentile groups classify colors on the SE legend, here based on the distribution of prediction standard errors across all time periods. The transition from low SE at sample sites to higher SE moving away from sample sites reflects the fact that the exact predictor (6) reproduces observations, so confidence intervals closer to sample sites are narrower than those further away.

This spatial trend in SEs is further illustrated by comparing locations of high SE in the same time period, which are also consistent over time. High SEs occur between the mouths of the Neuse and Pamlico Rivers and along a margin of varying width following the outline of the Outer Banks, areas within which sampling does not occur (**Figure 1**). We note here that because SEs increase as distance from sample site increases, we chose to generate only interpolated (and not extrapolated)

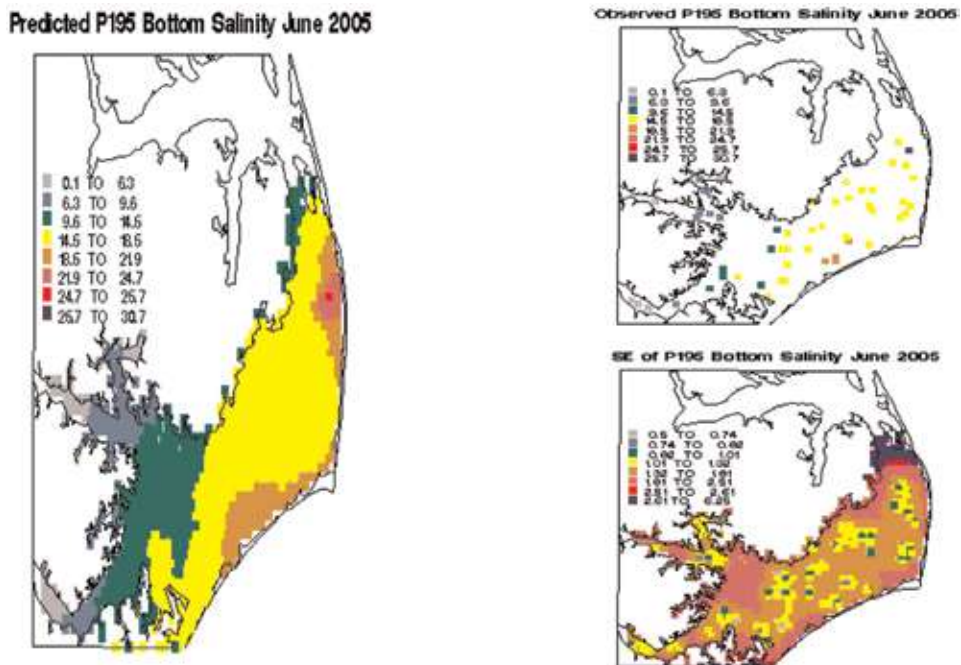


**Figure 4.** Salinity model predictions (left), prediction standard errors (bottom right), and P195 survey observations (top right) for June 2005, classified as moderate-to-moderate FWI.

salinity predictions. In June 2005, as in all other time periods, predictions were generated only for locations within S, which does not extend either to Albemarle Sound or to the heads of the Neuse and Pamlico Rivers (**Figure 4**).

*Low to low FWI in early and late-stage drought.* June 1999 (**Figure 5A**) and June 2002 (**Figure 5B**)—which mark early and late stages of North Carolina’s 1998–2002 drought [42]—experienced low long- and short-term FWI with predicted salinity ranking 12th and 4th, respectively. At every point in PS, predicted salinity in these two time periods was higher than in June 2005, and predicted salinity was much higher in June 2002 than June 1999, though both have similar values for  $1wkFWI_{r_t}$  and  $2moFWI_{r_t}$  variables from three of the four tributary rivers. The difference may be due to (1) the fact that in the fourth river, the Roanoke,  $1wkFWI_{r_t}$  and  $2moFWI_{r_t}$  in June 1999 were twice their values in June 2002, or (2) that by June 2002, NC had been experiencing drought conditions for 4 years (186 weeks) as opposed to less than one (30 weeks) and that this cumulative FWI deficit became more pronounced over time.

Though June 2002 salinity observations have a larger mean and greater variability, the majority of prediction standard errors are less than 1.01. In June 1999, however, SEs fell between 1.01 and 1.81 at all prediction locations except those that were very close to observations. This result shows that the conditions affecting salinity in PS were better represented by the mean function in June 2002 than they were in June 1999.

*Flood to flood FWI—with and without hurricanes.* FWI was extremely high in September 1999 (**Figure 5A**) as a result of the 500-year floods produced by Hurricanes Dennis and Floyd that occurred 24 and 12 days before the survey, respectively. In June 2003 (**Figure 5B**), extremely high FWI was due to an eight-month period of above-average precipitation totals prior to the survey. Though these are



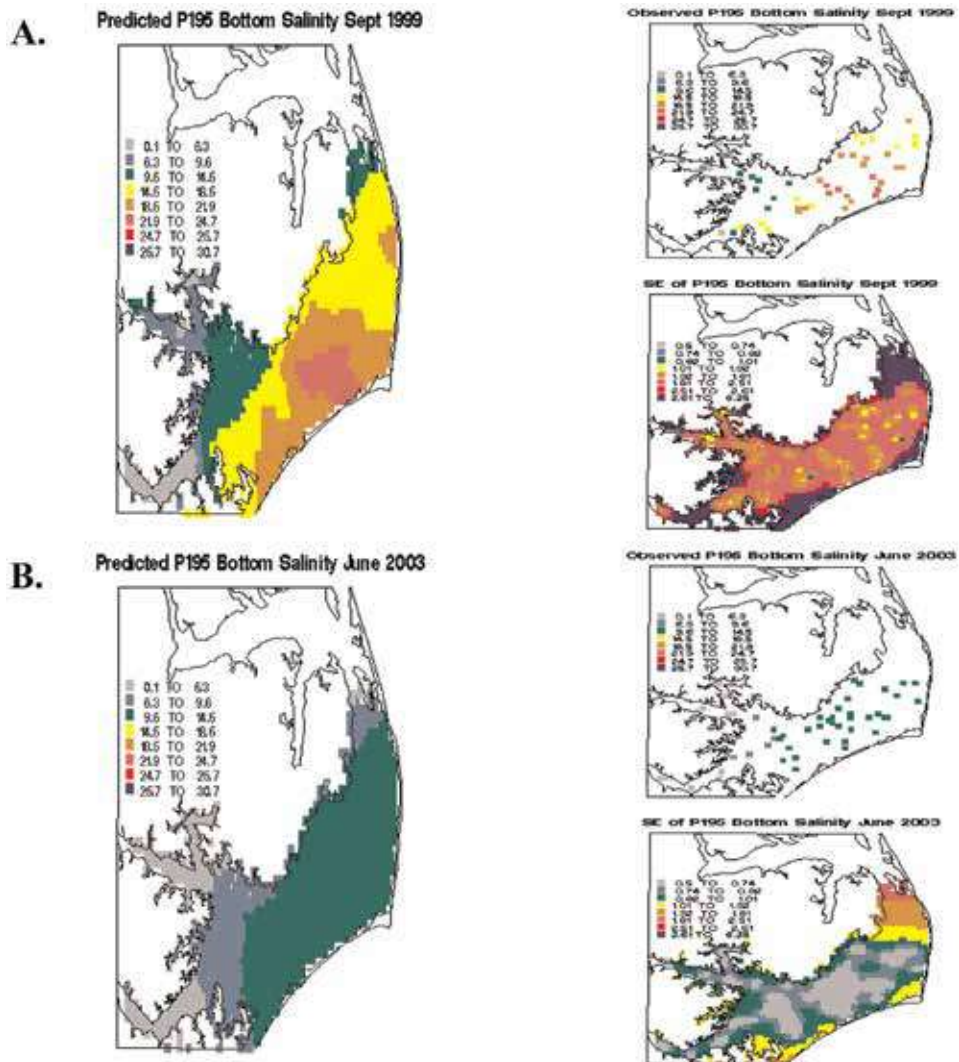


**Figure 6.** Salinity model predictions (left), prediction standard errors (bottom right), and P195 survey observations (top right) for September 1999 (A) and June 2003 (B), both classified as flood-to-flood FWI.

### 3. Discussion

Because water exchange between lagoonal estuaries and the open ocean can be relatively restricted, there is a relatively high potential in systems like PS for changes in precipitation patterns and storm frequencies associated with global climate change to result in changes in salinity patterns and subsequent ecosystem alterations. Changes in precipitation will affect the amount and timing of river flow, which will impact nutrient cycling, estuarine flushing rates, and salinity. Increased storm activity may open new inlets, which would alter current flow, increase tidal action, and allow a greater influx of seawater that carries with it both different chemical signals and mobile species. Salinity is therefore a practical estuarine characteristic to use to study the impacts of these changes, as both effects mentioned above include enhanced water exchange that impacts overall estuarine salinity content [43, 44].

We developed and evaluated two statistical models, using the best model to hindcast salinity in PS. The process mean function combined with the exponential covariance with a nugget explained 89% of the variability in a test dataset with a RMSE of 2.0 and produced relatively accurate retrospective salinity maps under a wide range of freshwater influx and system-state scenarios. Much of this accuracy was due to allowing the range and partial sill parameters of the spatial covariance to be time-period specific. We then examined variations in the spatial distribution of salinity under varying freshwater influx (FWI) conditions such as drought, average FWI, and flood conditions, and identified the following patterns. In years with moderate FWI, the salinity gradient increased from west to east in PS as expected, and was highest adjacent to the major inlets, with highest salinities near Oregon Inlet. In years with low FWI indicative of drought conditions, the overall mean and variance in salinity increased in PS. In years with floods, salinities displayed a high degree of spatial variation, with salinities being lower near the tributaries as expected, yet also displaying occasional sharp increases in salinity near inlets due to influx of ocean water into PS via the major inlets.

### 3.1 Improvements to model predictions

For retrospective prediction purposes, model improvements could focus on improvements to the mean trend, the covariance, or both, and such improvements could be evaluated using the test dataset. A reasonable goal might be to increase  $R^2$  to 0.93 or to reduce RMSE to 1.5. Improvements for the purpose of prospective prediction of salinity under hypothetical, unobserved conditions, a situation in which spatial covariance among observation deviations cannot be used, would entail improving the mean function exclusively. Locations and time periods with high SEs highlight conditions not well-represented by the current mean function. A reasonable goal here would be to produce a model for which all values of SE fall beneath the current median (1.32).

*Mean function.* The mean function alone explained over two-thirds of the variability in salinity in both process and time models. While this is a noteworthy accomplishment, there remains room for multiple improvements. High SE values in **Figure 5A** show that the mean function is unable to capture the interaction between high FWI in September 1999 and hurricane storm surges. One hurricane explanatory variable,  $inverse\_days\_survey_t$ , remained in the final process model. Its parameter estimate was positive, reflecting that strong hurricane winds push more saltwater into PS through inlets than would enter under typical seasonal wind conditions, but alone it explained only 4% of salinity variability in the full dataset. The  $inverse\_days\_survey_t$  variable did not differentiate between a year in which a single hurricane passed within 12 days of the survey and a year in which such a hurricane followed another that passed 12 days earlier. A future effort might attempt to account for cumulative build-up of storm surge on observed PS salinities.

Though  $closest\_inlet\_dist_{it}$  alone explained a third of the variability in salinity over all time periods, variability in inlet-plume size across **Figures 3–5** suggests that this distance metric should be modified based on wind speed and direction, using more finely resolved wind information than the  $month_t$  variable. Devising a way to use the  $u$  and  $v$  components of wind to interact with  $closest\_inlet\_dist_{it}$  could allow both the size and the direction of the inlet plume to vary such that east-to-west winds create different plume sizes and shapes than winds from the southeast-to-northwest. Considerable exploratory analysis would be needed to determine what pre-survey time lag should be considered to affect observed survey salinities.

Differences in both salinity values and SE estimates between early-stage drought during June 1999 and late-stage drought during June 2002 suggest accounting for

effects of FWI over a longer duration than 61 days. Doing so might explain differences in salinity patterns seen in time periods with similar one-week and two-month FWI conditions. Molina [45] calculated an 11 month mean residence time for freshwater in PS. We could incorporate this effect by adding a third freshwater influx index to the mean function or by adding an autoregressive component to the model so that salinity in a given time period was a function of mean salinity in the previous time period. The first option would be tedious from a data-manipulation standpoint, but much easier from a mathematical model-fitting standpoint, because SAS<sup>®</sup> Proc Mixed could still be used. The second option necessitates a change in the covariance function, as we can no longer assume that salinity deviations from the mean function at a given space-time point were independent in time. This second option would also require specialized hand-written code, as no current SAS<sup>®</sup> Proc allows such a dynamic space-time model to be fit.

Differences in salinity patterns between June 1999 and June 2002, our two low-to-low FWI time periods, could be attributed to differences in FWI from the Roanoke River, one of the two northern rivers whose connection to PS is indirect. This observation warrants further investigation into the calculation of the FWII indices; namely, an investigation of water-path distance as a possible substitute for crow-flies distance between river gauges and sites in PS. Although we did not find a study that demonstrated marked predictive improvement using water-path distance under all circumstances ([36, 46], and others), it would be interesting in future work to compare differences in PS salinity predictions using both distance methods. Recall that Gardner et al. [34] noted more accurate predictions of stream temperatures when models incorporated water-path distance, but only when this distance was further modified and weighted by stream order. It might be the case that water-path distance out-performs crow-flies distance in predicting estuarine salinity when care is taken to make all explanatory variables as meaningful as possible. Development of an automated procedure for calculating water-path distances similar to the one used in [47] would make such an investigation more practically feasible.

*Covariance function.* Two mutually-exclusive improvements to the covariance function, as implemented in SAS<sup>®</sup> Proc Mixed, could be investigated: using either the Matern covariance function or an anisotropic covariance function to achieve greater flexibility in each time period. The Matern covariance function has a smoothing parameter in addition to partial sill and range parameters. When the smoothing parameter takes the value of 0.5, the Matern covariance function is the same as the exponential covariance function—as the smoothness parameter approaches infinity, the covariance function approaches the Gaussian covariance function. Using the Matern covariance function is thus equivalent to allowing a third parameter to determine which two-parameter covariance function is appropriate, as opposed to using the same two-parameter covariance function for every time period. The computational cost of this flexibility is high—in a similar model with only four separate groups of covariance parameters, compared to the 40 groups in this paper—co-author Amy Nail experienced computation time of 2 h (versus a 2 min run time using the two-parameter exponential covariance function here). The added computational burden is due to the complex nature of the Matern covariance function and to the necessity of estimating one additional covariance parameter per time period (for a total of 40 additional parameters).

Another way to achieve flexibility while still specifying a single covariance function for every time period, would be to allow an anisotropic covariance function. Geometric anisotropy allows for different range parameters in different directions. For example, if the water current in PS were flowing directly north-to-south, two points separated by a north-to-south vector might have more similar values of salinity than would two points separated by a west-to-east vector of the same length.

Fortunately, the parameterization of a geometric anisotropic covariance function is such that if anisotropy were unnecessary, the parameters would take values that effectively result in an isotropic covariance function. The cost of this added flexibility is the need to estimate two additional covariance parameters per time period, for a total of 80 additional parameters. Computation time might be less here than for Matern, since anisotropic covariance functional forms are less complex.

#### 4. Conclusions

We created a statistical model combining a process mean function with an exponential spatial covariance function with a nugget to predict salinity in a lagoonal estuary. This model can generate predictions of bottom salinity for Pamlico Sound, NC that are more spatially-resolute than any previous bottom salinity predictions encountered in the literature for this system. The salinity maps produced using the model are useful for researchers to build an intuitive understanding of salinity dynamics under PS conditions covered by these 40 time periods. Salinity predictions can also be used to inform future analyses including, but not limited to, the examination of historical distribution patterns of estuarine species relative to salinity variability and the prediction of salinity changes under various global climate change scenarios.

#### Acknowledgements

We thank the North Carolina Division of Marine Fisheries and the United States Geological Survey for providing datasets used in this study. We also thank editor A. Manning for helpful comments that improved the manuscript. Funding for this project was provided by the Environmental Defense Fund (Program Manager Pam Baker), North Carolina Coastal Recreational Fishing License Program (Grant No. 2010-H-004), North Carolina Sea Grant (R12-HCE-2) and the National Science Foundation (OCE-1155609) to D. Eggleston. A. Nail was supported as a VIGRE Postdoctoral Fellow by NSF grant DMS 0354189.

#### Appendix

See **Table A1**.

Name of covariance function	Cov{ $\epsilon_{ii}, \epsilon_{ij}$ } =	
	With nugget effect	Without nugget effect
Exponential	$\sigma_n^2 I(d_{ij} = 0) + \sigma_t^2 \exp\left(\frac{-d_{ij}}{\theta_t}\right)$	$\sigma_t^2 \exp\left(\frac{-d_{ij}}{\theta_t}\right)$
Gaussian	$\sigma_n^2 I(d_{ij} = 0) + \sigma_t^2 \exp\left(\frac{-d_{ij}^2}{\theta_t^2}\right)$	$\sigma_t^2 \exp\left(\frac{-d_{ij}^2}{\theta_t^2}\right)$
Spherical	$\sigma_n^2 I(d_{ij} = 0) + \sigma_t^2 \left[1 - \left(\frac{3d_{ij}}{2\rho_t}\right) + \left(\frac{d_{ij}^3}{2\rho_t^3}\right)\right] I(d_{ij} \leq \rho_t)$	$\sigma_t^2 \left[1 - \left(\frac{3d_{ij}}{2\rho_t}\right) + \left(\frac{d_{ij}^3}{2\rho_t^3}\right)\right] I(d_{ij} \leq \rho_t)$

Note: For all models,  $\sigma_n^2, \sigma_t^2 > 0$ , and  $\theta_t \geq 0$ ,  $-\infty < \rho < \infty$ , and  $d_{ij}$  is the distance separating sites  $i$  and  $j$ .

Note:  $I(\text{statement}) = 1$  if statement is true and 0 otherwise.

**Table A1.**

Formulas for the three spatial covariance functions used in this analysis.

## Author details

Christina L. Durham<sup>1</sup>, David B. Eggleston<sup>1\*</sup> and Amy J. Nail<sup>2</sup>

<sup>1</sup> Department of Marine, Earth and Atmospheric Sciences, North Carolina State University, Raleigh, NC, United States

<sup>2</sup> Department of Statistics, North Carolina State University, Raleigh, NC, United States

\*Address all correspondence to: [eggleston@ncsu.edu](mailto:eggleston@ncsu.edu)

## IntechOpen

---

© 2019 The Author(s). Licensee IntechOpen. This chapter is distributed under the terms of the Creative Commons Attribution License (<http://creativecommons.org/licenses/by/3.0>), which permits unrestricted use, distribution, and reproduction in any medium, provided the original work is properly cited. 

## References

- [1] Cloern JE, Nichols FH. Time scales and mechanisms of estuarine variability, a synthesis from studies of San Francisco Bay. *Hydrobiologia*. 1985;**129**: 229
- [2] Anderson AM, Davis WJ, Lynch MP, Schubel JR. Effects of Hurricane Agnes on the Environment and Organisms of Chesapeake Bay. Baltimore, MD: The Chesapeake Bay Research Council, Johns Hopkins University; 1973
- [3] Bell GW, Eggleston DB. Species-specific avoidance responses by blue crabs and fish to chronic and episodic hypoxia. *Marine Biology*. 2005;**146**: 761-770
- [4] Mallin MA, Corbett CA. How hurricane attributes determine the extent of environmental effects: Multiple hurricanes and different coastal systems. *Estuaries and Coasts*. 2006;**29**:1046-1061
- [5] Bell GW, Eggleston DB, Wolcott TG. Behavioral responses of free-ranging blue crabs to episodic hypoxia. I. Movement. *Marine Ecology Progress Series*. 2003;**259**:215-225
- [6] Baird D, Christian RR, Peterson CH, Johnson GA. Consequences of hypoxia on estuarine ecosystem function: Energy diversion from consumers to microbes. *Ecological Applications*. 2004;**14**:805-822
- [7] Burkholder J, Eggleston D, Glasgow H, Brownie C, Reed R, Melia G, et al. Comparative impacts of major hurricanes on the Neuse River and Western Pamlico Sound ecosystems. *Proceedings of the National Academy of Science*. 2004;**101**: 9291-9296
- [8] Paerl HW, Pinckney JL, Fear JM, Peierls BL. Ecosystem responses to internal and watershed organic matter loading: Consequences for hypoxia in the eutrophying Neuse River Estuary, North Carolina, USA. *Marine Ecology Progress Series*. 1998;**166**:17-25
- [9] Paerl HW, Hall NS, Hounshell AG, Luettich RA, Rossignol KL, Osburn CL, et al. Recent increase in catastrophic tropical cyclone flooding in coastal North Carolina, USA: Long-term observations suggest a regime shift. *Scientific Reports*. 2019;**9**:10620. DOI: 10.1038/s41598-019-46928-9
- [10] Eggleston DB, Reyns NB, Etherington LL, Plaia G, Xie L. Tropical storm and environmental forcing on regional blue crab settlement. *Fisheries Oceanography*. 2010;**19**(2):89-106
- [11] Searcy S, Eggleston DB, Hare J. Environmental influences on the relationship between juvenile and larval growth for Atlantic croaker, *Micropogonias undulatus*. *Marine Ecology Progress Series*. 2007;**349**:81-88
- [12] Eggleston DB, Johnson E, Hightower J. Population Dynamics and Stock Assessment of the Blue Crab in North Carolina. Final Report for Contracts 99-FEG-10 and 00-FEG-11 to the North Carolina Fishery Resource Grant Program, NC Sea Grant, and the NC Department of Environmental Health and Natural Resources. Division of Marine Fisheries; 2004. p. 252
- [13] Lin G. A numerical model of the hydrodynamics of the Albemarle-Pamlico-Croatan Sounds system, North Carolina [M.S. thesis]. Raleigh, NC: North Carolina State University; 1992. 118 pp
- [14] Pietrafesa LJ, Janowitz GS. Physical oceanographic processes affecting larval transport around and through North Carolina inlets. *American Fisheries Society Symposium*. 1988;**3**:34-50

- [15] Bender MA, Knutson TA, Tuleya RE, Sirutis JJ, Vecchi GA, Garner ST, et al. Modeled impact of anthropogenic warming on the frequency of intense Atlantic hurricanes. *Science*. 2010;**327**:454-458
- [16] Federov AV, Brierley CM, Emanuel K. Tropical cyclones and permanent El Nino in the early Pliocene epoch. *Nature*. 2010;**463**: 1066-1070
- [17] Iglesias I, Avilez-Valente P, Pinho JL, Bio A, Vieira JM, Bastos L, et al. Numerical modeling tools applied to estuarine and coastal hydrodynamics: A user perspective. In: *Coastal and Marine Environments—Physical Processes and Numerical Modelling*. Rijeka: InTechOpen; 2019. pp. 1-20. DOI: 10.5772/intechopen.85521
- [18] Haase A, Eggleston D, Luettich R, Weaver R, Puckett B. Estuarine circulation and predicted oyster larval dispersal among a network of reserves. *Estuarine, Coastal & Shelf Science*. 2012;**101**:33-43
- [19] Puckett BJ, Eggleston DB, Kerr PC, Luettich R. Larval dispersal and population connectivity among a network of marine reserves. *Fisheries Oceanography*. 2014;**23**(4):342-361
- [20] Qiu C, Wan Y. Time series modeling and prediction of salinity in the Caloosahatchee River Estuary. *Water Resources Research*. 2013;**49**: 5804-5816. DOI: 10.1002/wrcr.20415
- [21] Ross AC, Najjar RG, Li M, Mann ME, Ford SE, Katz B. Sea-level rise and other influences on decadal-scale salinity variability in a coastal plain estuary. *Estuarine, Coastal and Shelf Science*. 2015;**157**:79-92
- [22] Lin J, Xie L, Pietrafesa LJ, Ramus JS, Paerl HW. Water quality gradients across Albemarle-Pamlico estuarine system: Seasonal variations and model applications. *Journal of Coastal Research*. 2007;**23**:213-229
- [23] Xia M, Xie L, Pietrafesa L. Modeling of the cape fear river estuary plume. *Estuaries and Coasts*. 2007;**30**: 698-709
- [24] Xu H, Lin J, Wang D. Numerical study on salinity stratification in the Pamlico River Estuary. *Estuarine, Coastal and Shelf Science*. 2008;**80**: 74-84
- [25] Hamrick JM. User's manual for the environmental fluid dynamics computer code. In: *Special Report in Applied Marine Science and Ocean Engineering No. 331*. Virginia: Virginia Institute of Marine Science/School of Marine Science, The College of William and Mary; 1996
- [26] Rathbun SL. Spatial modeling in irregularly shaped regions: Kriging estuaries. *Environmetrics*. 1998;**9**: 109-129
- [27] Chehata M, Jasinski D, Monteith MC, Samuels WB. Mapping three-dimensional water-quality data in the Chesapeake Bay using Geostatistics 1. *Journal of the American Water Resources Association*. 2007;**43**:813-828
- [28] Urquhart EA, Zaitchik BF, Hoffman MJ, Guikema SD, Geiger EF. Remotely sensed estimates of surface salinity in the Chesapeake Bay: A statistical approach. *Remote Sensing of the Environment*. 2012;**123**:522-531
- [29] Bales JD. Effects of hurricane Floyd inland flooding, September–October 1999, on tributaries to Pamlico Sound, North Carolina. *Estuaries and Coasts*. 2003;**26**:1319-1328
- [30] Bales JD, Robbins JC. Simulation of Hydrodynamics and Solute Transport in the Pamlico River Estuary, North Carolina. US Geological Survey, Raleigh,

NC (USGS Open-file Rep. No. 94-454); 1995

[31] Lilly JP. The Roanoke River and Albemarle sound. In: Jones FB, Phelps SB, editors. *Washington County, NC: A Tapestry*. Winston-Salem, NC: Jonsten Printing Company; 1998

[32] Paerl HW, Bales JD, Ausley LW, Buzzelli CP, Crowder LB, Eby LA, et al. Ecosystem impacts of three sequential hurricanes (Dennis, Floyd, and Irene) on the United States' largest lagoonal estuary, Pamlico Sound, NC. *Proceedings of the National Academy of Sciences*. 2001;**98**:5655-5660

[33] Ramus J, Eby LA, McClellan CM, Crowder LB. Phytoplankton forcing by a record freshwater discharge event into a large lagoonal estuary. *Estuaries and Coasts*. 2003;**26**:1344-1352

[34] Gardner B, Sullivan PJ, Lembo AJ. Predicting stream temperatures: Geostatistical model comparison using alternative distance metrics. *Canadian Journal of Fisheries and Aquatic Sciences*. 2003;**60**:344-351

[35] Peterson EE, Urquhart NS. Predicting water quality impaired stream segments using landscape-scale data and a regional geostatistical model: A case study in Maryland. *Environmental Monitoring and Assessment*. 2006;**121**:613-636

[36] Little LS, Edwards D, Porter DE. Kriging in estuaries: As the crow flies, or as the fish swims? *Journal of Experimental Marine Biology and Ecology*. 1997;**213**:1

[37] Pietrafesa LJ, Morrison JM, McCann MP, Churchill J, Bohm E, Houghton RW. Water mass linkages between the Middle and South Atlantic Bights. *Deep-Sea Research*. 1994;**41**: 365-389

[38] Xie L, Pietrafesa LJ. Systemwide modeling of wind and density driven

circulation in Croatan-Albemarle-Pamlico estuary system part I: Model configuration and testing. *Journal of Coastal Research*. 1999;**15**:1163-1177

[39] Pietrafesa LJ, Janowitz GS. Final Report on the Albemarle Pamlico Coupling Study. Raleigh, NC: NC Albemarle-Pamlico Estuarine Study; 1991. 223 pp

[40] Giese GL, Wilder HB, Parker GG. Hydrology of major estuaries and sounds of North Carolina. US Geological Survey Water-Supply Paper. 1979

[41] Paerl HW, Valdes LM, Peierls BL, Weaver RS, Gallo T, Joyner AR, et al. Ecological effects of a recent rise in Atlantic hurricane activity on North Carolina's Pamlico Sound System: Putting Hurricane Isabel in perspective. In: Sellner KG, Chesapeake Research Consortium, editors. *Hurricane Isabel in Perspective*. Edgewater, MD: CRC Publication 05-160; 2005

[42] Weaver JC. The drought of 1998–2002 in North Carolina—Precipitation and hydrologic conditions. Report U.S. Geological Survey Scientific Investigations Report 2005-5053. 2005. 88 pp

[43] Brinson MM, Bradshaw HD, Jones MN. Transitions in forested wetlands along gradients of salinity and hydroperiod. *Journal of the Elisha Mitchell Scientific Society*. 1985;**101**: 76-94

[44] Corbett DR, Vance D, Letrick E, Mallinson D, Culver S. Decadal-scale sediment dynamics and environmental change in the Albemarle Estuarine System, North Carolina. *Estuarine, Coastal and Shelf Science*. 2007;**71**: 717-729

[45] Molina JR. Estuarine exchange model of the Pamlico and Albemarle sounds [M.S. thesis]. Raleigh, NC: North Carolina State University; 2002. 56 pp

[46] Peterson EE, Merton AA, Theobald DM, Urquhart NS. Patterns of spatial autocorrelation in stream water chemistry. *Environmental Monitoring and Assessment*. 2006;**121**: 569-594

[47] Jensen OP, Christman MC, Miller TJ. Landscape-based geostatistics: A case study of the distribution of blue crab in Chesapeake Bay. *Environmetrics*. 2006; **17**:605-621



---

Section 4

# Bio-processes

---



# Subtropical Coastal Lagoon from Southern Brazil: Environmental Conditions and Phytobenthic Community Structure

*Leticia Donadel and Lezilda Torgan*

## Abstract

The chapter is about the study of environmental conditions and the structure of the benthic diatoms community in Peixe Lagoon, which is inserted in a National Park in southern Brazil. The study was carried out covering four seasons from 2011 to 2012. The system is shallow (<60 cm) located parallel to the coastline, and it is connected to the ocean through a single channel, which occurs naturally or through human action. In this lagoon, during the study, the water temperature ranged between 15.3 and 32.1°C, and the dissolved oxygen presented higher value in the winter (12.5 mg.L<sup>-1</sup>) and lower value in the summer (7.5 mg.L<sup>-1</sup>). The lagoon ranged from mesotrophic to hypereutrophic conditions. The salinity varied between 1.3 and 36.2‰, and these variations were mainly related to meteorological conditions. The community of diatoms in Peixe Lagoon is composed by 62 taxa distributed in 30 genera composed largely of marine, brackish, and few freshwater species. Among the attributes of the community, composition better reflects the environmental variations. The opening and closing of the channel, salinity, temperature, and the action and direction of the wind are variables influencing the dynamics of the microphytobenthic community.

**Keywords:** environmental variables, diatoms, community attributes, microphytobenthos, system dynamic

## 1. Introduction

The shallow coastal lagoons are low depth water column mixing systems in which phytoplankton and microphytobenthos communities, microscopic eukaryotic photosynthetic algae, and cyanobacteria which live on the seabed [1] play a key role in the primary production and recycling of matter and nutrients. The role of microphytobenthos is quite important where macrophytes are absent and light radiation penetrates down to the bottom [2].

Microphytobenthos are composed of a set of microorganisms distributed in very diversified taxonomic groups, among which the diatoms are an important and often dominant component in estuarine and shallow coastal environments. These algae have varied adaptive strategies for adhesion and migration on different substrates, and there is a very large number of species sensitive to environmental changes.

Traditionally, benthic diatoms are classified according to the substrate in which they live. Those that live on thin sediment are called epipellic and those that live on sandy substrate are called epipsammic [3].

Diatoms studies in coastal lagoon were mainly concentrated in the world's largest water bodies, the Baltic, Black, and Caspian seas, which are ecosystems impacted by the anthropogenic actions and global climate changes. The eutrophication happened due to the increased nitrogen and phosphorus loads during the last century, and the increase in water temperature related to climate was detected by the changes in subfossil diatom assemblages. The accumulation of heavy metals from surrounded waters can be monitored due to the capacity of these algae to accumulate metals attached to the outside of the cell wall. There is an excellent literature review about these and other impacts; see the Snoeijs and Weckström chapter [4]. We can also find excellent information about the composition, spatial distribution of modern diatom assemblages, diversity, production, and ecology of the sediment-inhabiting diatoms in the estuaries [5–11]. In the smaller shallow lagoon from the east coast of Uruguay (South America) the diatoms studies were used to infer the paleosalinity, trophic and climate changes in relation to the sea level variation [12–16].

So far, most studies concentrated on phytoplankton at Patos Lagoon [17–24], Tramandaí-Armazém Lagoon [25–29], and Peixe Lagoon [30–34]. Regarding microphytobenthic, studies were limited to salt marshes and to the Patos Lagoon estuary [35–43].

The knowledge of the diatoms at Peixe Lagoon began with investigations on diatom assemblages in current and fossil sediments that allowed paleoenvironmental reconstruction. It demonstrated that the lagoon behaved as a deeper and more extensive lagoon system connected to the ocean by one or more permanent linking channels during the Holocene [44]. Later, studies were carried out on the taxonomic composition of diatoms in the marginal sediment of the lagoon. One study emphasizes the genus *Diploneis* Ehrenb. ex Cleve, rich in species [45]. Another investigation highlights the occurrence of *Cocconeis sawensis* Al-Handal et Riaux-Gobin, recently described for saline lakes in southern Iraq as an epiphyte in *Chara* sp. Linnaeus (1753: 1156). It was also recorded on an island in the South Pacific and epizoic on manatee in Florida Bay, USA [46]. The other species of the community were described, illustrated, and compiled with information on ecology and distribution in these coastal systems [47].

Studies about phytoplankton in subtropical coastal lagoon from south of Brazil showed that the structure and dynamic of the phytoplanktonic community were regulated by hydrological factors (inflow-outflow of continental and coastal waters in the system) as well as by meteorological conditions (wind and rainfall) and limnological variables (temperature and salinity) [18, 19, 33]. We have a set of factors that can act simultaneously while being difficult to recognize a main factor. Our question is to know if the structure and dynamic of the benthic diatoms in the Peixe Lagoon are related with these same factors. In order to answer this question, the study objectives were: (1) to know the composition of the diatoms community; (2) to verify the community structure and its spatial and temporal variation; and (3) to relate the variations of the community to environmental variables over an annual cycle.

In this chapter, firstly, we present information about the geographic, environmental, and climatic features where the Peixe Lagoon is situated. To be a case study, the methods are also included. Secondly, we describe the physical and chemical conditions of the lagoon and the benthic diatoms composition. Thirdly, we present and discuss the environmental variables related to the composition and spatial and temporal variation of the community attributes. Finally, we review the relationships of organisms occurring in plankton and sediment that should not be overlooked in studies in shallow coastal lagoons.

## 2. Study area

Peixe Lagoon is the only intermittent lagoon of the extreme south of Brazil and it is situated in the Lagoa do Peixe National Park (31°00'46" S; 51°09'51" W and 31°29'00" S; 50°46'31" W). This park is recognized by the Ramsar Convention as a Wetlands site, as well as an area of the UNESCO Atlantic Forest Biosphere Reserve, an Important Bird and Biodiversity Area (IBA) and a designated site of international importance by the Western Hemisphere Shorebird Reserve Network (WHSRN). The coast is characterized by a microtidal regime, with a mean amplitude of 0.45 m [48].

Peixe Lagoon is a shallow, elongated system (35 km long and 1 km wide), parallel to the coastline (**Figure 1**) connected to the Atlantic Ocean through a single narrow channel (choked lagoon) (**Figure 2**). The channel occlusion occurs due to deposition of sand caused by the predominance of the north and northeast winds [49, 50]. The connection with the ocean usually occurs during winter and spring, when the precipitation becomes more pronounced and the marshes and fields marginal to the lagoon are flooded. During these periods, an artificial opening of the channel is carried out by means of machines, since a natural opening only occurs sporadically [50]. The margins of the lagoon are covered by salt marshes vegetation dominated by *Paspalum vaginatum* Sw., *Cotula coronopifolia* L., *Sporobolus montevidensis* (Arechavaleta) P.M. Peterson & Saarela (= *Spartina densiflora* Brong), *Hydrocotyle bonariensis* Lam., *Androtrichum trigynum* (Spreng.) H. Pfeiff., *Bacopa monnieri* (L.) Wettst., and *Juncus acutus* L. [51]. The surface sediments at the bottom are essentially sandy. On the sites with greater depth of the lagoon, the sediments are thinner, with addition of silt and clay [49].

The system is located in subtropical climate where the rainfall is distributed throughout the year. In the period of studies, the highest rainfall (145.8 mm) occurred at the end of the fall (June 2011), decreasing in the following months and then increasing (131.2 mm) in early spring (October 2011). November had the lowest cumulative precipitation (23.0 mm). The average monthly temperature varied between 12.6 and 18°C in the autumn/winter seasons and between 18.3 and 24.4°C in spring/summer (**Figure 3**).

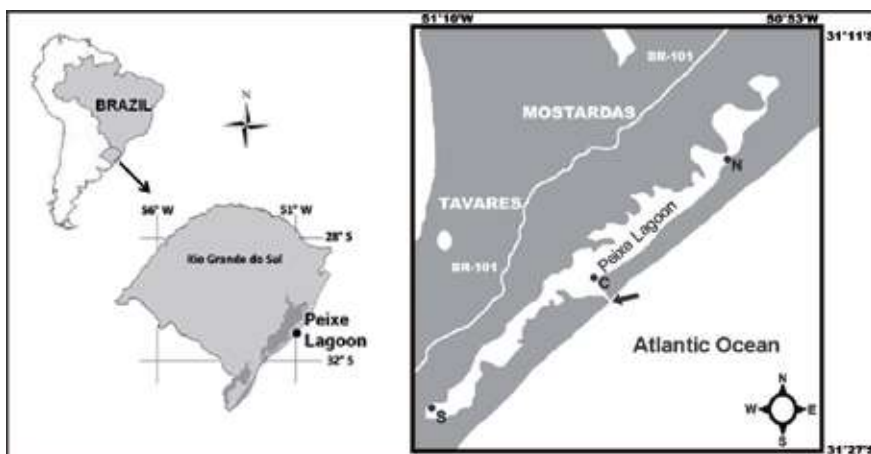


**Figure 1.** Location of Peixe Lagoon area in the state of Rio Grande do Sul, southern Brazil, the sampling stations (North = N, Center = C, South = S) and the channel of connection with ocean (arrow).



**Figure 2.**  
Aerial view of the Peixe Lagoon channel. Source: Lagoa do Peixe National Park (PNLP).

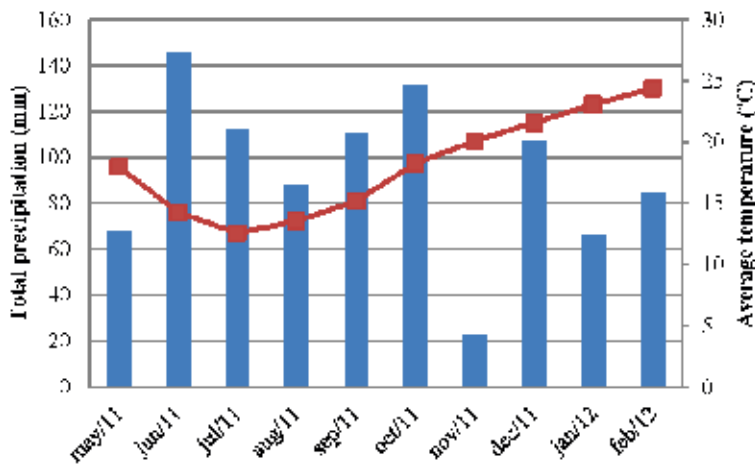


**Figure 3.**  
Total precipitation (mm) and average monthly temperature (°C) recorded by the meteorological station of Mostardas/RS. Source: National Institute of Meteorology (INMET).

### 3. Methods

#### 3.1 Sampling

The study was based on samples collected at three sampling stations in the lagoon. North (**Figure 4**) is close to a narrow channel that interconnects the northernmost sealed bodies with a central portion of the lagoon; Center (**Figure 5**) is next to the channel that connects to the ocean; and South (**Figure 6**) is at the south end of the lagoon. Sampling occurred in the four seasons, fall (June 2011), winter (August 2011), spring (November 2011), and summer (February 2012). During the first sampling, in the fall, the channel was closed. It was open days before winter sampling and remained open for the remainder of the sampling period. For the diatoms analysis, sediment samples were collected at depths of 2 cm with a spatula, at the lagoon margin, and packed in glass pods for transport to the laboratory.

#### 3.2 Abiotic variable

Conductivity ( $\text{mS}\cdot\text{cm}^{-1}$ ), salinity, pH, water temperature ( $^{\circ}\text{C}$ ), dissolved oxygen—DO ( $\text{mg}\cdot\text{L}^{-1}$ ), and oxidation-reduction potential—ORP ( $\text{mg}\cdot\text{L}^{-1}$ ) were



**Figure 4.**  
*Sampling station: North.*



**Figure 5.**  
*Sampling station: Center.*



**Figure 6.**  
*Sampling station: South.*

measured with a HORIBA U52 probe. Depth and water transparency (cm) were measured with a Secchi disk. Precipitation, wind velocity, and wind direction data were obtained from the National Institute of Meteorology—INMET.

Laboratory analyses were performed as follows: total phosphorus—TP ( $\text{mg.L}^{-1}$ ) by absorptiometry reduction of ascorbic acid, total nitrogen—TN ( $\text{mg.L}^{-1}$ ), according to the Kjeldahl method (NBR 10560-1988, 13796-1997), and total silicate ( $\text{mg.L}^{-1}$ ) with the silicomolybdate method [52]. The classification of salinity was based on the Venice System [53]. Trophic level was determined by the modified system of Vollenweider [54].

### 3.3 Diatom analysis

The sediment samples (1g) were dried in an oven and cleaned with potassium permanganate and hydrochloric acid according to the Simonsen technique [55]. For light microscopy (LM) analyzed, a Zeiss Axioplan Microscope (Carl Zeiss, Oberkochen, Germany) was used. The relative abundance of the taxa was carried out in slides seeking the minimum sample efficiency of 80% [56]. Species richness was estimated by the number of taxa present in the samples. The specific diversity was assessed using Shannon index ( $H'$ ) [57] and Evenness equitability ( $E$ ). The analysis of variance (ANOVA) was applied to test the significance among the community attributes, since the data presented a normal distribution. The PAST® software was used for these analyzes. The relationship between biotic and abiotic variables with canonical correspondence analysis (CCA), PC-ORD® version 6.08 was used. For the construction of the biotic matrix, only species with a frequency equal to or >5% were considered in at least one sample unit and for the abiotic matrix, 10 environmental variables were included (**Table 1**). The data were transformed into  $\log_{10}(x + 1)$  in order to normalize the variances [58]. The Monte Carlo permutation test was carried out to verify the significance of the ordination axes.

	Fall			Winter			Spring			Summer		
	N	C	S	N	C	S	N	C	S	N	C	S
Depth	67	25	25	60	20	20	80	30	30	50	25	42
Secchi	67	15	25	30	20	0	60	25	30	50	25	12
Temp	15.5	17.2	17.5	17.0	7.6	17.4	26.5	26.	29.3	29.8	32.1	31.9
pH	7.9	7.6	8.1	7.6	8.0	7.7	7.9	8.2	8.5	8.1	8.5	8.2
ORP	275	282	262	230	297	253	275	205	202	211	108	214
Cond	10.7	13.3	12.3	12.3	11.5	12.1	10.7	9.8	9.3	7.5	9.0	9.4
Salin	31.2	28.3	30.8	4.5	17.0	1.3	7.3	30.2	30.0	31.9	36.0	29.5
Cond	10.7	13.3	12.3	12.3	11.5	12.1	10.7	9.8	9.3	7.5	9.0	9.4
Sil	1.8	1.7	1.1	1.0	18.0	1.4	1.0	2.7	6.6	7.8	0.0	0.1
PT	0.03	0.07	0.08	0.15	0.12	0.06	0.08	0.13	0.07	0.07	0.03	0.06
NT	0.6	0.10	0.43	0.87	0.68	0.90	0.01	0.09	0.02	0.55	0.65	0.50

**Table 1.**

Physical and chemical variables analyzed in Peixe Lagoon in the four seasons, from June 2011 to February 2012, in the North (N), Center (C), and South (S) sampling stations. Depth (cm); Secchi = Secchi transparency (cm); temp = temperature ( $^{\circ}\text{C}$ ); ORP = oxide-reduction potential (mV); cond = conductivity ( $\text{mS}\cdot\text{cm}^{-1}$ ); DO = dissolved oxygen, salin = salinity (ppt); sil = silica ( $\text{mg}\cdot\text{L}^{-1}$ ); PT = total phosphorus ( $\text{mg}\cdot\text{L}^{-1}$ ); NT = total nitrogen ( $\text{mg}\cdot\text{L}^{-1}$ ).

## 4. Environmental conditions

The lagoon has a mean depth (<60 cm) and the Secchi disk depth generally coincides with the total depth. The water temperature varies between 15.3 and 17.6 $^{\circ}\text{C}$  in the colder seasons (fall and winter) and from 26.1 to 32.1 $^{\circ}\text{C}$  in the hottest seasons (spring and summer). The pH varies from 7.6 to 8.8 and the oxidation-reduction potential as well as the dissolved oxygen present similar trends, with higher values in the cold seasons and lower in the hot seasons (**Table 1**).

In relation to nutrients, total phosphorus varies between 0.03 and 0.08  $\text{mg}\cdot\text{L}^{-1}$  in fall and summer at 0.12–0.15  $\text{mg}\cdot\text{L}^{-1}$  in winter and spring, from eutrophic to hyper-eutrophic conditions. Total nitrogen presented higher values (0.68–0.90  $\text{mg}\cdot\text{L}^{-1}$ ) in winter (mesoeutrophic conditions), with a decline in spring (0.01–0.09  $\text{mg}\cdot\text{L}^{-1}$ ) and elevation in the summer (0.55–0.65  $\text{mg}\cdot\text{L}^{-1}$ ), changing to mesotrophic conditions. Silica concentrations are higher in winter sampling (mean of 17.5  $\text{mg}\cdot\text{L}^{-1}$ ). When the

channel of connection with ocean was open, the total nitrogen concentrations at all stations elevated as well as the total phosphorus in the north and center in winter. This may have been due to the water runoff from the land around the lagoon, used for livestock (**Table 1**).

The salinity demonstrated outstanding spatial and seasonal variations. These variations were mainly related to the meteorological conditions. Spatially, the salinity varies between 1.3‰ in the South station in the winter (oligohaline zone) and 36.2‰ in the Center during the summer (euhaline zone). The station with the highest salinity variation is the North (4.5‰ min./winter and 34.9‰ max./summer), followed by the South station (1.3‰ min./winter and 29.5‰ max./summer). The Center station maintained higher values of salinity in all the climatic seasons due to its proximity with the ocean. Seasonally, salinity has the highest values in summer and the lowest in winter. These low values can be attributed to the action of the wind, predominantly northeast, that propelled the waters from the Ruivo Lake which are less saline, to the Peixe Lagoon [33]. In the summer, the decrease of the precipitation and intensity of the wind causes the outstanding increase of the salinity. This dynamic was also observed in the system from 1991 to 1996 [50]. The South station of the lagoon presents less marine influence, therefore, lower salinity.

The variation of water levels of the lagoon is also strongly controlled by the winds regime, both intensity and direction, as well as precipitation. In the periods of predominant south wind (fall) and low precipitation (spring), the lowest levels of depth were observed. The Center is located next to the connection channel with the ocean and has a low average depth (30 cm). It is constantly saline (poly to euhaline zone). Due to the predominant northeasterly winds for most of the year, the water body of the lagoon is pushed to the west bank. The variation of the intensity of the winds can vary in the periods of day and night, causing great extensions of marginal sediment to be exposed and to be submerged again in a matter of hours [50].

The wind velocity during the period of studies had the lowest averages in the fall. It intensified in the following months of winter, with a peak in August

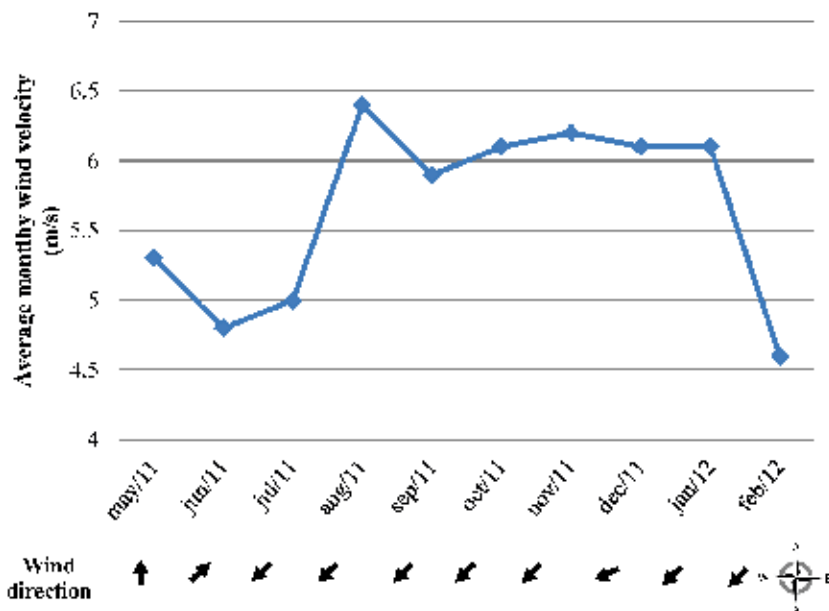


**Figure 7.** Average monthly wind velocity (m/s) and predominant monthly wind direction (arrows indicate direction). Data recorded by the Meteorological Station of Mostardas/RS. Source: INMET.



the predominance of biraphid and monoraphid diatoms, which are organisms that have raphe. This structure is a selective characteristic of the epipelagic species [59–63] because it promotes the movement of organisms in search for better light and humidity conditions, since it allows the secretion of polymeric substances produced by their cells.

## 6. Structure of the community *versus* environmental conditions

### 6.1 Spatial and temporal variation

The community attributes (richness, diversity, and evenness) showed a decreasing spatial gradient from the North to the South stations. The specific diversity ranged between 2.3 bits/ind. at North and 0.4 bits/ind. at South and the evenness varied between 74 and 20% at North and South stations.

Seasonally, in fall, without connection with the ocean, the community attributes presented the highest values. After the channel opening, the richness was similar in winter and spring, rising in the summer. The values of evenness and diversity increased from winter (0.6–1.7 bits/ind.) to summer (0.8–2.3 bits/ind.) (**Figure 8**). However, these attributes did not differ significantly between the seasons and the station sampling.

### 6.2 Diatoms composition related to environmental variables

The composition of the diatoms and the physical and chemical variables of the water in the canonical correspondence analysis (**Figure 9**) of the abundant species (25 species with more than 5% abundance) can better demonstrate the community dynamics in the system.

The sampling units of the South station are grouped on the negative side of axis 1. They were related to the lower values of conductivity and salinity. The species associated with this axis were *Cocconeis sawensis*, *Fragilaria eichhornii*, *Cocconeis euglypta*, *Fallacia florinae*, and *Halamphora coffeaeformis*. In this axis, it is also possible to observe the separation of the sampling units from the North, mainly due to the difference in temperature between hot and cold seasons, in fall and winter months. The related species were *Nitzschia scalpelliformis*, *Luticola simplex*, *Ehrenbergia granulosa*, *Rhopalodia runrichiae*, *Diploneis smithii*, and *D. didyma*. The sampling units of the Center station are grouped on the positive side of axis 2, where higher values of salinity and temperature were observed in the hotter seasons, as well as the lower values of silica and ORP. The species *Opephora pacifica*, *Catenula adhaerens*, and *Opephora* aff. *mutabilis* were related to this axis (**Figure 10**).

During the study, we observed periods with higher and lower marine influence, due to the opening of the channel. In fall, the only season in which the channel was closed, the composition of diatom species was distinct in the north and south of the lagoon. The south and south-west quadrant wind might also have been an influence factor for the distinction of community composition.

After the channel opening, it is possible to observe the difference in the composition of the community at the southern portion in relation to the north and center portions of the lagoon. The species highlighted in the south (*Cocconeis sawensis*, *C. euglypta*, *Fallacia florinae*, and *Halamphora coffeaeformis*) are found in brackish and marine waters, with the exception of *C. euglypta*, a characteristic species of freshwater, but it supports high conductivity water [64]. So, the marine influence appeared as one of the main factors affecting spatial diatom composition and spatial distribution in the lagoon.

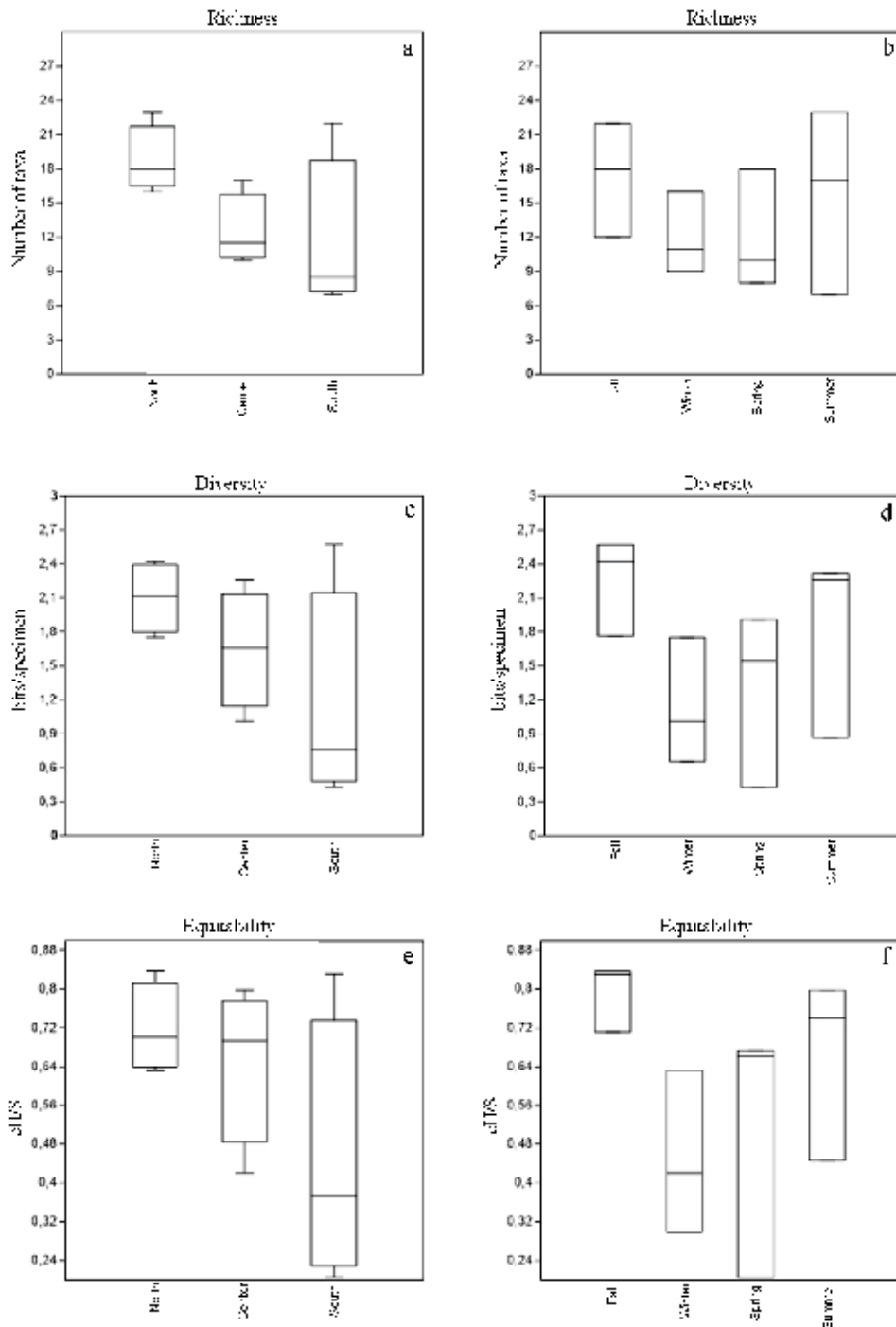


**Figure 8.** (a-f) Distribution of community attributes related to sampling stations and the seasons of the year in Peixe Lagoon from June 2011 to February 2012.

However, the salinity cannot be considered as the only driving force that determines the composition of diatom species in environments with marine influence in subtropical and temperate regions. Temperature is also considered a very important environmental factor [11]. In Peixe Lagoon, the temperature difference between hot seasons (spring and summer) and cold seasons (fall and winter) also differentiated

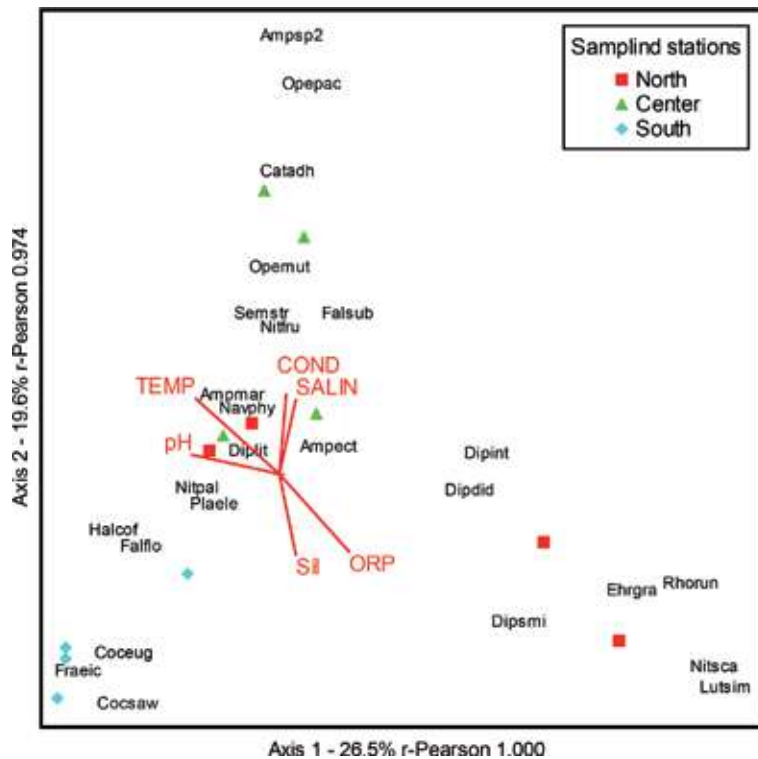


**Figure 9.** Canonical correspondence analysis (CCA) of the abundant species in the sampling stations and seasons fall, winter, spring, summer in Peixe Lagoon. For legends of the variables, see **Table 2**. *Amphora ectorii* (*Ampect*), *A. maracaiboensis* (*Ampmar*), *Amphora* sp.2 (*Ampsp2*), *Catenula adhaerens* (*Catadh*), *Cocconeis euglypta* (*Coceug*), *C. sawensis* (*Cocsaw*), *Diploneis didyma* (*Dipdid*), *D. interrupta* (*Dipint*), *D. litoralis* (*Diplit*), *D. smithii* (*Dipsmi*), *Ehrenbergia granulosa* (*Ehgrva*), *Fallacia florinae* (*Falflo*), *F. subforcipata* (*Falsub*), *Halamphora coffeaeformis* (*Halcof*), *Luticola simplex* (*Lutsim*), *Navicula phylleptosomaformis* (*Navphy*), *Nitzschia frustulum* (*Nitfru*), *N. palea* (*Nitpal*), *N. scalpelliformis* (*Nitsca*), *Opephora aff. mutabilis* (*Opemut*), *O. pacifica* (*Opepac*), *Placoneis elegantula* (*Plaele*), *Rhopalodia runrichiae* (*Rhorun*), *Seminavis strigosa* (*Semstr*), *Fragilaria eichhornii* (*Fraeic*).

the composition of the species. *Diploneis interrupta*, *D. didyma*, *D. smithii*, *N. scalpelliformis*, and *Luticola simplex* were related to the colder seasons. This was also observed for species of *Diploneis* in the sediment of sublittoral zone of the Gulf of Trieste [65]. *Catenula adhaerens*, *Nitzschia frustulum*, *Opephora aff. mutabilis*, *O. pacifica*, and *Seminavis strigosa* were related to the sampling units with higher temperatures and salinities.

### 6.3 Diatoms related to sediment

Another important factor regarding diatom distribution is the sediment characteristic [66, 67]. In the Center and South stations, the surface of the Peixe Lagoon is essentially covered by sandy sediments, in which we find *Campylosira cymbelliformis*, *Catenula adhaerens*, *Dimeregramma minus*, and *Stauropora soodensis* species usually associated with sand grains.

In deeper sites of the lagoon, such as near the North, the sediments are thinner, with addition of silt and clay [49]. In this station, where muddy sand is present, we observed more clearly the seasonal variation of the diatom community. This site also showed highest diversity (1.7–2.4 bits/ind.) and richness (16–26 táxons) and the presence of more exclusive epipelagic species; among these are the following: *Caloneis permagna*, *Luticola simplex*, *Nitzschia dissipatoides*, *N. scalpelliformis*,

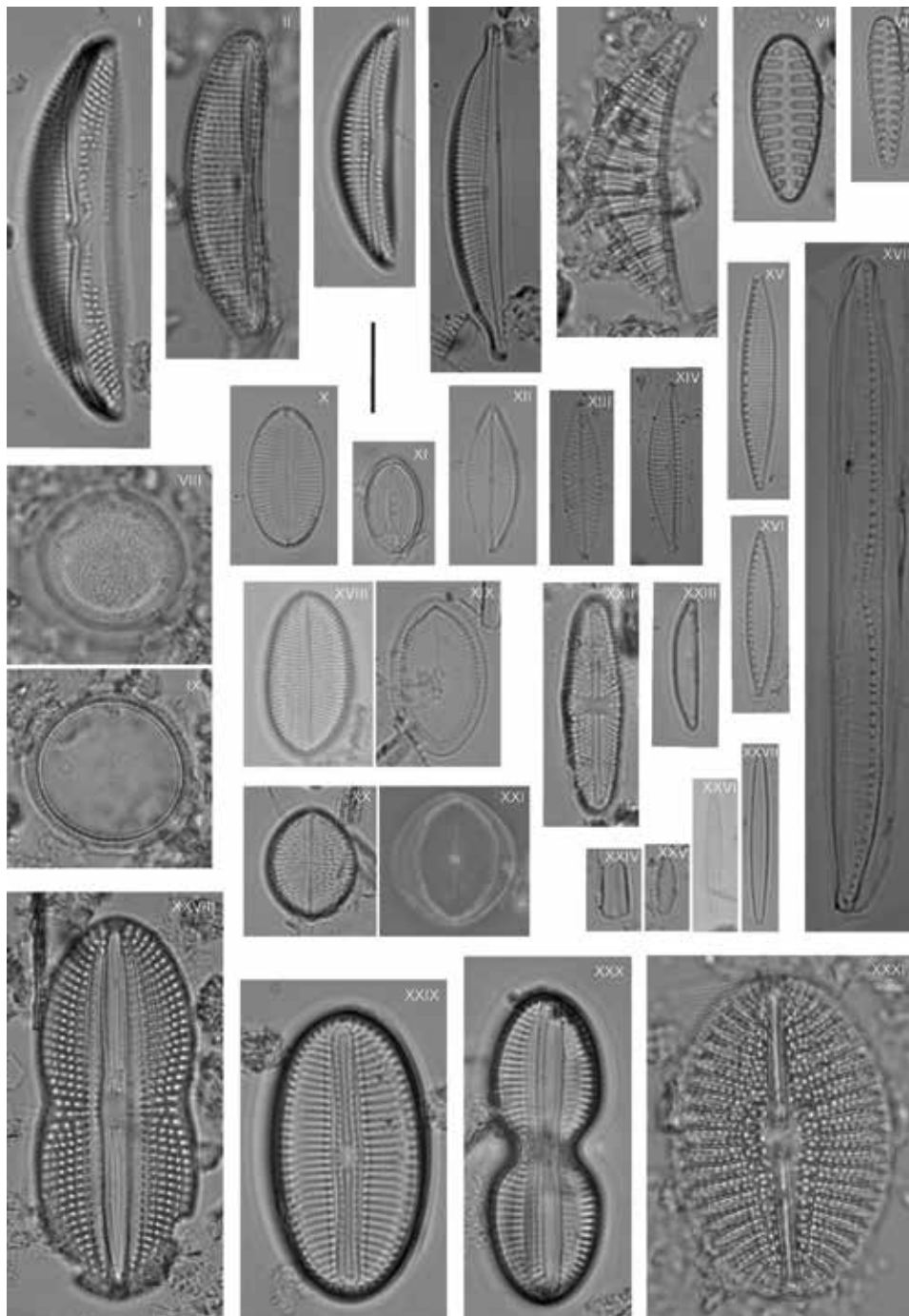


**Figure 10.**

I. *A. maracaiboensis*. II. *Amphora* sp. 2. III. *A. ectorii*. IV. *Halamphora coffeaeformis*. V. *Rhopalodia runrichiae*. VI. *Opephora pacifica*. VII. *O. aff. mutabilis*. VIII, IX. *Erhembergia granulosa*. X. *Fallacia subforcipata*. XI. *F. florinae*. XII. *Placoneis elegantula*. XIII. *Navicula phylleptosomaformis*. XIV. *Seminavis strigosa*. XV. *Nitzschia frustulum*. XVI. *N. palea*. XVII. *N. scalpelliformis*. XVIII, XIX. *Cocconeis euglypta*. XX, XXI. *C. sawensis*. XXII. *Luticola simplex*. XXIII. *Catenula adhaerens*. XXIV-XXVII. *Fragilaria eichhornii*. XXVIII. *Diploneis didyma*. XXIX. *D. litoralis* var. *clathrata*. XXX. *D. interrupta*. XXXI. *D. smithii*. Scale bar = 10  $\mu$ m.

*N. vitrea* var. *salinarum*, *Rhopalodia runrichiae*, and *Terpsinöe americana* (Table 2). In agreement with other studies, the epipsammic fraction appeared to be much more stable than epipellic assemblage [9, 67].

## 7. Sediment and water interaction

We expected to find planktonic forms in the sediment due to the low depth of the lagoon and because of the fact that the sediment usually integrates planktonic and periphytic taxa [3]. The absence of planktonic forms could be explained by the hydrographic processes that tend to transport nonliving, unattached forms out of the system, similar to estuaries [67]. Furthermore, the location of the sampling stations, since the material was collected on the lagoon margin, was outside the water surface. However, it is known that in periods with decreasing wind intensity, water tend to return flooding areas that had been exposed [50]. A few planktonic species in the sediment were also recorded in a study of microphytobenthos in the Gulf of Trieste, Europe, although the collections were made in submerged sediment [65].

Comparing with an earlier study about phytoplankton at Peixe Lagoon, with sampling performed during the same period, *Asterionellopsis glacialis* (Castracane) Round, *Chaetoceros gracillis* Pantocsek, and *Skeletonema potamos* (Weber) Hasle were found in abundance in plankton samples. In this study, however, these species were not found in the sediment; whereas *Diploneis didyma*, a highlighted species found in benthos, was also present in the plankton. The species *Cocconeis sawensis* was recorded at the southern benthos of the lagoon, and it was also observed in the plankton and epiphyton in association with the macroalgae *Cladophora* sp. in the fall and winter seasons [33, 46]. This suggests that in shallow environments, the plankton receives a greater contribution of benthic species than the opposite. Similar results were found in shallow estuarine zone of Patos Lagoon [19].

Estuary and shallow coastal waters develop the process of resuspension whereby sediment particles with diatoms enter the water column. Examination of diatoms in the water revealed that 75% of frustules belonged to pennate forms and we concluded that flooding tides were responsible for a net transport of epipelagic diatoms from the mudflat to a salt marsh. The resuspension of the diatoms can be the source of the chl *a* peak in the plankton [68]. So, this organism may greatly augment the primary production in water [69, 70]. Other investigations have showed large number of benthic diatoms in the water column [71, 72]. The wind, flooding tides, and tidal inducing waves and currents are the causes of this process.

## 8. Conclusions

In the Peixe Lagoon, the benthic diatoms were present in high diversity. Among the attributes of the community, the taxonomic composition best responded to the environmental variables. The quantitative attributes did not show significant relationships. The connection with the ocean, salinity, rainfall, wind action, and temperature were strongly related to the spatial and seasonal variation of the composition of the diatom community in this lagoon system. These organisms substantiate their use as indicators of environmental variations, mainly regarding salinity and temperature in subtropical coastal systems.

## Acknowledgements

We thank the Conselho Nacional de Desenvolvimento Científico e Tecnológico-Programa de Capacitação em Taxonomia (CNPq-PROTAX) for the financial support and Coordenação de Aperfeiçoamento de Pessoal de Nível Superior (CAPES) for a doctoral grant to the first author and to CNPq for Productivity Grant to the second author. This study was financed in part by the Coordenação de Aperfeiçoamento de Pessoal de Nível Superior—Brasil (CAPES)—Finance Code 001.

## **Author details**

Leticia Donadel\* and Lezilda Torgan  
Postgraduate Program in Botany, Department of Botany, Federal University of Rio Grande do Sul, Porto Alegre, Rio Grande do Sul, Brazil

\*Address all correspondence to: leticiadonadel@yahoo.com.br

## **IntechOpen**

---

© 2019 The Author(s). Licensee IntechOpen. This chapter is distributed under the terms of the Creative Commons Attribution License (<http://creativecommons.org/licenses/by/3.0>), which permits unrestricted use, distribution, and reproduction in any medium, provided the original work is properly cited. 

## References

- [1] MacIntyre HL, Geider RJ, Miller DC. Microphytobenthos: The ecological role of the “Secret Garden” of unvegetated, shallow-water marine habitats. I. Distribution abundance and primary production. *Estuaries*. 1996;**19**:186-201
- [2] Facca C, Sfriso A, Socal G. Temporal and spatial distribution of diatoms in the surface sediments of the Venice Lagoon. *Botanica Marina*. 2002;**45**:170-183
- [3] Round F, Crawford R, Mann D. *The Diatoms. Biology and Morphology of the Genera*. 1st ed. Cambridge: Cambridge University Press; 1990. p. 747
- [4] Snoeijs P, Weckström K. Diatoms environmental change in large brackish-water ecosystems. In: Stoermer EF, Smol JP, editors. *The Diatoms: Applications for the Environmental and Earth Sciences*. 2nd ed. United Kingdom: Cambridge University Press; 2010. pp. 287-308
- [5] Admiraal W. The ecology of estuarine sediment-inhabiting diatoms. In: Round FE, Chapman D J, editors. *Progress in Phycological Research*. Bristol: Biopress. 1984;**3**:269-322
- [6] Cahoon LB, Cooke JE. Benthic microalgal production in Onslow Bay, North Carolina, USA. *Marine Ecology Progress Series*. 1992;**84**:185-196
- [7] Cahoon LB, Beretich GR, Thomas CJ, McDonald AM. Benthic microalgal production at Stellwagen Bank, Massachusetts Bay, USA. *Marine Ecology Progress Series*. 1993;**102**:179-185
- [8] Trobajo R, Sullivan MJ. Applied diatom studies in estuaries and shallow coastal environments. In: Stoermer EF, Smol JP, editors. *The Diatoms: Applications for the Environmental and Earth Sciences*. 2nd ed. United Kingdom: Cambridge University Press; 2010. pp. 309-323
- [9] Ribeiro LLCS. Intertidal benthic diatoms of the Tagus estuary: Taxonomic composition and spatial-temporal variation [thesis]. Lisboa: Universidade de Lisboa; 2010
- [10] Hassan GS, Espinosa MA, Isla FI. Modern diatom assemblages in surface sediments from estuarine systems in the southeastern Buenos Aires Province, Argentina. *Journal of Paleolimnology*. 2006;**35**:39-53. DOI: 10.1007/s10933-005-6444-8
- [11] Espinosa MA, Isla FI. Modern diatom assemblages in surface sediments from meso-macrotidal estuaries of Patagonia, Argentina. *Pan-American Journal of Aquatic Sciences*. 2015;**10**:20-43
- [12] García-Rodríguez F, Metzeltin D, Sprechmann P, Trettin R, Stams G, Beltrán-Morales LF. Upper and Holocene paleosalinity and trophic state changes in relation to sea level variation in Rocha Lagoon, southern Uruguay. *Journal of Paleolimnology*. 2004;**32**:117-135
- [13] García-Rodríguez F, Sprechmann P, Metzeltin D, Scafati L, Melendi DL, Volkheimer W, et al. Holocene trophic state changes in relation to sea level variation in Lake Blanca, S E Uruguay. *Journal of Paleolimnology*. 2004;**31**: 99-115. DOI: 10.1023/B:JOPL.0000013281.31891.8e
- [14] García-Rodríguez F. Inferring paleosalinity trends using the chrysophyte cyst to diatom ratio in coastal shallow temperate/subtropical lagoons influenced by the sea level changes. *Journal of Paleolimnology*. 2006;**36**:165-1173. DOI: 10.1007/s10933-006-0011-9

- [15] del Puerto L, García-Rodríguez F, Inda H, Bracco R, Castineira C, Adams JB. Paleolimnological evidence of Holocene climate changes in Lake Blanca, southern Uruguay. *Journal of Paleolimnology*. 2006;**36**:151-163. DOI: 10.1007/s10933-006-0012-8
- [16] García-Rodríguez F, Stutz S, Inda H, Puerto Ld, Bracco R, Panario D. A multiprox approach to inferring Holocene paleobotanical changes linked to sea-level variation, paleosalinity levels, and shallow lake alternative states in Negra Lagoon, SE Uruguay. *Hydrobiologia*. 2010;**646**:5-20. DOI: 10.1007/s10750-010-0184-0
- [17] Torgan L, Garcia-Baptista M, Odebrecht C, Möller O. Distribuição vertical do fitoplâncton na Laguna dos Patos, Rio Grande do Sul, Brasil (verão, 1986). *Acta Limnologica Brasiliensia*. 1995;**7**:67-77
- [18] Torgan L. Estrutura e dinâmica da comunidade fitoplanctônica na Laguna dos Patos, Rio Grande do Sul, Brasil, em um ciclo anual [thesis]. São Paulo: Universidade Federal de São Carlos; 1997
- [19] Torgan L, Tundisi J, Niencheski L. Seasonal variation of planktonic diatoms in Patos Lagoon, Southern Brazil. In: Jacob J editor. *Proceedings of the 15th Diatom Symposium*. Tuggell: A.R.G. Gantner Verlag; 2002. pp. 459-470
- [20] Torgan L, Odebrecht C, Niencheski L. Variação espacial da estrutura de tamanho do fitoplâncton na Laguna dos Patos, Sul do Brasil. *Atlantica*. 2000;**22**:95-111
- [21] Torgan L, Raupp S. Morfologia externa de *Melosira moniliformis* (O.F. Müller) C. Agardh var. *moniliformis* (Bacillariophyta) do estuário da laguna dos Patos, Rio Grande do sul, Brasil. *Iheringia, Série Botânica*. 2001;**56**:185-196
- [22] Torgan L, Pillar V, Niencheski F. Phytoplankton associations of a coastal lagoon in south of Brazil. *Journal of Coastal Research*. 2006;**39**:1149-1151
- [23] Torgan L, Becker V, Santos C. *Skeletonema potamos* (Bacillariophyta) in Patos Lagoon, southern Brazil: Taxonomy and distribution. *Revista Peruana de Biología*. 2009;**16**(1):93-96
- [24] Odebrecht C, Bergesch M, Medeanic S, Abreu P. A comunidade de microalgas. In: Seeliger U, Odebrecht C, editors. *O estuário da Lagoa dos Patos: um século de transformações*. Editora da FURG: Rio Grande; 2010. pp. 49-63
- [25] Rosa Z, Callegaro V. Diatomáceas da Lagoa Tramandaí e da Lagoa do Armazém, Rio Grande do Sul, Brasil: I—Gênero *Navicula* Bory. *Iheringia, Série Botânica*. 1988;**37**:17-32
- [26] Rosa Z, Miranda-Kiesslich A. O gênero *Pediastrum* Meyen (Chlorococcales-Hydrodictyceae) no sistema lagunar da Região Litoral do Rio Grande do Sul, Brasil. *Iheringia, Série Botânica*. 1988;**38**:149-169
- [27] Werner V. Cianofíceas planctônicas da Lagoa de Tramandaí e da Lagoa do Armazém, Rio Grande do Sul, Brasil. *Iheringia, Série Botânica*. 1988;**37**:33-70
- [28] Rosa Z, Werner V. Diatomáceas da Lagoa Tramandaí e da Lagoa do Armazém, Rio Grande do Sul, Brasil: II—Gêneros *Gyrosigma* Hassal, *Pleurosigma* W. Smith e *Mastogloia* Thwaites. *Iheringia, Série Botânica*. 1993;**43**:67-87
- [29] Rosa Z, Werner V, Dacroce L. Diatomáceas da Lagoa de Tramandaí e da Lagoa Armazém, Rio Grande do Sul, Brasil: III—Ordem Centrales. *Iheringia, Série Botânica*. 1994;**45**:29-55
- [30] Werner V. Cyanophyceae/ Cyanobacteria no sistema de lagoas e lagunas da planície costeira do Estado do

Rio Grande do Sul, Brasil [thesis]. São Paulo: Universidade Estadual Paulista; 2002

[31] Werner V, Sant'anna C. A new species of *Aphanothece* (Cyanophyceae, Chroococcales) from a shallow coastal lagoon, south Brazil. Nova Hedwigia. 2000;**70**:113-125

[32] Werner V, Sant'anna C. Occurrence of the rare genus *Microcystis* P. Richter (*Chroococcales*, *Cyanobacteria*) in a coastal lagoon from southern Brazil. Revista Brasileira de Botânica. 2006;**29**:183-186. DOI: 10.1127/nova.hedwigia/70/2000/113

[33] Donadel L, Cardoso L, Torgan L. Plankton community dynamics in a subtropical lagoonal system and related factors. Anais da Academia Brasileira de Ciências. 2016;**88**:249-267. DOI: 10.1590/0001-3765201520150022

[34] Donadel L, Torgan L. *Falcula hyalina* (Fragilariaceae, Bacillariophyta) from a coastal lagoon, southern Brazil: An additional approach on its morphology. Phytotaxa. 2016;**243**:185-189. DOI: 10.11646/phytotaxa.243.2.10

[35] Bergesch M, Odebrecht C, Abreu P. Microalgas do estuário da Lagoa dos Patos: Interação entre o sedimento e a coluna de água. Oecologia Brasiliensis. 1995;**1**:273-289

[36] Garcia M. The transfer of *Fragilaria obtusa* Hustedt to the genus *Staurosira* Ehrenberg (Bacillariophyceae). Phycological Research. 2006;**54**:87-93. DOI: 10.1111/j.1440-1835.2006.00412.x

[37] Garcia M, Talgatti D. The diatom *Anorthoneis dulcis* Hein from southern Brazil: Morphology and ecology. Research Letters in Ecology. 2008;**1**:1-5. DOI: 10.1155/2008/140245

[38] Torgan L, Donadel L, Silva J. A transferência de *Navicula sovereignae* Hustedt para o gênero *Placoneis*

Mereschkowsky (Bacillariophyta). Iheringia, Série Botânica. 2010;**65**:107-114

[39] Silva J, Torgan L, Cardoso L. Diatomáceas (Bacillariophyceae) em marismas no sul do Brasil. Acta Botânica Brasílica. 2010;**24**:935-947

[40] Talgatti D. Diatomáceas (Bacillariophyta) em marismas do sul do Brasil: Estudo da comunidade bentônica [thesis]. Porto Alegre: Universidade Federal do Rio Grande do Sul; 2014

[41] Talgatti D, Bertolli L, Torgan L. *Seminavis recta* comb. nov. et stat. nov.: Morphology and distribution in salt marshes from southern Brazil. Fottea. 2014;**14**:141-148. DOI: 10.5507/fot.2014.011

[42] Talgatti D, Sar E, Torgan L. *Haslea sigma* (Naviculaceae, Bacillariophyta) a new sigmoid benthic species from salt marshes of southern Brazil. Phytotaxa. 2014;**177**:231-238. DOI: 10.11646/phytotaxa.177.4.4

[43] Talgatti D, Wetzel C, Morales E, Ector L, Torgan L. Transfer of *Fragilaria atomus* Hust. To the genus *Stauroforma* (Bacillariophyta) based on observation of type and newly collected material. Phytotaxa. 2014;**158**:43-56. DOI: 10.11646/phytotaxa.158.1.3

[44] Santos C. Assembléias de diatomáceas em sedimentos Holocênicos no extremo sul do Brasil: Reconstruções paleoambientais [dissertation]. Porto Alegre: Universidade Federal do Rio Grande do Sul; 2011

[45] Pacheco C, Bertolli L, Donadel L, Torgan L. O gênero *Diploneis* Ehrenberg ex Cleve (Bacillariophyceae) em marismas do sul do Brasil. Iheringia, Série Botânica. 2016;**71**:331-355

[46] Donadel L, Torgan L, Al-Handal A. Additional morphological features of the epiphytic diatom *Cocconeis*

- sawensis* Al-Handal & Riaux-Gobin (*Cocconeidaceae*, *Bacillariophyta*) from a coastal lagoon, southern Brazil. *Phytotaxa*. 2018;**371**:217-229. DOI: 10.11646/phytotaxa.371.3.5
- [47] Donadel L, Torgan L. Benthic diatoms from lagoon system in the National Park Lagoa do Peixe southern Brazil. *Biota Neotropica*. (forthcoming)
- [48] Toldo EE Jr, Dillenburg SR, Almeida LESB, Tabajara LL, Martins RR, Cunha LOBP. Parâmetros morfodinâmicos da praia de Imbé, RS. *Pesquisas em Geociências*. 1993;**20**:27-32
- [49] Arejano T. Geologia e Evolução Holocênica do Sistema Lagunar da “Lagoa do Peixe”, Litoral Médio do Rio Grande do Sul, Brasil [dissertation]. Porto Alegre: Universidade Federal do Rio Grande do Sul; 2006
- [50] Knak R. Relatório Técnico Final. In: Knak R. (coord.) Projeto caracterização ambiental do Parque Nacional da Lagoa do Peixe. Rio Grande: Fundação Universidade de Rio Grande; 1998. p. 1-327
- [51] Costa CS, Tagliani PR. Cobertura vegetal e uso preponderante do espaço. In: Tagliani PRA, editor. *Ecologia da paisagem da restinga da Lagoa dos Patos: Uma contribuição para o manejo e conservação da Reserva da Biosfera*. Rio Grande: Editora da Furg; 2011. p. 184
- [52] American Public Health Association (APHA). *Standard Methods for Examination of Water and Wastewater*. 20nd ed. Washington: American Public Health Association and Water Environment Federation; 1998. p. 964
- [53] Anonymous. Final resolution of the symposium on the classification of brackish waters. *Archivio di Oceanografia e Limnologia*. 1959;**11**(Supplement):243-245
- [54] Wetzel RG. *Limnologia*. 2nd ed. Lisboa: Fundação Calouste Gulbenkian; 1993. p. 919
- [55] Simonsen R. The diatom plankton of the Indian Ocean Expedition of R/V “Meteor” 1964-1965. *Meteor Forschungen Ergebniss*. 1974;**19**(Série D):1-107
- [56] Pappas J, Stoermer E. Quantitative method for determining a representative algal sample count. *Journal of Phycology*. 1996;**32**:693-696
- [57] Shannon CE, Weaver W. *The Mathematical Theory of Communication*. Urbana: The University of Illinois Press; 1949. p. 125
- [58] Ter Braak C. Canonical correspondence analysis: A new eigenvector technique for multivariate direct gradient analysis. *Ecology*. 1986;**67**:1167-1179
- [59] Lund J. Observations on soil algae. I. The ecology size and taxonomy of British soil diatoms. *New Phytologist*. 1945;**44**:56-110
- [60] Stoermer EF. Notes on Iowa diatoms. II. Species distribution in a subaerial habitat. *Proceedings of the Iowa Academy of Science*. 1962;**69**:87-96
- [61] Hay S, Maitland T, Paterson D. The speed of diatom migration through natural and artificial substrata. *Diatom Research*. 1993;**8**:371-384
- [62] Underwood G, Paterson D. The importance of extracellular carbohydrate production by marine epipelagic diatoms. *Advances in Botanical Research*. 2003;**40**:183-240. DOI: 10.1016/S0065-2296(05)40005-1
- [63] Witkowski A, Brehm U, Palińska K, Rhiel E. Swarm-like migratory behaviour in the laboratory of a pennate diatom isolated from

North Sea sediments. Diatom Research. 2012;**27**:95-100. DOI: 10.1080/0269249X.2012.690204

[64] Romero OE, Jahn R. Typification of *Cocconeis lineata* and *Cocconeis euglyta* (Bacillariophyta). Diatom Research. 2013;**28**:175-184. DOI: 10.1080/0269249X.2013.770801

[65] Cibic T, Blasutto O, Falconi C, Umani S. Microphytobenthic biomass, species composition and nutrient availability in sublittoral sediments of the Gulf of Trieste (northern Adriatic Sea). Estuarine, Coastal and Shelf Science. 2007;**75**:50-62. DOI: 10.1016/j.ecss.2007.01.020

[66] Ampsoker MC, McIntire CD. Distribution of intertidal diatoms associated with sediments in Yaquina estuary, Oregon. Journal of Phycology. 1978;**14**:387-395. DOI: 10.1111/j.1529-8817.1978.tb02457.x

[67] Sabbe K. Short-term fluctuation in benthic diatom numbers on an intertidal sandflat in the Westerschelde estuary (Zeeland, the Netherlands). Hydrobiologia. 1993;**269/270**:275-284. DOI: 10.1007/BF00028026

[68] Baillie PW, Welsh BL. The effect of tidal resuspension on the distribution of intertidal epipelagic algae in an estuary. Estuarine and Coastal Marine Science. 1980;**10**:165-180. DOI: 10.1016/S0302-3524(80)80056-9

[69] Riaux-Gobin C. Phytoplankton, tripton et microphytobenthos: échanges au cours de la marée, dans un estuaire du Nord-Finistère. Cahiers du Biologie Marine. 1987;**28**:159-185

[70] Shaffer GP, Sullivan MJ. Water column productivity attributable to displaced benthic diatoms in well-mixed shallow estuaries. Journal of Phycology. 1988;**24**:132-140. DOI: 10.1111/j.1529-8817.1988.tb04226.x

[71] Gallagher JB. The significance of the surface film in salt marsh plankton metabolism. Limnology and Oceanography. 1975;**29**:120-123. DOI: 10.4319/lm.1975.20.1.0120

[72] Lukatelich RJ, McComb AJ. Distribution and abundance of benthic microalgae in a shallow southwestern Australian estuarine system. Marine Ecology Progress Series. 1986;**27**:287-297



# Lagoons Reefs of Alacranes Reef and Chinchorro Bank: Ocean Reef of Mexican Atlantic

*Daniel Torruco, M. Alicia González-Solis  
and Ángel Daniel Torruco González*

## Abstract

Coral reef lagoons are one of the parts of the reef with the largest biotopes, making it an area with great inequalities. Under this perspective we try to compare the lagoons of the biggest ocean reefs in Mexico, which despite belonging to the Mexican Atlantic depend on two different systems: Alacranes Reef of the Gulf of Mexico and Banco Chinchorro of the Mexican Caribbean. From the results the proportion of living substrate is higher were obtained in Banco Chinchorro; however, the richness of species and diversity is greater in Alacranes (58 versus 39 species and 4.44 versus 4.38 bits/ind., respectively). *Lobophora variegata* (algae) is the only species whose dominance was proportionately consistent in both reefs; the similarity of sites identifies specific zones of the lagoons in both reefs, in the space the species are distributed close to the center of the axes, but many remain solitary or assembled in pairs. Despite the differences between the reefs according to the community descriptors, the location of the sites and their position in relation to the wind are relevant to the understanding of the dynamics of the lagoons.

**Keywords:** lagoon reefs, macroalgae, invertebrate coral reef, Atlantic reef, natural protected areas

## 1. Introduction

Coral reefs are one of the most diverse communities on the planet and the most diverse in the marine environment; they occupy less than 1% of the bottom of the ocean but are inhabited by 25% of all the marine species currently present [1]. In the Caribbean, coral reefs emerged about 27–30 million years ago in the mid-Oligocene, reaching outstanding development during the Miocene and part of the Pliocene (23–2.5 million years) due to the enrichment of species from the Pacific Ocean to the closure of the Isthmus of Panama [2], which confers it to be one of the oldest environments of the Earth [3].

It is built by living beings of the Scleractinia group that are the main builders and that rise from the bottom to the surface and that by its dimensions and physical structure, influence the environment. Its inhabitants are very diverse and have specific adaptations to each part of this system; therefore, the system has high sensitivity to external agents and an enormous complexity. They are systems located between the tropics, with high temperatures of 18–28°C, surrounded by

clear oligotrophic waters, with high oxygenation, and a salinity of 35 parts per thousand [4].

In addition to the high diversity in which these ecosystems live and develop, they are very productive marine communities. They play a critical role as habitat and protection areas of approximately 10–20% of the world's fisheries [5, 6]. This great system consists of sections that confer zoning. These sections can or will not be presented according to the type of reef in question, providing a distinctive and unique trait to each one. In our case, we will focus on the description of one of these sections, the reef lagoon, and we will do this by confronting the two largest reefs in Mexico, Alacranes Reef and Chinchorro Bank, both of them belong to the Atlantic Ocean, but their structures, characteristics, and components are different.

Both reefs have been studied under different aspects ranging from shipwrecks, [5] ecology [6, 7], biology [8], sociology [9], and paleontology [10], which gives us an idea of the importance of these ocean reefs to the country in relation to the exploitation of its natural resources, conservation, and even its importance in the delimitation of the territorial sea and consequently its sovereignty.

One of the main questions, however, was: are these reefs subject to the same ecological-environmental pressures and controllers even though they belong to two different ocean systems? To get closer to this response, we try to put the reader in context by making a wide description of each reef highlighting its ecological, fishing, and tourist importance, showing the results obtained through two sampling periods in the lagoon in particular and discussing them in relation to the southern, central, and northern areas of each of them, the leeward and windward zones and above all their membership in one or another ocean system.

One of the objectives of this research is to determine whether there are differences in the processes that occur in a given area of the reef, and this will lead to different ideas about whether it is possible to propose conservation and management plan differentials; different surveillance efforts, in the case of protected areas; differences in the natural resources exploitation, etc. That is the importance of this study. In the biological-ecological sense, there are also a number of objectives such as identifying the most important species in the structure of the lagoon community, knowing the dominant species in each area, and determining whether there is a substitution of species in each time period and above all knowing how stability is in the broader sense of this area of the reefs, recognizing that corals can be under such pressure that they can suffer disease and even death when the ambient conditions change rapidly without giving time to acclimatization. Around the world there is concern about coral reef conditions, especially because of the multiple problems they face such as coastal development and alterations by human influence that lead to a higher rate than estimated. Solutions to this problem can only be given through a vigorous drive for scientific research, particularly ecological and necessarily multidisciplinary that proposes informed procedures with firm scientific foundations. Fortunately, there are national and international efforts to preserve the health of reefs by restraining their arguments and procedures in scientific discoveries; we are sure that our contribution will serve as a further support to the efforts of conservation of these reefs.

## **2. Material and methods**

In this section we will present the study areas, the general characteristics of each reef, as well as the methodology used to obtain the data and the subsequent numerical analysis.

## 2.1 Study area

Both reefs are oceanic and the largest in Mexico and are marine protected areas: Alacranes reef with the National Park status and Chinchorro Bank as a biosphere reserve.

The physiographic reef structure makes it possible to recognize two sections, windward and leeward, and at least four main areas, South Lagoon, Central Lagoon, North Lagoon, and reef crest that border each reef.

### 2.1.1 Alacranes reef

Their geographical location is 22°23'N, 89°41'W, and 135 km off coast of Port Progreso on the Yucatan Shelf. This reef is the largest and most complex of the series of reef lying along the edge of the Campeche Sound. The reef has the form of the atoll with northwest trend, due in part by winds and strong westerly currents. Its sub-oval pattern of outer reefs encloses shallow lagoon, and relationship to the Campeche Sound characterizes it as a shallow lagoon shelf atoll [11, 12]. The surrounding waters are 52 m deep. The lagoon reef maximum depth is 20 m in the north. We recognize a semicircular well-developed windward reef on the eastern side and leeward margin less sharply defined belt of reef growth. The windward reef forms a continuous barrier along the north, east, and southeast. The leeward side is characterized by small patch reefs and submerged sandbars. The lagoon is filled with microatolls giving a reticular pattern. There are five sand cays on the leeward rim of the reef: Bird or White Island, Isla Chica, Pérez Island, Dead Island, or Deserter and Banished Island. The total area recorded for the five islands is 530.407 m<sup>2</sup>, representing 1.7% of the area [13]. By virtue of the intense dynamics of the islands, their shape and dimensions can vary from the order of meters or tens of meters in short periods of time [11]. All cays are very low with maximum height of 3–4 m. A *Thalassia testudinum* seagrass bed and other algae are frequent in the lagoon reef. The cays are important site for nesting seabirds and nesting green turtles. Sharks are abundant in shallow waters; the management program [5] reported 116 bird species, 136 fishes, 24 species of shark, and 34 coral species. The reef is currently visited by fishermen who collect queen conch and other shells. Lobsters and grouper are also taken, mainly by skin diving and spear gun. The tourism is more and more frequent. The area has frequent climatological disturbance (winds of the north and hurricanes). The area has a forbidden period for the conch and lobster for the Fish Secretary decree.

### 2.1.2 Chinchorro Bank

Their geographical location is 18°47'–18°23'N, 87°14'–87°27'W, and 24 km off coast of southeastern Quintana Roo, México, between Xcalak and the Ubero and about 100 km north from Turneffe Island in Belize. This reef is part of the Great Atlantic Reef Belt (second world barrier). Chinchorro has an area of 53.379 ha. It is a kidney-shaped prominence and is separated from the mainland by a 1000-m-deep channel [14]. The current is very strong (often over two knots). There are four cays: Cayo Norte (two mangrove-covered islands with an area of 2645.2 ha, destined for the protection of the reef); Cayo Centro, the largest, is a mangrove island with few little inner lagoons with an area of 1263.76 ha, comprises the entire cay and adjacent waters; and Cayo Sur (or Lobos), the smallest (300 m long), is a sandy bank, the only close to the windward margin of the atoll, with 678.53 ha, destined mainly to the protection of the elkhorn corals; all the cays represent 5.82% of the total area of the reserve [15]. The reef has an area of 1443.6 km<sup>2</sup>; lagoon reef maximum depth is

21 m in the south, 3–4 m near Cayo Centro, and 2 m in the north. A *Thalassia testudinum* seagrass bed and garden eels, sometimes at high densities, are found in the reef lagoon. The reef lagoon extends for several tens of kilometers west of the bank and is extremely productive [13]. Under its waters the first thing we identify are sponges, fans and sea whips, and isolated colonies of stony corals and a huge diversity of multicolored reef fishes or small fish that are by hundreds hidden under the rocky cavities of where they come out and create a lively silver spot. However, the diversity and abundance of someone groups (e.g., the management program [14] reports 95 species of Cnidaria, 35 sponges, 96 birds, 11 reptilian, 135 algae, and 104 species of mollusk), the main fauna inhabiting this tropical ecosystem is practically unknown (cichlid, crocodiles, etc.). Some of this species have never been described; maybe others are relict species, and others are a complex of subspecies interacting biologically and ecologically between them. Aggregation of the queen conch (*Strombus gigas*) and spiny lobsters (*Panulirus argus*) and abundance of large fish are frequent; turtles probably occur too. Cayo Centro is an important breeding site for frigate birds (*Fregata magnificens*) and olivaceous cormorant (*Phalacrocorax olivaceous*). The area is fished for queen conch (*Strombus gigas*) and lobster (*Panulirus argus*) by fishermen from Xcalac and Chetumal; there are three fishery cooperatives with 60–70 elements each one; the current disturbance for fishing is probably small, because of a forbidden period for the Fishery Secretary decree [14]. There are two lighthouses and many wrecks. The reef is gradually becoming popular with scuba divers who make 4- to 5-day trips from Cancún, Cozumel, and Quintana Roo coasts. The area has frequent climatological disturbance (winds of the north and south and hurricanes) (Figure 1).



**Figure 1.**  
Sampling sites in both oceanic reefs.

## 2.2 Methods

### 2.2.1 Sampling

The sampling was developed in two periods with a 2-year interval (2015–2017), for each reef. Each reef complex was divided into three main areas: north, central, and south. We established 35 sites for Alacranes reef and 36 stations for Chinchorro Bank, positioned with GPS (Garmin inReach Explorer+). The stations were distributed in the following ways: 16 sites in the southern zone of both reefs; 10 and 17 for Alacranes and Chinchorro, respectively, in the central zone and 9 and 3 for Alacranes and Chinchorro, respectively, in the north zone. The differences between the south and central areas with the northern area were mainly the difficulty and risks of navigating the low sand and shallow depths.

Two 20-m-long randomized photographic transects [16] for each site, transect consisted of 20 photographs that covered each one an area of  $(56 \times 34 \text{ cm})$   $1904 \text{ cm}^2$ , were used [17]. The photographs were taken with a Nikonos V camera, and the total number of photographs analyzed was 2802 ( $533.5 \text{ m}^2$ ); 38 photographs were disposed by out of focus. To obtain the coverage of the species, each photograph was superimposed on a grid with  $10 \text{ cm}^2$  divisions for the coverage calculation. In parallel with the photographic transects, a selective collection of species was carried out for their precise identification in the laboratory and to serve as a basis for photointerpretations. The bibliography used depended on the phylum [18–23].

### 2.2.2 Data analysis

The coralline coverage data matrix for each reef was used in different numerical analyses. A single matrix was formed by reef, where the most common community parameters were determined in the sites, with the purpose of obtaining a robust quantitative descriptive synthesis: the dominance was determined by the index of the importance value [24]; its formula is as follows:

$$IVI = A\% + F\% \quad (1)$$

where A—relative abundance, F—relative frequency  
and biological diversity was quantified with the Shannon-Wiener index [25]  
whose expression is

$$H' = - \sum_{i=1}^S p_i \log p_i \quad (2)$$

where  $p_i$  is the proportion of the abundance of the species  $i$ .

The sites were classified with the Bray-Curtis similarity index, using the flexible union criterion with a  $\beta = 0.25$  [26]; the coefficient has the following equation:

$$d_{i,k} = \frac{\sum_{i=1}^Z |X_{i,j} - X_{i,k}|}{\sum_{i=1}^Z (X_{i,j} + X_{i,k})} \quad (3)$$

where  $j, k$ —objects  $j$  and  $k$  that are evaluated,  $i$ — $i$ -ésimo descriptor,  $Z$ —number of descriptors,  $d_{j,k}$ —affinity value determined as geometric distance,  $X_{i,j}$ —descriptor value  $i$  in the entity  $j$ .

A main coordinate analysis was used for spatial distribution of the species [27].

### 3. Results

#### 3.1 Biodiversity

Biodiversity is a characteristic of nature and a property of living beings. It is a highly complex and nonlinear system, which is produced from a complex dynamic of interactions between living beings and their nonliving supports (physical, chemicals, etc.) through different contexts of time, geography, and cultures. The reef system is among the most biodiverse, equated with the tropical rain forest and linked to the ecological services provided by this interaction that finally integrates the environment and reflects the sensitivity of these services with concerning the depletion and disappearance of resources, communities, and populations. In this case we present the results obtained when investigating two lagoons of Atlantic Ocean reefs.

In both reefs the nonliving substrate generally has a higher percentage (**Figure 2**); however, in some places living coverage exceeds the substrate. On the other hand, on the Alacranes reef, only three sites are given this situation also in the southern part (**Figure 2A**). Some areas of the Chinchorro Bank, especially the southern part, show greater coverage than inert substrate (**Figure 2B**). Generally, the tendency for Alacranes reef is a decrease in living coverage from the south to the north, and consequently an increase of the substrate does not live in that

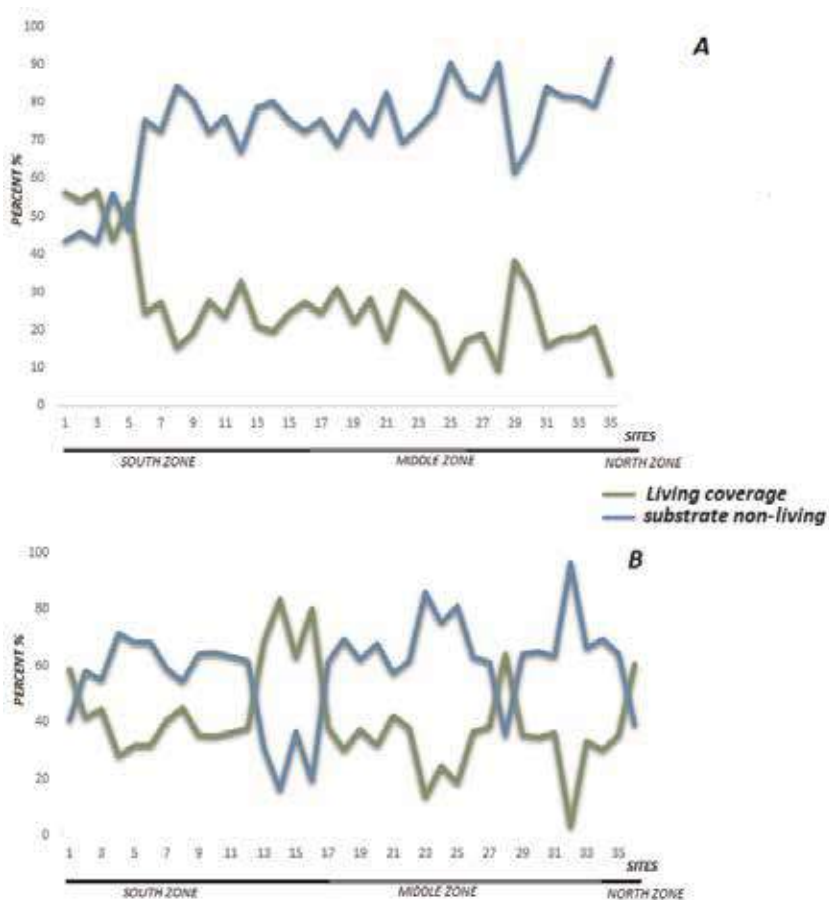


**Figure 2.** Live coverage and inert substrate percentages in the reef lagoons. (A) Alacranes reef, (B) Chinchorro Bank.

direction. Chinchorro Bank shows a similar tendency to Alacranes, where there is a descent from the south to the north, only that the trend slope is lower. The living substrate increases also from the south to the north with a similar slope.

In relation to the organisms collected in the reef lagoons, three phyla with 70 species were registered, the disposition of the groups in each reef is presented in **Table 1**, and in the annex the presence of the species in each lagoon is recorded.

Even though some species are presented in both reefs, the dominance percentage of the five most representative species is shown in **Figure 3**; they show that the dominance percentage of *Orbicella annularis* for Chinchorro Bank is higher and that for Alacranes reef decreases until the fourth place. On the other hand, the alga *Lobophora variegata* is presented in the second place in Chinchorro Bank but rises to the first in Alacranes reef; however, the dominance percentage is similar.

The richness of species is lower in Chinchorro, since the sites that present the greatest richness reach only seven species, while in Alacranes most sites are between 15 and 20, reaching in the southern area up to 40 species (**Figure 4A, D**). Diversity in Chinchorro Bank goes from 0 (one species) to 2.4 bits/ind., while in the Alacranes reef, it goes from 1 to 4.3 bits/ind. (**Figure 4B, E**). Equitability has similar behavior to diversity in both reefs, reaching 0.9 as its maximum value (**Figure 4C, E**).

**Table 2** seeks to gather the general information of the two ocean reefs, their origin, presenting the totals in terms of their size, as well as the parameters of total diversity that are presented in both lagoons.

Groups	Alacranes reef	Chinchorro Bank
Algae	11	8
Sponges	18	4
Hydrozoa	2	2
Hard corals	18	16
Soft corals	9	9
Total	58	39

**Table 1.**  
 Species number per group registered in Alacranes reef and Chinchorro Bank lagoons.

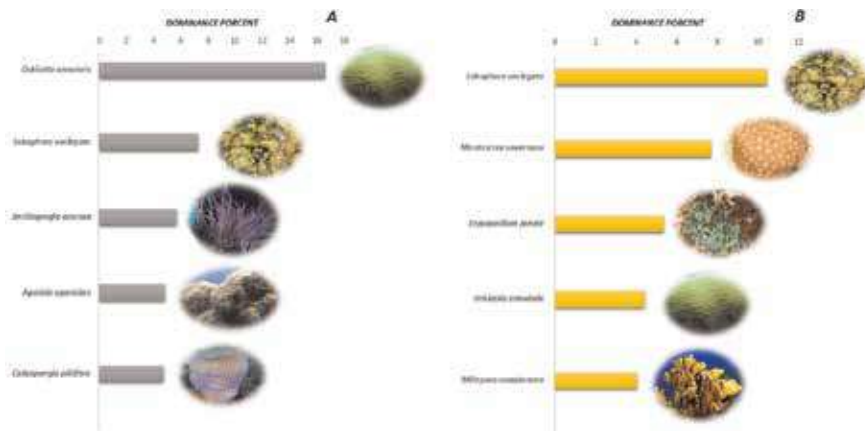


**Figure 3.**  
 The five species with the highest percentage of dominance. (A) Alacranes reef, (B) Chinchorro Bank lagoons.

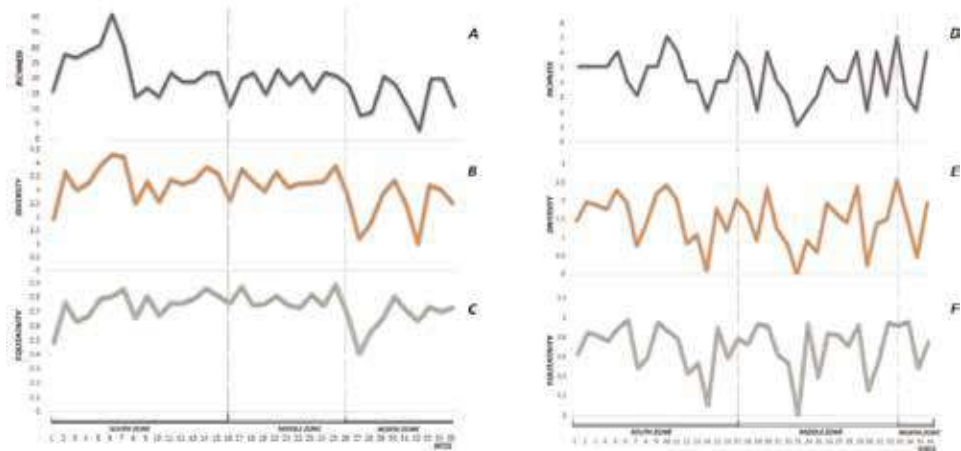


**Figure 4.** Richness (A, D), diversity (B, E), and equitability (C, F) in the lagoons of Alacranes (ABC) and Chinchorro (D,E,F) reefs. The three areas are south, central, and north.

Attribute	Alacranes reef	Chinchorro Bank
Origin	Pleistocene-Cretaceous	Cenozoic: Pliocene-Pleistocene
Area (km <sup>2</sup> )	300	1443.6
Islands	5	4
Island area [km <sup>2</sup> ]	0.53	5.82
Insular percentage	1.7	0.40
Lagoon area [km <sup>2</sup> ]	299.755	533.79
Surrounding water depth (m)	52 m	+500 m
S (species no.)	58	39
H' (bits/ind.)	4.44	4.38
H' <sub>max</sub> (bits/ind.)	5.85	5.25
H' <sub>min</sub> (bits/ind.)	0.127	0.308
J'	0.759	0.834

**Table 2.** Alacranes reef and Chinchorro Bank characteristics.

### 3.2 Site affinity

The similarity given by the Bray-Curtis index, of the Alacranes Reef, forms seven groupings: The first is formed by two sites in the northern area. The second clusters more sites (11), which are distributed throughout the reef; however, at lower levels, sites of the same area or at least contiguous areas such as stations 8, 12, and 18 are associated. The third group joins two stations: one from the central zone and the other from the north.

The four clusters include five stations that although they identify some area, some site of another area is joined as is the case of sites 19, 20, 21, and 23, elements of the central zone to which site 28 of the north zone is joined. The fifth group relates eight sites, showing an association that completely identifies the area in the south. The sixth cluster has five sites, most of them from the south zone and only one from the north zone (site 29). The seventh group has only two sites: one of the south zone and one of the north (**Figure 5A**).

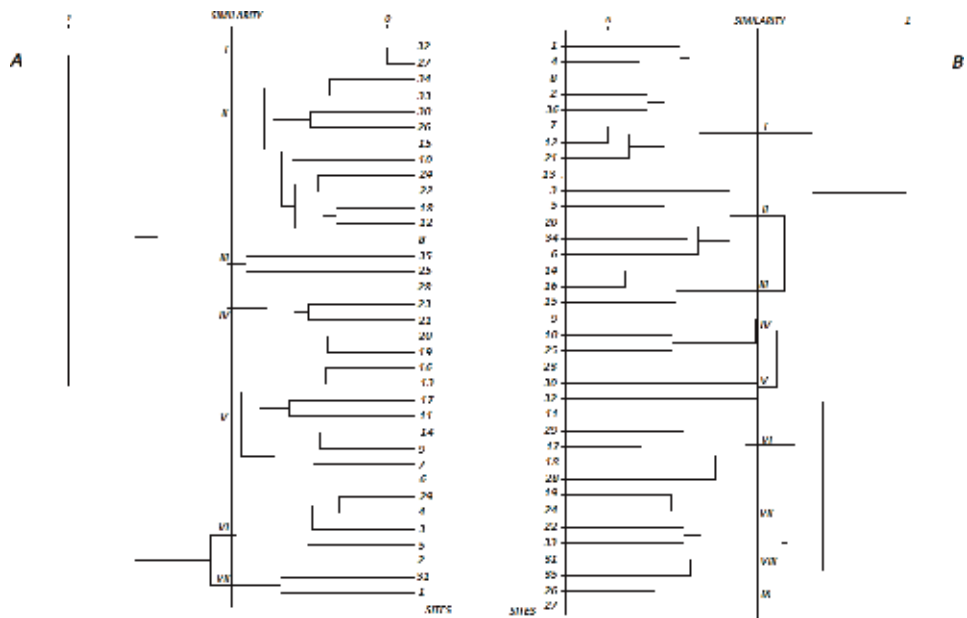


**Figure 5.** Sites similarity given by the Bray-Curtis index. (A) Alacranes reef, (B) Chinchorro Bank lagoons.

The Chinchorro Bank sampling sites form nine groups at a level of 50%. The largest of them includes eight stations, of which six belong to the south zone, one to the central part on windward, and one of the north zone in leeward. Group II gathers five sites of which three are in the south zone, one in the central part on windward, and one in the north area in leeward. The third cluster is exclusive to the southern zone. Cluster IV is made up of two sites in the south windward area and one in the center of the central area. Group V has three exclusive sites in the middle area, two of them close to the island of Cayo Centro and one of them on the windward edge. The sixth cluster has five stations, almost all of them from the middle area, except for a site located in the south area. Group VII has four locations, close to each other in the central area except for one of them located in the leeward area. The eighth cluster is formed by two stations in the central zone and the other in the north. The last group consists of two sites in the central area, one on the windward edge and the other in the leeward (**Figure 5B**).

### 3.3 Spatial species distribution

In relation to the spatial distribution of species of Alacranes reef, there were 58 species (flora and fauna) that also form, most of them, a large conglomerate close to the three axes of coordinates. There were paired associations as in the case of *Amphimedon compressa* with *Stephanocoenia intersepta*, *Siderastrea siderea*, and *Millepora alcicornis*, among others; *Antillogorgia bipinnata*, *Porites astreoides*, *Agaricia agaricites*, *Dictyota* sp., *Acanthophora spicifera*, and *Isophyllia sinuosa* move away from any grouping (**Figure 6A**).

In Chinchorro Bank, it has to be generally presented that for 39 species most of them cluster at the origin of the three axes, forming a large group. The species *Halimeda incrassata* and *Lobophora variegata* show a very close relationship, while the species *Callyspongia plicifera*, *Antillogorgia acerosa*, *Agaricia agaricites*, *Orbicella annularis*, *Eunicea mammosa*, *Eunicea flexuosa*, and *Gorgonia flabellum* are out of any conglomerate (**Figure 6B**).

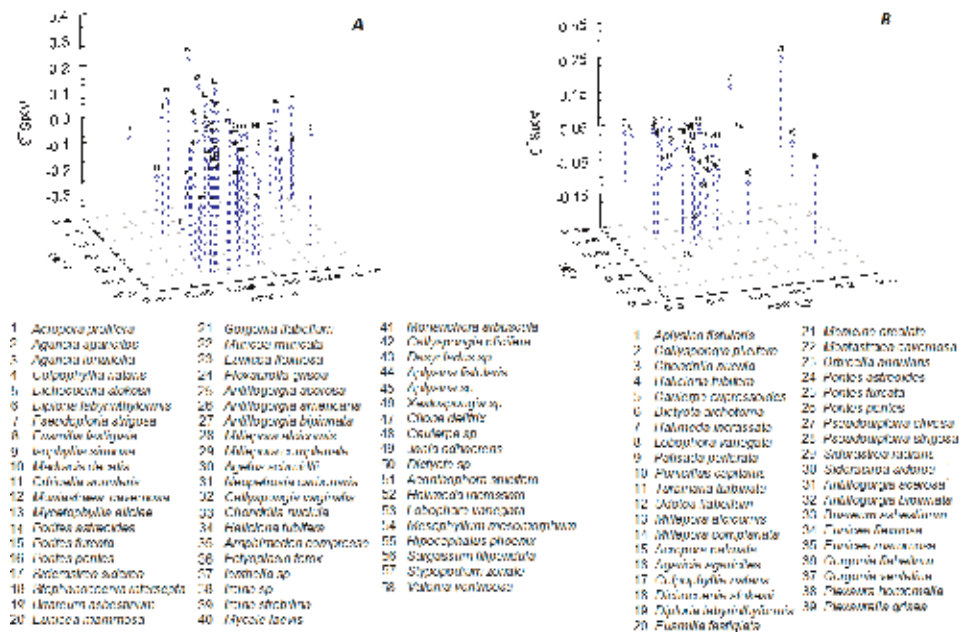


**Figure 6.** Spatial ordination of the species found in the reef lagoons. (A) Alacranes reef, (B) Chinchorro Bank.

## 4. Discussion

### 4.1 Biodiversity

The marine benthic communities have been evaluated from different points of view, which respond to their distribution, interests, or incidental events. The most common assessments are those focused on establishing the community structure and distribution patterns of temperate and boreal zones [28, 29], while in the tropical coastal zone are the evaluations focused on determining the response of these communities to changes caused by seasonal fluctuations and/or physico-chemical or structural modifications of the environment, by natural or anthropogenic sources [30–32]. Precisely, an indicator related to environmental services is biodiversity. It is essential to know the ecological characteristics of reefs and coral-line communities, because it allows to identify the stability of these ecosystems as well as the manifestations that these present in the face of natural and anthropogenic disturbances. The most obvious indication of the effect of natural and anthropogenic disturbances on coral systems is the death of corals. However, if the damage is not massive, sometimes there is a change of species, in which other types of coral species or various organisms in the bottom, such as carbonated or fleshy algae, arrive and occupy the position of the species that originally resided in the site, causing the so-called phase change [33, 34]. Consequently, the functions of the system are affected, since the corals that arrive are not always so efficient to produce carbonate, to generate sediments or sands, and above all, to give food or refuge to other species, so even if there is live coral, the environmental service is not the same.

Meanwhile, environmental variability is one of the two forms of environmental change, with alterations in the intensity or frequency of stochastic events [35, 36]. Its raise is associated with the increment in disturbances and variability of resources, imposing challenges that have a greater influence on biological communities, than those generated by changes in the average environmental condition

(the second form of environmental change). In turn, environmental variability has been conceptually used to frame all possible values that may exhibit the physical and chemical characteristics of a benthic habitat [37, 38].

Alacranes reef can be considered as the most studied coral complex of the Mexican seas due to its extraordinary characteristics, which place it within the most extensive and important coralline masses of the country [39]. The reef was described for more than a century [40] but, until the late 1950s, began to be studied more or less constantly, mainly by foreigners [41]. Alacranes has a vast history of shipwrecks and has been a point of attraction of visitors since colonial times [42].

The Yucatan Peninsula is a platform of sedimentary origin, constituted by a karstic Quaternary complex. It is the most recent emersion area in the country, and its growth is associated with sediment coastal transport processes and marine transgression and regression cycles. Therefore, Alacranes is of recent formation, originated by the biological action of the corals with the gradual deposit of calcareous material during the Pleistocene and Cretaceous, favored by the slow immersion of the Yucatan Peninsula [43]. Alacranes sits on a terrace of 51–64 m that is supposed to be carved during the descent eustatic sea level at the end of Wisconsin or at the beginning of the transgression Holocene (11,000 years ago), hence began the modern reef growth, arriving some 5000 years, both the reef and the sea level, to its current values [44]. The area is a platform reef of approximately 300 km<sup>2</sup>, which rises 50 m from the seabed. According to several investigations [45], it is known that the pattern of currents and the contribution of nutrients for the Alacranes reef come from the upwelling process that originates in the eastern end of the Yucatecan platform. The current of the Caribbean, as it passes through the Yucatán Strait and ascends on the platform, contributes high values of nutrients and therefore a high productivity [46]. Thanks to this contribution, there are commercial fisheries of lobster (*Panulirus argus*) and the groupers (*Epinephelus* sp.) [47]. The general state of conservation of the reef can be considered good [48].

Alacranes is a resting area for migratory birds that cross the Gulf of Mexico; particularly one of the islands of the Alacranes reef is considered one of the most important breeding areas in the world for the bird *Sula dactylatra*. Thus, it is considered an important area for the conservation of birds of the country [49], especially with a record of 110 species between accidental and permanent residents in the reef. In the reef environment, the management program has registered 34 species of corals, some of which are considered species under special protection [50]—in this assessment we report 28. According to the Alacranes bathymetric characterization, the slope of windward descends to an average of 55 m of depth; in the north part there is a marked inflection of the profile in comparison of the areas center and south, where the slope descends gently. The windward slope is the only site on the Alacranes reef where the stony corals of the genus *Orbicella/Montastraea* are not dominant. The dominance corresponds to *Siderastrea radians*. One of the characteristics of this area is the high density of soft corals or octocorals; the dominant genus is *Pseudopterogorgia*, although *Gorgonia flabellum* is also frequent and reaches large size. In addition to these, the genera *Eunicia*, *Plexaura*, and *Plexaurella* are represented in this part, like the one reported by other studies [42, 51]. The barrier reef is physiographically one of the most conspicuous elements of the system, and like any barrier reef, in turn is divided into outer barrier, west in the case of Alacranes, reef crest, and inner barrier [52]. The outside is the one that is exposed to the prevailing winds and the persistent swell train. Along the barrier at different points, it reaches the surface. The notorious dominance of the *Palythoa caribbeaerum* colonial anemone extends to the areas of the crest and the inner barrier. In the shallow part, between three and four meters of depth, the Hydrozoa *Millepora alcicornis* is frequent, like *Gorgonia flabellum*. In this area, the hard corals

are represented by *Porites asteroides*, *Pseudodiploria strigosa*, *Acropora palmata*, and *A. cervicornis*, mainly. In the southern part of the barrier, *Acropora prolifera*, a rare species in the Caribbean reefs, is located. The reef crest reaches up to 400 m wide and marks the maximum growth of the reef and is only interrupted by two channels of flow and reflux tidal in the area known as the flooded. The boundary between the crest and the inner barrier is not clearly defined, but it can be said that it starts in the area where the swell train begins to disappear. In the inner barrier, in the closest part to the crest, *Acropora palmata*, *A. cervicornis*, *Porites porites*, *P. astreoides*, and *Millepora alcicornis* are the corals competing with *Palythoa*. To the west the inner barrier comprises the meadows of seagrass and the canals near the barrier. Of these components, the seagrass meadows play an important role in the system [53]. They are presented in shallows of sandy bottoms covered by meadows of *Thalassia testudinum*, *Cymodocea manatorum*, and *Diplanthera wrightii* whose roots and rhizomes form a dense plot that functions as a sediment trap and stabilizes the substrate. Associated with the meadows are presented corals *Manicina areolata*, *Oculina diffusa*, and *Porites porites*. The reef plateau is the most complex area of reef lagoon and includes shallow seagrass meadows, pinnacular reefs, and microatolls, as well as an intricate network of canals, the result of these morphological structures that rise abruptly from 12 to 15 m deep, until almost reaching the surface. *Orbicella annularis* is dominant and accompanies *M. cavernosa*, *Pseudodiploria strigosa*, *Colpophyllia natans*, *Porites porites*, *P. astreoides*, and *Stephanocoenia intersepta*.

For its biological characteristics, the reserve of Chinchorro Bank is a natural laboratory, practically unaltered, partially known, and even unknown in many of its aspects, to develop innovative scientific research and quality focused both on the execution of floristic and faunal inventories that enrich and update existing ones, as well as to understand in detail the biological and ecological relationships and processes that develop there. Due to Chinchorro Bank's geographical isolation and its position in the hurricanes and tropical storms route, it is important to establish mechanisms to facilitate the knowledge of the prevailing meteorological conditions to increase the safety degree of visitors and fishermen. Unlike other Mexican reefs, Banco Chinchorro does not develop on a continental or insular shelf but on a deep underwater crest (more than 400 m deep about 30 km out coast), which rises like a pinnacle [54, 55]. Little is known of its origin; we have the theory that in the past, the reef complex was formed by separation and derives from a portion of the continental coastal area, possibly in the Cenozoic era in the late Tertiary period or early Quaternary (in the Pliocene-Pleistocene age). The separate fraction of the coastline contained a fringe or marginal reef and coastal lagoons with typical fauna. The detachment of part of the coast was possibly of a single plate, which took with it a large reservoir of ancient water which possessed characteristics of a continental mass of water, which has maintained its characteristics with the contribution of the rains. Due to its geographical position in the Western Caribbean and their influence in the Gulf Stream, it is an intermediate point compared to other reef systems located downstream in the Lesser Antilles, which allows it to receive larvae of these distant places and in turn export larvae of different organisms generated in Chinchorro to systems located upstream, like Cozumel, Alacranes reef, and the keys of Florida, among others [56].

The Chinchorro Bank is of great ecological importance due to the high diversity of organisms that are there. By remaining practically isolated for a long time, some areas are unchanged, allowing for a comparable study with other similar ecosystems. Banco Chinchorro is nominated by UNESCO as a World Heritage Site and as a Ramsar site for the protection of migratory birds and wetlands. It was recently designated as the Man and Biosphere (MAB) site [50]. The fauna inventoried by the management program [14] is dominated by local and migratory birds that use the keys permanently or during the time of migration to rest and feed. Ninety-six

species of birds are registered. Several of them registered in NOM-059-ECOL-1994 as subject to special protection, for example, the blue-winged teal (*Anas discors*) and the roadside hawk (*Buteo magnirostris*). The brown heron (*Ardea herodias*) is considered rare. For example, the blue-winged teal (*Anas discors*) and the road hawk (*Buteo magnirostris*), the brown heron (*Ardea herodias*) is considered rare, the stork (*Mycteria americana*) and the rabies or rabihorcado (*Fregata magnificens*) as it is known in the locality where, according to fishermen's reports, this bird reached great abundance they have the category of threatened. Within the reptiles, the American crocodile (*Crocodylus acutus*) is listed as endangered, although apparently in the bank, this species is abundant.

The known composition of the coral taxa is represented by hexacorals, octocorals, and hidrozoarios with 95 species reported [14]; in this assessment we report 31. Among the Scleractinian *Orbicella annularis*, *M. cavernosa*, *Porites astreoides*, *Agaricia tenuifolia*, *A. agaricites*, *Acropora palmata*, and *A. cervicornis* dominate, while of the gorgonian the dominant ones correspond to *Eunicea mammosa*, *Gorgonia flabellum*, *P. americana*, *Briareum asbestinum*, and *Plexaura flexuosa*. The hidrozoarios are represented by *Millepora complanata* and *M. alcicornis* like the report by other investigation [57]. The macroinvertebrates are conspicuous elements of the coral reef; they are even organisms of great scientific, tourist, and commercial interest, but little is known of those that are presented in the reserve. The available records, which are not exhaustive, correspond to 35 species of sponges, 78 gastropods, 26 bivalves, and 6 crustaceans [14]. For Chinchorro Bank, faunal and floristic inventories with which it is counted in the reserve are partial. It is not known the composition of zooplankton, phytoplankton, microzoobenthos, and microphytobenthos, among others, as well as taxonomic groups of which there are no records such as the case of echinoderms, jellyfish, anemones, crustacean by marine fauna, and arachnids, insects, and mammals for terrestrial fauna is not known.

With the high values of diversity in Alacranes reef, one would think that it is the most diverse and most conserved reef; however, the high coverage values in Chinchorro Bank belie that assumption. It is very important to mention that the coverage composition of benthic organisms is a variable that determines total biodiversity or specific group biodiversity, such as benthic organisms, invertebrates, or reef fish [58]. Both lagoons have hard and soft corals in different proportions, but abundance has a high variation in soft corals. This may be related to the high colonization capacity of soft corals which adhere to different types of substrate.

The south part of Chinchorro Bank recorded the highest diversity of benthic groups, but Alacranes reef was in the north. Density and percentage of live coral coverage, particularly reef building corals in these areas, are slightly over the average recorded in coral reefs from the Mesoamerican Reef [59]. It is possible that these corals enhance considerably the growth of new colonies, which will make possible the persistence of reefs and the habitat they provide to other species. In the north of Chinchorro and the south of Alacranes, it is highly probable that sedimentation condition will affect and reduce the live coral coverage, since this condition persists for a period; about 7% of coral coverage in this area could be lost because it is well known that sediments damage coral polyp tissues by abrasion and asphyxia.

#### 4.2 Site affinity

There are distinct morphological variations between leeward and windward sectors. A shallow and extensive reef flat is a common feature in most of leeward part of these reefs. Coralline algae are quite abundant in these flats, and rubble of coral skeletons in ample dead beds of hard corals is evident. With both data sets, the classification

analysis leads to effectively recognizing the quantitative differences between the different zones. It extracts subjective considerations and discovers the importance of the ecological attributes identified in the field. However, in some cases the factors that originate the distribution patterns are not clearly discovered, since the analysis conducted suggests that significant changes with the depth occurs in the populations and shows that the different parts of the same reef system can be subjected to different pressures and combinations in the selection process, even in physiographical areas related to the frequency and intensity of disturbance by the wave.

The affinities between the sites showed strong identities toward identifying areas with particular characteristics such as windward, leeward, and the reef ridge; however, the inclusion of some site of the reef plain in these groups can be caused by the depth and the type of biotope that develops there (availability of free substrate, coral fragments, etc.) as happens in other reef sites [60]. Chinchorro Bank presented a greater number of groupings, showing particular areas with strong characterization, where slight changes in some parameters is sufficient for the index to detect and separate them; Alacranes gathers more sites in its clusters, which would allow to think that their affinities are maintained in a larger area.

### 4.3 Spatial species distribution

In stable ecological systems, it is possible to recognize the dynamic state in which all the interactions and variations of a community are centered and nullified at a point of equilibrium to which all the components of the community are directed after a disturbance, allowing the community to be recognized as an entity based on its attributes [61–63], which are the total abundance of species, the total abundance of the dominant species, the biomass of the community, and the composition of species [64, 65]. With the analysis of Main Coordinates, it's possible to identify a community for the species that most influence its community spatial structure [66]; however, this community could present different points of stability, in which the dominance of different species is present, which they present specific equilibrium points, providing different levels of resistance to disturbances, as could create the differences between windward and leeward levels. In both reefs and analysis strategies, the species that takes advantage of the largest amount of resources for its benefit and consequently is the most dominant is *Orbicella annularis*, which is similar to that reported for the Netherlands Antilles [67], on both reefs was a species that separates from any grouping, being more evident in Chinchorro Bank. However, in areas with a certain degree of disturbance, the scheme changes dramatically, and other species replace *O. annularis* in its dominance. In the first case, when solid substrate is available, the gorgonians are those that have more aggressiveness and in the second when missing a solid substrate, the group of sponges has some advantage. In fact, these data confirm what was partially found by other research [68–70] who defined areas or biotopes with strong ecological differences. Coral reefs in the Caribbean and Gulf of Mexico have a similar coral biota. Nevertheless, there is a reduction in the number of common Scleractinian coral species from the Alacranes reef to Chinchorro Bank. Coral species richness, however, does not seem to decrease drastically as it does with gorgonians [71].

## 5. Conclusions

The conclusions of this research are as follows:

- The two lagoons have different dynamics.

- The proportion of live coverage in Chinchorro Bank is higher than in the Alacranes reef.
- While the richness is greater in the lagoon of the Alacranes reef, the magnitude of the Chinchorro Bank lagoon may result in an undervaluation due to insufficient sampling.
- The abundance-rich ratio of species given by diversity is similar in both lagoons.
- *Orbicella annularis* is the coral that is among the five most dominant species in both lagoons.
- In the lagoons there were site affinities, especially at the edges, that faithfully identify windward and leeward areas, which allow to infer the importance of this element and what originates in relation to wave force, oxygenation, etc.
- The analyses show areas with large ecological differences in the lagoons.

By virtue of its insular nature and the scarcity of freshwater, both reefs have remained safe from major alterations. Alacranes reef and Chinchorro Bank are a distant paradise that still have abundant fishing resources and diverse underwater life to marvel, as well as the possibility of discovering hidden secrets kept by the sea and time. However, we must consider and not forget that the overexploitation of resources can deplete the productivity of this place, which until now is one of the last places where coral reefs and memories of other times remain intact. The knowledge obtained from these systems must serve to conserve their natural resources, with special emphasis on endemic species, threatened, endangered, special protection, and those of current and potential economic importance, as well as preserving the reef landscape and its natural elements, for the enjoyment, recreation, exploitation, and elevation of the quality of life of social groups and visitors and for future generations. It should also encourage the conduct of research and studies that broaden and deepen this knowledge and contribute to the development of methods and alternatives for the sustainable use of resources.

The benchmarks of reefs in Mexico are changing, and they need to be redefined frequently to update them, in order for the management tools to be more effective and accurate; we hope that this contribution will go in that direction of conservation and maintenance of these magnificent ecosystems.

## Acknowledgements

We would like to extend our thanks to the National Council of Science and Technology for the support given to the realization of several projects in which this field work is included. Likewise, we thank the Marine Secretariat and the fishermen of several cooperatives, for the transfer of personnel and students to the different reefs and to all the people and institutions that contributed resources, time, and knowledge to carry out this research.



Alacranes reef lagoon																																			
Species	1	2	3	4	5	6	7	8	9	10	11	12	13	14	15	16	17	18	19	20	21	22	23	24	25	26	27	28	29	30	31	32	33	34	35
18 <i>Chondrilla nucula</i> Schmidt, 1862	†	†	†	†	†	†	†	†	†	†	†	†	†	†	†	†	†	†	†	†	†	†	†	†	†	†	†	†	†	†	†	†	†	†	†
19 <i>Cliona delitrix</i> Pang, 1973	†	†	†	†	†	†	†	†	†	†	†	†	†	†	†	†	†	†	†	†	†	†	†	†	†	†	†	†	†	†	†	†	†	†	†
20 <i>Dasycladus</i> sp. C. Agardh, 1828	†	†	†	†	†	†	†	†	†	†	†	†	†	†	†	†	†	†	†	†	†	†	†	†	†	†	†	†	†	†	†	†	†	†	†
21 <i>Ectyoplasia ferox</i> (Duchassaing & Michelotti, 1864)	†	†	†	†	†	†	†	†	†	†	†	†	†	†	†	†	†	†	†	†	†	†	†	†	†	†	†	†	†	†	†	†	†	†	†
22 <i>Ianthella</i> sp. Gray, 1869	†	†	†	†	†	†	†	†	†	†	†	†	†	†	†	†	†	†	†	†	†	†	†	†	†	†	†	†	†	†	†	†	†	†	†
23 <i>Ircinia strobilina</i> (Lamarck, 1816)	†	†	†	†	†	†	†	†	†	†	†	†	†	†	†	†	†	†	†	†	†	†	†	†	†	†	†	†	†	†	†	†	†	†	†
24 <i>Ircinia</i> sp. Nardo, 1833	†	†	†	†	†	†	†	†	†	†	†	†	†	†	†	†	†	†	†	†	†	†	†	†	†	†	†	†	†	†	†	†	†	†	†
25 <i>Haliclona tubifera</i> (George & Wilson, 1919)	†	†	†	†	†	†	†	†	†	†	†	†	†	†	†	†	†	†	†	†	†	†	†	†	†	†	†	†	†	†	†	†	†	†	†
26 <i>Mycale Laevis</i> (Carter, 1882)	†	†	†	†	†	†	†	†	†	†	†	†	†	†	†	†	†	†	†	†	†	†	†	†	†	†	†	†	†	†	†	†	†	†	†
27 <i>Monanchora arbuscula</i> Duchassaing & Michelotti, 1864	†	†	†	†	†	†	†	†	†	†	†	†	†	†	†	†	†	†	†	†	†	†	†	†	†	†	†	†	†	†	†	†	†	†	†
28 <i>Neopetrosia carbonaria</i> (Lamarck, 1814)	†	†	†	†	†	†	†	†	†	†	†	†	†	†	†	†	†	†	†	†	†	†	†	†	†	†	†	†	†	†	†	†	†	†	†
29 <i>Xestospongia</i> sp. Laubenfelds, 1932	†	†	†	†	†	†	†	†	†	†	†	†	†	†	†	†	†	†	†	†	†	†	†	†	†	†	†	†	†	†	†	†	†	†	†
30 <i>Millepora alcicornis</i> Linnaeus, 1758	†	†	†	†	†	†	†	†	†	†	†	†	†	†	†	†	†	†	†	†	†	†	†	†	†	†	†	†	†	†	†	†	†	†	†
31 <i>Millepora complanata</i> Lamarck, 1816	†	†	†	†	†	†	†	†	†	†	†	†	†	†	†	†	†	†	†	†	†	†	†	†	†	†	†	†	†	†	†	†	†	†	†
32 <i>Acropora proliferata</i> (Lamarck, 1816)	†	†	†	†	†	†	†	†	†	†	†	†	†	†	†	†	†	†	†	†	†	†	†	†	†	†	†	†	†	†	†	†	†	†	†
33 <i>Agaricia agaricites</i> (Linnaeus, 1758)	†	†	†	†	†	†	†	†	†	†	†	†	†	†	†	†	†	†	†	†	†	†	†	†	†	†	†	†	†	†	†	†	†	†	†
34 <i>Agaricia tenuifolia</i> Dana, 1848	†	†	†	†	†	†	†	†	†	†	†	†	†	†	†	†	†	†	†	†	†	†	†	†	†	†	†	†	†	†	†	†	†	†	†
35 <i>Colpophyllia natans</i> (Houttelyn, 1772)	†	†	†	†	†	†	†	†	†	†	†	†	†	†	†	†	†	†	†	†	†	†	†	†	†	†	†	†	†	†	†	†	†	†	†
36 <i>Dichocoenia stokesii</i> Milne Edwards & Haime, 1848	†	†	†	†	†	†	†	†	†	†	†	†	†	†	†	†	†	†	†	†	†	†	†	†	†	†	†	†	†	†	†	†	†	†	†

Alacranes reef lagoon																																				
Species	1	2	3	4	5	6	7	8	9	10	11	12	13	14	15	16	17	18	19	20	21	22	23	24	25	26	27	28	29	30	31	32	33	34	35	
37 <i>Diploria laberynthiformis</i> (Linnaeus, 1758)	†	†	†	†	†	†	†	†	†	†	†	†	†	†	†	†	†	†	†	†	†	†	†	†	†	†	†	†	†	†	†	†	†	†	†	
38 <i>Isophyllia sinuosa</i> (Ellis & Solander, 1786)	†	†	†	†	†	†	†	†	†	†	†	†	†	†	†	†	†	†	†	†	†	†	†	†	†	†	†	†	†	†	†	†	†	†	†	
39 <i>Eusmilia fastigiata</i> (Pallas, 1766)	†	†	†	†	†	†	†	†	†	†	†	†	†	†	†	†	†	†	†	†	†	†	†	†	†	†	†	†	†	†	†	†	†	†	†	
40 <i>Madracis decarctis</i> (Lyman, 1859)	†	†	†	†	†	†	†	†	†	†	†	†	†	†	†	†	†	†	†	†	†	†	†	†	†	†	†	†	†	†	†	†	†	†	†	
41 <i>Montastrea cavernosa</i> (Linnaeus, 1767)	†	†	†	†	†	†	†	†	†	†	†	†	†	†	†	†	†	†	†	†	†	†	†	†	†	†	†	†	†	†	†	†	†	†	†	
42 <i>Mycetophyllia aliciae</i> Wells, 1973	†	†	†	†	†	†	†	†	†	†	†	†	†	†	†	†	†	†	†	†	†	†	†	†	†	†	†	†	†	†	†	†	†	†	†	
43 <i>Orbicella annularis</i> (Ellis & Solander, 1786)	†	†	†	†	†	†	†	†	†	†	†	†	†	†	†	†	†	†	†	†	†	†	†	†	†	†	†	†	†	†	†	†	†	†	†	
44 <i>Porites astreoides</i> Lamarck, 1816	†	†	†	†	†	†	†	†	†	†	†	†	†	†	†	†	†	†	†	†	†	†	†	†	†	†	†	†	†	†	†	†	†	†	†	
45 <i>Porites furcata</i> Lamarck, 1816	†	†	†	†	†	†	†	†	†	†	†	†	†	†	†	†	†	†	†	†	†	†	†	†	†	†	†	†	†	†	†	†	†	†	†	
46 <i>Porites porites</i> (Pallas, 1766)	†	†	†	†	†	†	†	†	†	†	†	†	†	†	†	†	†	†	†	†	†	†	†	†	†	†	†	†	†	†	†	†	†	†	†	
47 <i>Pseudodiploria strigosa</i> (Dana, 1846)	†	†	†	†	†	†	†	†	†	†	†	†	†	†	†	†	†	†	†	†	†	†	†	†	†	†	†	†	†	†	†	†	†	†	†	†
48 <i>Siderastrea siderea</i> (Ellis & Solander, 1786)	†	†	†	†	†	†	†	†	†	†	†	†	†	†	†	†	†	†	†	†	†	†	†	†	†	†	†	†	†	†	†	†	†	†	†	†
49 <i>Stephanocoenia intersepta</i> (Lamarck, 1816)	†	†	†	†	†	†	†	†	†	†	†	†	†	†	†	†	†	†	†	†	†	†	†	†	†	†	†	†	†	†	†	†	†	†	†	†
Soft corals	†	†	†	†	†	†	†	†	†	†	†	†	†	†	†	†	†	†	†	†	†	†	†	†	†	†	†	†	†	†	†	†	†	†	†	†
50 <i>Antillogorgia americana</i> (Gmelin, 1791)	†	†	†	†	†	†	†	†	†	†	†	†	†	†	†	†	†	†	†	†	†	†	†	†	†	†	†	†	†	†	†	†	†	†	†	†
51 <i>Antillogorgia acerosa</i> (Pallas, 1766)	†	†	†	†	†	†	†	†	†	†	†	†	†	†	†	†	†	†	†	†	†	†	†	†	†	†	†	†	†	†	†	†	†	†	†	†
52 <i>Antillogorgia bipinnata</i> (Verrill, 1864)	†	†	†	†	†	†	†	†	†	†	†	†	†	†	†	†	†	†	†	†	†	†	†	†	†	†	†	†	†	†	†	†	†	†	†	†
53 <i>Briareum asbestinum</i> (Pallas, 1766)	†	†	†	†	†	†	†	†	†	†	†	†	†	†	†	†	†	†	†	†	†	†	†	†	†	†	†	†	†	†	†	†	†	†	†	†
54 <i>Eunicea flexuosa</i> (Lamouroux, 1821)	†	†	†	†	†	†	†	†	†	†	†	†	†	†	†	†	†	†	†	†	†	†	†	†	†	†	†	†	†	†	†	†	†	†	†	†
55 <i>Eunicea mammosa</i> Lamouroux, 1816	†	†	†	†	†	†	†	†	†	†	†	†	†	†	†	†	†	†	†	†	†	†	†	†	†	†	†	†	†	†	†	†	†	†	†	†
56 <i>Gorgia flabellum</i> Linnaeus, 1758	†	†	†	†	†	†	†	†	†	†	†	†	†	†	†	†	†	†	†	†	†	†	†	†	†	†	†	†	†	†	†	†	†	†	†	†
57 <i>Muricea muricata</i> (Pallas, 1766)	†	†	†	†	†	†	†	†	†	†	†	†	†	†	†	†	†	†	†	†	†	†	†	†	†	†	†	†	†	†	†	†	†	†	†	†
58 <i>Plexaurella grisea</i> Kunze, 1916	†	†	†	†	†	†	†	†	†	†	†	†	†	†	†	†	†	†	†	†	†	†	†	†	†	†	†	†	†	†	†	†	†	†	†	†





## Author details

Daniel Torruco<sup>1\*</sup>, M. Alicia González-Solis<sup>1</sup> and Ángel Daniel Torruco González<sup>2</sup>

<sup>1</sup> Research Center and Advance Studies of the National Polytechnic Institute, Merida, Yucatan, Mexico

<sup>2</sup> Vizcaya of the Americas University, Merida, Yucatán, Mexico

\*Address all correspondence to: [dantor@cinvestav.mx](mailto:dantor@cinvestav.mx)

## IntechOpen

---

© 2019 The Author(s). Licensee IntechOpen. This chapter is distributed under the terms of the Creative Commons Attribution License (<http://creativecommons.org/licenses/by/3.0>), which permits unrestricted use, distribution, and reproduction in any medium, provided the original work is properly cited. 

## References

- [1] Zlatarski V, Martínez-Estalella N. Les Scleractinaires de Cuba avec des Données sur les Organismes Associes. Annex 1. Sofía: Editions de l'Académie Bulgaria des Sciences; 1982. 200p
- [2] Torruco D, González-Solis MA. Estado actual de los corales de Yucatán. In: Duran R, Méndez M, editors. Biodiversidad y desarrollo humano en Yucatán. Mérida, Yucatán: CICY, PPD-FMAM, Conabio, Seduma; 2010. pp. 204-209
- [3] Macintyre IG, Burke RB, Stuckenrath R. Thickest recorded Holocene reef section, Isla Pérez core hole, Alacran Reef, Mexico. *Geology*. 1977;5:749-754
- [4] Lalli C, Parsons T. Biological Oceanography. An Introduction. 2nd ed. Vol. 335. Burlington: Elsevier Butterworth-Heinemann; 1997
- [5] CONANP. Programa de Conservación y Manejo Parque Nacional Arrecife Alacranes. CDMEX: SEMARNAP; 2006. p. 169
- [6] Garduño MA. Distribución de la ictiofauna asociada a los arrecifes del Caribe mexicano [thesis]. Mérida: Centro de Investigación y de Estudios Avanzados del IPN; 1988
- [7] Jordán-Dahlgren E. El ecosistema arrecifal coralino del Atlántico mexicano. *Revista de la Sociedad Mexicana de Historia Natural*. 1993;44: 157-175
- [8] Kornicker LS, Bonet F, Cann R, Hoskin CM. Alacran Reef, Campeche Bank, Mexico. *Publications of the Institute of Marine Science, University of Texas*. 1959;6:1-22
- [9] Comisión Intersecretarial para el Manejo Sustentable de Mares y Costas. Política Nacional de Mares y Costas de México: Gestión Integral de las Regiones más Dinámicas del Territorio Nacional. CD México: Gobierno Federal; 2017. 81p
- [10] Bonet F. Biogeología subsuperficial del arrecife Alacranes, Yucatán. *Boletín del Instituto Geológico de México - UNAM*. 1967;80:1-191
- [11] Rezak R, Bright TJ, McGrail DW. Reefs and Banks of the Northwestern Gulf of Mexico. USA: Wiley; 1985. 259p
- [12] Logan BW. Coral reefs and banks, Yucatan shelf, Mexico. *American Association of Petroleum Geologists*. 1969;11:129-198
- [13] Jordán-Dahlgren E. Atlas de los Arrecifes Coralinos del Caribe Mexicano. In: El sistema Continental. Vol. 1. ICMYL-UNAM/CIQRO: CDMX; 1993. 110p
- [14] INE. Programa de manejo Reserva de la Biosfera Banco Chichorro. CDMEX: SEMARNAP/INE; 2000. p. 192
- [15] Tunnell JW Jr. Regional comparison of Southwestern Gulf of Mexico to Caribbean Sea coral reefs. In: *Proceedings of the 6th International Coral Reef Symposium*. Vol. 3. Australia; 1988. pp. 303-308
- [16] Bohnsack JA. Photographic quantitative sampling of hard bottom benthic communities. *Bulletin of Marine Science*. 1979;29:242-252
- [17] Leujak W, Ormond RFG. Comparative accuracy and efficiency of six coral community survey methods. *Journal of Experimental Marine Biology and Ecology*. 2007;351:168-187
- [18] Gómez P. Esponjas marinas (Porifera) de la Reserva de la Biosfera de SianKa'an. In: Navarro D, Suárez E, editors. *Diversidad Biológica en la Reserva de la Biosfera de Sian Ka'an*,

Quintana Roo, México. Vol. 2.  
Chetumal: CIQRO; 1992. pp. 23-33

[19] Littler DS, Littler MM, Bucher KE, Norris JN. Marine Plants of the Caribbean: a field guide from Florida to Brazil. Washington: Smithsonian Institution Press; 1989

[20] Bayer FM. The Shallow-Water Octocorallia of the West Indian Region. The Hague: Martinus Nijhoff; 1961

[21] Humann P. In: Deloach N, editor. Reef corals identification; Florida, Caribbean, Bahamas. Jacksonville, Florida: New World Publications; 2002. 253p

[22] González-Solis MA, Torruco D, Torruco-González AD. Biodiversidad de macroalgas en arrecifes coralinos de la Sonda de Campeche, el Caribe Mexicano y Belice. Gayana Botánica. 2018;75(1): 501-511

[23] Humann P. In: Deloach N, editor. Reef Creature Identification. Florida, Caribbean, Bahamas. Jacksonville, Florida: New World Publications; 1992. 328p

[24] Orlóci L. Ecological Program for Institutional Computing on the MacIntosh. Ecological Computations Series. SPB. The Hague: Academic Publishing; 1990. 61p

[25] Magurran AE. Ecological Diversity and Its Measurement. New York: Princeton University Press; 1988. 179p

[26] Pielou EC. The Interpretation of Ecological Data: A Primer on Classification and Ordination. New York: Wiley; 1984. 147p

[27] Orlóci L. Multivariate Analysis in Vegetation Research. 2nd ed. The Hague: Dr. Junk WBV; 1978. 451p

[28] Ambroso S, Gori A, Dominguez-Carrió C, Gili JM, Berganzo E,

Teixidó N, et al. Spatial distribution patterns of the soft corals *Alcyonium acaule* and *Alcyonium palmatum* in coastal bottoms (Cap de Creus, northwestern Mediterranean Sea). Marine Biology. 2013;160: 3059-3070

[29] Carrasco FD. Organismos del bentos marino sublitoral: algunos aspectos sobre la abundancia y distribución. In: Werlinger C, editor. Biología Marina y Oceanografía: Conceptos y Procesos. Concepción: Trama; 2004. p. 650

[30] Loya Y, Rinkevich B. Effects of oil pollution on coral reef communities. Marine Ecology Progress Series. 1980;3: 167-180

[31] Liddell WD, Ohlhorst SL. Patterns of reef community structure, North Jamaica. Bulletin of Marine Science. 1987;40(2):311-329

[32] Bertolino M, Calcinai B, Cattaneo-Vietti R, Cerrano C, Lafratta A, Pansini M, et al. Stability of the sponge assemblage of Mediterranean coralligenous concretions along a millennial time span. Marine Ecology. 2014;35:149-158

[33] Dudgeon SR, Aronson RB, Bruno JF, Precht WF. Phase shifts and stable states on coral reefs. Marine Ecology Progress Series. 2010;413:201-216

[34] Hughes TP, Rodrigues MJ, Bellwood DR, Ceccarelli D, Hoegh-Guldberg O, McCook L, et al. Phase shifts, herbivory, and the resilience of coral reefs to climate change. Current Biology. 2007;17:360-365

[35] Parepa M, Fischer M, Bossdorf O. Environmental variability promotes plant invasion. Nature Communications. 2013;4:1604

[36] Rahel F. The hierarchical nature of community persistence: A problem of

- scale. *American Naturalist*. 1990;**136**: 328-344
- [37] Valanko S, Norkko J, Norkko A. Does stability in local community composition depend on temporal variation in rates of dispersal and connectivity? *Journal of Sea Research*. 2015;**98**:24-32
- [38] Viaroli P, Bartoli M, Giordani G, Naldi M, Orfanidis S, Zaldivar JM. Community shifts, alternative stable states, biogeochemical controls and feedbacks in eutrophic coastal lagoons: A brief overview. *Aquatic Conservation: Marine and Freshwater Ecosystems*. 2008;**18**:105-117
- [39] Antoine JW, Gilmore JG. Geology of the Gulf of Mexico. *Ocean Industry*. 1970;**5**(5):34-38
- [40] Smith FGW. Atlantic reef corals. In: *A Handbook of the Common Reef and Shallow-Water Corals of Bermuda, the Bahamas, Florida, the West Indies and Brazil*. Coral Gables, Florida: University of Miami Press 1976. 164p
- [41] Fosberg FR. A brief study of the cay of Arrecife Alacranes, a Mexican atoll. *Atoll Research Bulletin*. 1962;**93**:1-25
- [42] Martínez E. Estudio Comparativo de los Escleractinios de Sotavento y Barlovento del Arrecife Alacranes. Campeche: Folletos de Divulgación, Secretaría de Marina. Direcc. Gral. *Ocean. Naval Est*; 1989. 25p
- [43] Folk R, Robles R. Carbonate Sands of Isla Pérez, Alacran Reef Complex, Yucatán. *Journal of Geology*. 1964;**72**: 255-292
- [44] Antoine JW. Structure of the Gulf of Mexico. 1-34. In: Rezak R, Henry VJ, editors. *Contributions on the Geological and Geophysical Oceanography of the Gulf of Mexico*. Vol. 3. Texas: Gulf Publ. Co., Texas A&M Univ; 1972. pp. 1-34
- [45] Capurro FR. La circulación oceánica en el Golfo de México. México: Mem. V Congr. Nac. Ocean; 1972. pp. 3-12
- [46] Johnson K, Kristiina V, Clark H, Schmitz O, Vogt D. Biodiversity and the productivity and stability of ecosystems. *Trends in Ecology & Evolution*. 1996; **53****47**:372-377
- [47] Rodríguez-Zaragoza FA, Ortiz M, Berrios F, Campos L, de Jesús-Navarrete A, Castro-Pérez J, et al. Trophic models and short-term dynamic simulations for benthic-pelagic communities at Banco Chinchorro Biosphere Reserve (Mexican Caribbean): A conservation case. *Community Ecology*. 2016;**17**(1):40-60
- [48] Spalding MD, Ravilious C, Green EP. *World Atlas of Coral Reefs* United Nations, Environment Programme-World Conservation Monitoring Centre. Los Angeles: University of California Press; 2001. 424p
- [49] AIDA. La Protección de los Arrecifes en México. Rescatando la Biodiversidad Marina y sus Beneficios para la Humanidad. CDMX: Asociación Interamericana para la Defensa del Ambiente; 2015. 40p
- [50] Canela RJ. Conocimiento y uso de los Recursos del Arrecife Alacranes por Pescadores de la zona maya de la península de Yucatán. *Reporte del proyecto de sostenibilidad maya*. Vol. 4. Los Angeles: Universidad de California-Riverside y Fundación MacArthur; 1992. 62p
- [51] Rice WH, Kornicker LS. Mollusks of Alacran Reef, Campeche Bank, México. *Publications of the Institute of Marine Science, University of Texas*. 1962;**8**: 366-403
- [52] Torruco D. Faunística y ecología de los corales escleractinios en los arrecifes de coral del sureste de México [thesis]. Barcelona: Universitat de Barcelona; 1995

- [53] Chávez EA, Hidalgo E, Izaguirre MA. Comparative analysis of Yucatan coral reefs. In: Proceedings of the 5th International Coral Reef Congress; Vol. 2; 1985. pp. 355-361
- [54] González-Solis MA, Torruco D, Liceaga A, Ordaz J. The shallow and deep bathymetry of the Chinchorro Bank reef in the Mexican Caribbean. *Bulletin of Marine Science*. 2003;73(1): 15-22
- [55] Torruco D, González-Solis MA, Ordaz J. The role of environmental variables in the lagoon coral community structure on the Chinchorro Bank, México. *Bulletin of Marine Science*. 2003;73(1):23-36
- [56] Gutiérrez D, García-Saez C, Lara M, Padilla C. Comparación de arrecifes coralinos: Veracruz y Quintana Roo. In: Salazar-Vallejo S, González N, editors. *Biodiversidad Marina y Costera de México*. CDMX: CONABIO/CIQRO; 1993. pp. 787-806
- [57] James NP, Ginsburg RN. The seaward margin of Belize barrier and atoll reefs. *International Association of Sedimentologists*. 1979;3:191
- [58] Chávez EA. Observaciones generales sobre las comunidades del arrecife de Lobos, Veracruz. *Anales. Escuela Nacional de Ciencias Biológicas*. 1973;20:13-21
- [59] Polunin VC, Sánchez C, Schep S, Stevens RJ, Vallés H, MJA V, et al. *Towards Reef Resilience and Sustainable Livelihoods: A Handbook for Reef Managers Caribbean Coral*. Exeter: University of Exeter; 2014. 172p
- [60] Ainsworth CH, Mumby PJ. Coral-algal phase shifts alter fish communities and reduce fisheries production. *Global Change Biology*. 2015;21:165-172
- [61] May R. Will a large complex system be stable? *Nature*. 1972;238:413-414
- [62] Fung T, Seymour RM, Johnson CR. Alternative stable states and phase shifts in coral reefs under anthropogenic stress. *Ecology*. 2011;92:967-982
- [63] Grimm V, Schmidt E, Wissel C. On the application of stability concepts in ecology. *Ecological Modelling*. 1992;63: 143-161
- [64] Connell JH, Slatyer RO. Mechanisms of succession in natural communities and their role in community stability and organisation. *The American Naturalist*. 1977;111: 1119-1144
- [65] Folke C, Carpenter S, Walker B, Scheffer M, Elmqvist T, Gunderson L, et al. Regime shifts, resilience, and biodiversity in ecosystem management. *Annual Review of Ecology, Evolution, and Systematics*. 2004;35:557-581
- [66] Guerra C, Cobo F, Gonzalez M, Alonso J. Stability and resilience in macrobenthic communities: The role of habitat disturbance. *WIT Transactions on Ecology and the Environment*. 2007; 106:215-223
- [67] Scatterday JW. Low water emergence of Caribbean Reefs and effects of exposure on coral diversity observations off Bonaire Netherlands Antilles. In: Frost SH, Weiss MP, Saunders JB, editors. *Reefs and Related Carbonates Ecology and sedimentology. Studies in Geology*. Vol. 4. Tulsa, Oklahoma: American Association of Petroleum Geologist; 1977. pp. 155-169
- [68] Jordán E, Martín E. Chinchorro: Morphology and composition of a Caribbean atoll. *Atoll Research Bulletin*. 1987;310:1-33
- [69] Tunnell JW. Reef distribution. In: Tunnell JW Jr, Chávez EA, Withers K,

editors. Coral Reefs of the Southern Gulf of Mexico. College Station, Texas: Texas A&M University Press; 2007. pp. 14-22

[70] Armenteros M, Saladrigos D, González-Casuso L, Estévez ED, Kowalewski M. The role of hábitat selection on the diversity of macrobenthic communities in three gulfs of the Cuban archipelago. *Bulletin of Marine Science*; **94**(2):249-268

[71] Torruco D, González-Solis MA, Liddell WD. Integración ecológica de grupos funcionales en la laguna arrecifal de Alacranes, Yucatán, México. *Brenesia*. 1993; **39-40**:37-49





*Edited by Andrew J. Manning*

*Lagoon Environments Around the World - A Scientific Perspective* covers a wide range of topics. Typically bordering between land and sea, lagoons are among the most diversely utilized waterways on the planet. Lagoons are extremely important environments socio-economically, and their usage places ever increasing stress on these very sensitive aquatic regions. The effective management of shallow aquatic environments requires a detailed scientific understanding of the various contributory natural processes. This has both environmental and economic implications, especially where there is any anthropogenic involvement. This book draws on international scientific research to examine the following lagoon related issues: classification, circulation hydrodynamics, ecosystems, sedimentation, anthropogenic stresses, and response to extreme events. The research was carried out by researchers who specialize in shallow water processes and related issues.

Published in London, UK

© 2020 IntechOpen

© Lennons Daughter / unplash

**IntechOpen**

ISBN 978-1-78985-953-9



9 781789 859539

